Investigating the role of PARylation in regulating Skeletal Muscle Mass and Function in Healthy Mature Mice

Dheeraj Pandey

A thesis submitted in partial fulfillment of the requirements for the degree Master of Science in Biochemistry

Supervisor Dr. Keir J. Menzies

Department of Biochemistry, Microbiology, and Immunology

Faculty of Medicine

University of Ottawa

Abstract

Adenosine diphosphate (ADP) ribosylation is a post-translational modification dependent on the transfer of ADPr units from nicotinamide adenine dinucleotide (NAD+) on to a plethora of biomolecules (i.e., proteins, DNA, RNA, etc.) in response to physiological stressors (i.e., nutrient deprivation, oxidative stress, DNA strand breaks). Poly-ADP-ribosylation (PARylation) is primarily mediated by the family of poly(ADP-ribose) polymerases (PARPs) and enzymatically degraded (dePARylation) by hydrolases such as poly(ADP-ribose) glycohydrolase (PARG). This thesis characterizes the role of poly(ADP-ribose) polymerase 1 (PARP1) and PARG in the skeletal muscle of healthy mature mice under normal physiological conditions. Specifically, we validate the deletion of *Parp1* and *Parg* in inducible skeletal muscle-specific KO mouse models followed by performing general phenotyping of both male and female mice. The thesis concludes that under normal physiological conditions the activity of *Parp1* or *Parg* in (de)PARylation is dispensable for maintaining skeletal muscle mass, function, and homeostasis in healthy mature mice.

Keywords: poly(ADP-ribose) polymerase 1 (PARP1), poly(ADP-ribose) glycohydrolase (PARG), PARylation, muscle health.

Acknowledgements

Firstly, I would like to thank Dr. Keir J. Menzies for providing me with the opportunity to join his lab and for the guidance and supervision to complete this project. I am immensely grateful for the experience that I gained through conducting research in the Menzies laboratory. Thank you to my thesis advisory committee members, Dr. Nadine Wiper-Bergeron and Dr. Yan Burelle for their support, feedback, and suggestions to further my research project.

Thank you to Dr. Alex E. Green for his excellent mentorship and for inculcating scientific expertise in me. My research would not have been complete without the continuous support of everyone from the animal care and veterinary services committee and the behavior and physiology core for providing impeccable service. Special thanks to the people in and outside the lab for making these past two years memorable. Finally, thank you to my family and friends for their endless love and faith in me.

Table of Contents

List of Abbreviations

Abbreviation	Definition
ADP	Adenosine diphosphate
ADPR	Adenosine diphosphate ribose
AMPK	AMP-activated protein kinase
AP1	Activator protein 1
APLF	Aprataxin and PNKP like factor
ARH	ADP-ribosyl hydrolase 3
ART	ADP-ribosyl transferase
ARTC	ADP-ribosyl transferases clostridia toxin-like
ARTD	ADP-ribosyl transferases diphtheria toxin-like
ATP	Adenosine triphosphate
BRCA	Breast cancer gene
BRCT	BRCA1 C terminus
CHFR	Checkpoint with forkhead and ring finger domain
CLAMS	Comprehensive laboratory animal monitoring system
C/EBP	CCAAT-enhancer-binding proteins
DMD	Duchenne muscular dystrophy
GAPDH	Glyceraldehyde-3-phosphate dehydrogenase
HSA	Human skeletal actin
HSP-90	Heat shock protein-90
MACROD	Macro domain
MCM	Mer-Cre-Mer
MER	Mutated estrogen receptor
MyHC	Myosin heavy chain
MYOD	Myoblast determination protein 1
MYOG	Myogenin
NAM	Nicotinamide
NFKB	Nuclear factor kappa-light-chain-enhancer of activated B cells
NMN	Nicotinamide mononucleotide
NAD+	Nicotinamide adenine dinucleotide
NUDT	Nudix hydrolase
PAR	Poly ADP-ribosylation

PARP1	Poly ADP-ribose polymerase
PARG	Poly ADP-ribose glycohydrolase
PBM	PRMT5 binding motif
PBZ	Poly ADP-ribose-binding zinc finger domain
PTM	Post translational modification
RER	Respiratory exchange ratio
TARG1	Terminal ADP-ribose protein glycohydrolase 1
TNKS	Tankyrase
TNNT1	Troponin T1
XRCC1	X-Ray repair cross complementing 1
YY1	Yin yang 1

Note: Abbreviations are listed in the alphabetical order

List of Tables

Note: Complete list of tables

List of Figures

Note: Complete list of figures listed in the order of appearance in the chapters, Ch = chapter, Supp = supplementary

Chapter I

General Introduction

1.1 Post-translational modification as an adaptation to environmental stressors

All living organisms have evolved certain mechanisms to survive through suboptimal growth conditions by initiating transcriptional regulation of stress genes to generate a cellular defense response against a variety of environmental stressors (physical, chemical, or nutritional). Cellular stress can be detected and mediated by effector proteins downstream of the signaling cascade which then initiate a response to the stimuli through the activation of signaling pathways through transcription factors. This allows the cell to fine tune the cellular response via the expression of genes, to regulate the adaptation to stress and maintain homeostasis. All living organisms have evolved more immediate responses to stress that include cellular processes known as post-translational modifications (PTMs). PTMs provides a dynamic and rapid response to physiological stressors as an alternate adaptive mechanism as (1) the macromolecules involved in the PTMs are ubiquitous in the cells and (2) do not have to be synthesized, thus reducing time and energy consumption while initiating a stress response (Palazzo et al., 2017; Zhang et al., 2015).

PTMs are reversible or irreversible covalent additions of functional groups primarily to the amino side chains of the target proteins, nucleic acids, and lipids. Thus, enhancing the complexity of the proteins and their biological functions, hence, increasing their functional diversity. PTMs modulate protein folding, function, activity, turnover and mediate interactions with proteins and other cellular macromolecules to regulate cellular

signal transduction, gene transcription, DNA damage repair, cell fate and others (Ramazi & Zahiri, 2021). Of note, there are over 600 classes of PTMs that have been known to span in an order 10^6 unique target sites (Bradley, 2022). Some of the most well-known PTMs include phosphorylation, acetylation, and ubiquitination which covers more than 90% of all the PTMs (Ramazi & Zahiri, 2021). However, the focus of this thesis is on a highly conserved PTM known as ADP-ribosylation. It is one of the oldest and most well preserved PTM in all eukaryotes, bacteria, and viruses (Palazzo et al., 2017; Perina et al., 2014). Evidence links its evolutionary history dating back to early common ancestors (Palazzo et al., 2017; Perina et al., 2014).

1.2 ADP-ribosylation as a reversible post-translational modification

ADP-ribosylation is an NAD+ dependent reversible PTM. It is involved in several cellular processes such as DNA repair, apoptosis, stress response, signal transduction and others (Perina et al., 2014). ADP-ribosylation modifies target proteins by covalently attaching single or multiple ADP ribose (ADPr) units by cleaving nicotinamide adenine dinucleotide (NAD+) in processes called mono-ADP ribosylation (MARylation) or poly-ADP ribosylation (PARylation), respectively. ADPr units can be attached on to proteins at various amino acid residues, including arginine, serine, glutamate, aspartate, lysine, threonine amongst others (Teloni & Altmeyer, 2016).

ADP-ribosyl transferases (ARTs) consists of a superfamily of two different enzymatic classes based on their catalytic domains and are referred as ADP-ribosyl diphtheria toxin like transferases (ARTDs), also know as Poly(ADP-ribose) Polymerases (PARPs) and ADP-ribosyl cholera toxin like transferases (ARTCs). The ARTD superfamily consists of 17 family members, whereas ARTCs include 5 family members

(Lüscher et al., 2021; Poltronieri et al., 2021). Depending on the number of ADPr motifs attached to the target protein by these enzymes, they can be classified as mono-ADP-ribosyl transferases (mono-ARTs) that perform MARylation or poly-ADP-ribosyl transferases (poly-ARTs or PARPs) that perform PARylation (Qi et al., 2019). Concomittantly, these MAR and PAR chains from the target protein are hydrolyzed by hydrolase enzymes such as Poly-ADP-ribosyl glycohydrolase (PARG) (**Figure 1.**, as discussed later in **section 1.11.)**.

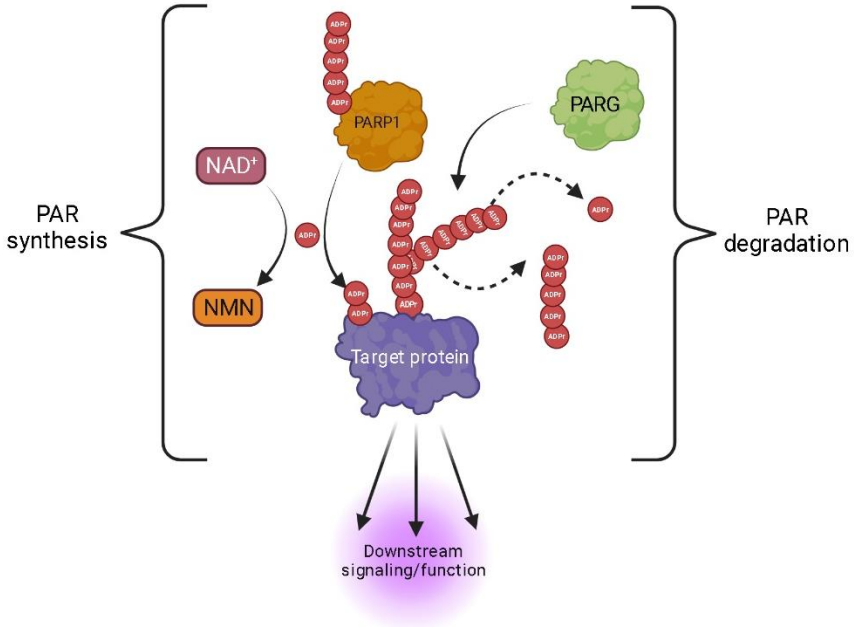

Figure 1. Schematic representing the processes of (de)PARylation. Created with Biorender.

1.3 Mono ADP-ribosylation

Even though the nomenclature suggests that PARPs catalyze multiple ADPr units on to the target protein, there are many PARPs that perform MARylation including PARP3,

PARP4, PARP6-8, PARP10-12 and PARP14-16. Of note, PARP9 and PARP13 are enzymatically inactive (Gupte et al., 2017; Liu et al., 2017; Vyas et al., 2014). Additionally, ARTCs 1 and 5 have also been found to perform MARylation (Lüscher et al., 2021). ARTCs involve four structurally related ecto-mono-ADP ribosyl transferases that are either secreted into the extracellular compartments or expressed at the surface of cells ectopically. Out of these ARTCs, ARTC1 and ARTC5 contain the catalytic domain required for polymer elongation whereas ARTC3 and ARTC4 lack the catalytic glutamate residue required for polymer elongation (Di Girolamo & Fabrizio, 2019).

The majority of the MARylating enzymes are primarily present in the cytoplasm but some can be found in the nucleus through cell cycle dependent shuttling (Challa et al., 2021). Even though the role of MARylation is not well understood, recent studies with the help of new techniques have begun to shed light on the biological functions of these MARylating enzymes in regulating cellular processes such as maintenance of cytoskeleton, focal adhesion and motility of cells (PARP14) (Vyas et al., 2013, 2014), RNA metabolism (PARP7,10,12, and 14) (Bock et al., 2015), and are involved in various stress responses (PARP12,14 and 15) (Challa et al., 2021; Leung et al., 2011; Vyas et al., 2014). PARP14 has also been found to regulate immune cell response (Cho et al., 2011), whereas PARP16 regulates the unfolded protein response pathway (Jwa & Chang, 2012). Moreover, the roles of PARP6 and PARP7 have been implicated in neuronal development.

1.4 Poly-ADP-ribosylation

PAR synthesis was first identified by Chambon et al. (Chambon et al., 1963). PARylation attaches a branch of repeating ADPr units linked through α(1”→2’) ‘O’-

glycosidic ribose-ribose bonds. PAR chain length can vary from 2 to 200 ADPr units branching off at every 20-50 ADPr units (D'Amours et al., 1999; Kim et al., 2005). Each ADPr residue carries two phosphate groups attached to the 5' carbon atom of a ribose group, which is linked to nicotinamide adenosine through its 1' carbon atom. The two phosphate groups contribute to the negative charge on the PAR motif (Reeder et al., 1967; Sugimura et al., 1967; Thomas & Tulin, 2013).

The significance of PAR heterogeneity on cellular physiology is yet to be uncovered, although it has been said to modulate crucial cellular processes, including the DNA damage response and chromatin regulation (Aberle et al., 2020; Dantzer & Santoro, 2013; De Vos et al., 2012; Javle & Curtin, 2011), transcription, translation and protein degradation(Bai, 2015a; Kim et al., 2005; Kraus & Hottiger, 2013), mitochondrial regulation and metabolism (Bai, Cantó, et al., 2011; Bai et al., 2015), inflammation and immunity (Fehr et al., 2020; Mangerich & Bürkle, 2012), cancer and cell death (Aberle et al., 2020; Curtin & Szabo, 2013; Kim et al., 2005; Krishnakumar & Kraus, 2010; Lüscher et al., 2018; Masutani & Fujimori, 2013; Talhaoui et al., 2016). PAR synthesis is tightly regulated and is present at lower levels in the mammalian cells (D'Amours et al., 1999a; M. Li & Yu, 2015; Liu et al., 2017). PAR chains are transient in nature and are rapidly degraded within the order of minutes (Alvarez-Gonzalez & Althaus, 1989; Bernardi et al., 1997). Other than the allosteric modification of acceptor proteins by direct covalent binding, PAR polymers can regulate biological processes by interacting with reader proteins belonging to four distinct groups: PAR binding motifs (PBM), PAR binding macro domains, PAR binding zinc-finger domains (PBZ) and Try-Try-Glu (WWE) domains. This in turn allows PAR to exert its function by providing a docking site for several nuclear proteins such as DNA repair and

transctiption factors, chromatin remodellers, DNA and RNA binding proteins and cell-cycle regulators to perform their functions in various situations (Barkauskaite et al., 2015; Lüscher et al., 2018; Teloni & Altmeyer, 2016) (**Figure 2.**).

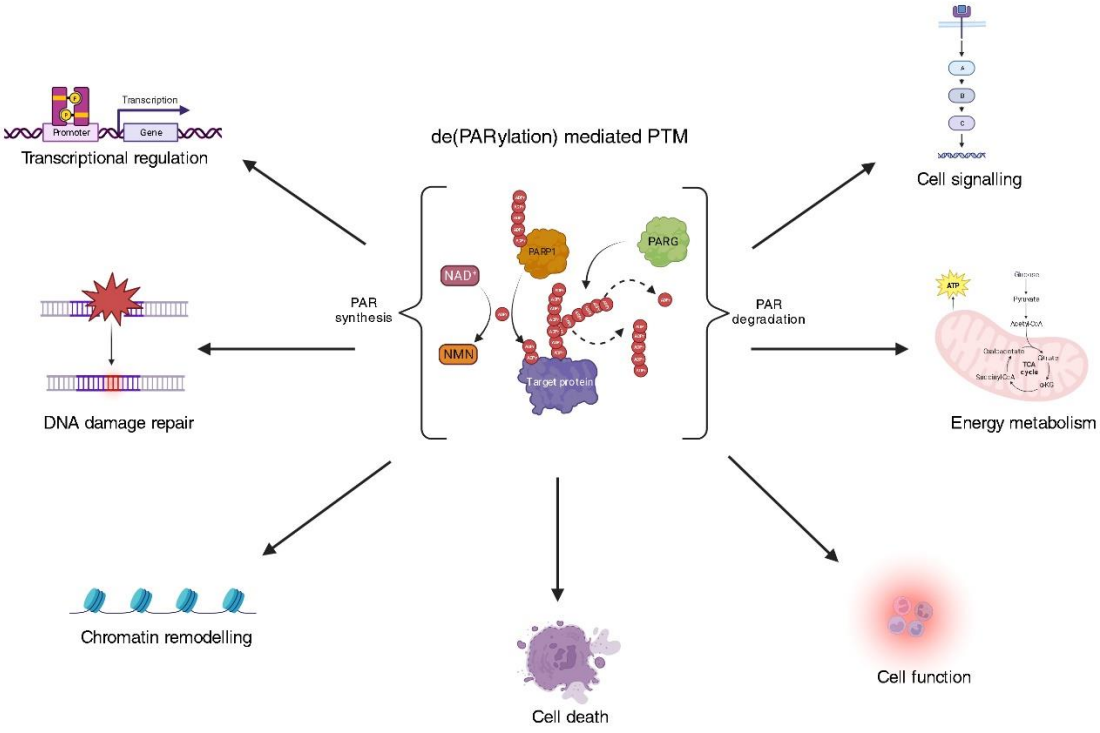

Figure 2. The various biological roles of (de)PARylation . Created with Biorender.

1.5 Poly(ADP-ribose) Polymerases

There are only four enzymes that catalyze PAR synthesis in vivo namely PARP1 and PARP2, PARP5a (TNKS1) and PARP5b (TNKS2) (Leung et al., 2011; Lüscher et al., 2018). Based on homology, these proteins share a common 'ART signature' composed of Histidine-Tyrosine-Glutamine (H-Y-E) triad in the catalytic domain, which is required for NAD+ cleavage to nicotinamide adenine mononucleotide (NAM) and ADPr (Hassa, 2008). In addition, PARP1-2 and PARP5a-5b have been shown to contain a variable secondary structure in the donor site as a D-loop, which affects the way catalytic domain of these enzymes interact with NAD+ (Vyas et al., 2014; Wahlberg et al., 2012). PARP1 and PARP2 are capable of synthesizing PAR polymers in linear or branched fashion (Alvarez-Gonzalez & Althaus, 1989; Chen et al., 2018; Izumi & Mellon, 2021; Miwa & Sugimura, 1971; Tanaka et al., 1977), whereas, PARP5a and PARP5b can only catalyze linear ADPr oligomers up to 20 ADPr units in length (Cook et al., 2002; De Rycker & Price, 2004; Rippmann et al., 2002; Smith et al., 1998a). PARP1-2 are localized in the nucleus (Meder et al., 2005; Rancourt & Satoh, 2009; Riccio et al., 2016), whereas PARP5a-5b are localized to the cytoplasm, golgi, endoplasmic reticulum, peroxisomes and cytoskeleton (X. Li et al., 2017). One of the main roles for PARPs are to act as a DNA damage sensor through their DNA binding domains, and initiate a DNA repair response through PAR synthesis within the order of seconds of DNA lesion recognition (Pandey & Black, 2021). Dysregulation of PAR homeostasis sensitizes cells to DNA damaging agents, embryonic development, cellular differentiation, metabolism, inflammation, diabetes, cancer and aging (Bai, 2015; Barkauskaite et al., 2015; Gupte et al., 2017; Hottiger, 2015; Krishnakumar & Kraus, 2010).

PARylation is predominantly catalyzed by PARP1 (85-90%), the founding member of the PARP family and a target of PARylation itself (D'Amours et al., 1999; Harrision et al., 2020; Shieh et al., 1998). Previous study by (Bai, Cantó, et al., 2011) has shown that *Parp1* deletion improves whole-body muscle metabolism through SIRT1 mediated upregulation of mitochondrial biogenesis. In contrast, a separate study has shown exacerbated obesity in 129/SVJ mice fed on a high fat diet after *Parp1* germline deletion (Devalaraja-Narashimha & Padanilam, 2010). This ambiguity in the phenotype of *Parp1* null mice may be due to the different mouse strains used in these different studies. Nonetheless, PARP2 shares more than 60% of sequence homology with PARP1 and is structurally similar with overlapping functions, albeit it lacks the zinc finger domain at the N-terminus that is present in PARP1 (Schreiber et al., 2006). PARP2 has been found to engage in DNA damage repair by attaching through its tryptophan-glycine-arginine (WGR) DNA-binding domain in response to genotoxic stress (Obaji et al., 2018). PARP2 has an overlapping PAR synthesis function during genotoxic stress, as double knockout of *Parp1*/*Parp2* in mice is embryonically lethal and increases genomic instability in embryonic fibroblasts (Menissier de Murcia, 2003; Teloni & Altmeyer, 2016). PARP2 has been studied for its role in PARylation of core histone proteins and its interaction with chromatin like PARP1 (Kurgina et al., 2021). However, in contrast to predominant linearized PAR chains synthesized by PARP1, PARP2 synthesizes branched PAR polymers at a higher frequency compared to PARP1 while facilitating DNA double stranded break repair (Chen et al., 2018; Izumi & Mellon, 2021). In the absence of PARP2, the branch chain formation is reduced, affecting the recruitment of APLF histone chaperone to the branched chain required for chromatin relaxation during DNA damage repair (Chen et al., 2018). Using in vivo

germline KO mice, loss of *Parp2* demonstrates a leaner phenotype, leading to lower body weight, and protection against diet-induced obesity in mice on a C57BL6J background (Bai, Canto, et al., 2011). Outside of PARP2, PARP5a and PARP5b also known as Tankyrases, were also recognized as proteins associated with genomic maintenance and telomere associated proteins (Smith et al., 1998). Additionally, PARP5a-5b have been shown to modulate spindle formation and centrosome function. They have been involved in regulating proteasome assembly and turnover rate, fine tuning several signaling transduction pathways such as Hippo signaling and Wnt/β-catenin (Teloni & Altmeyer, 2016). Either knockout of PARP5a or 5b in mice are viable and display only a mild phenotype, however, deletion of both the Tankyrases cause embryonic lethality in mice suggesting an overlapping role for these Tankyrases (Chiang et al., 2008; X. Li et al., 2017).

1.6 Poly(ADP-ribose) Polymerase 1 structure

The majority of PARylation in cells is driven by PARP1 during DNA damage (Satoh & Lindahl, 1992). PARP1 can attach up to 200 PAR polymers to the target protein with branching at every 20-50 ADPr units. (Kiehlbauch et al., 1993). Structurally, PARP1 contains three zinc finger DNA binding domains (Zn 1-3) at the N-terminal, followed by a nuclear localization sequence domain (NLS), a BRCA1 C-terminal (BRCT) auto-modification domain (Langelier et al., 2010, 2011), a tryptophan-glycine-arginine (WGR) domain and a highly conserved catalytic domain on the C-terminal for its enzymatic activity (Iwashita et al., 2005), and is between 110-116 kDa in size (D'Amours et al., 1999, Iwashita et al., 2005, Langelier et al., 2010, 2011) (**Figure 3.**). PARP1 catalytic activity can be regulated by auto-PARylation, which inhibits its activity, or through other PTMs that can activate or inhibit activity such as mono-ADP-ribosylation (Dasovich & Leung,

2023; Loseva et al., 2010; Mao et al., 2011), phosphorylation (Gagné et al., 2005; Z. Li et al., 2021), methylation (Wang et al., 2022), acetylation (Hassa et al., 2005; Rajamohan et al., 2009) and deacetylation (Rajamohan et al., 2009).

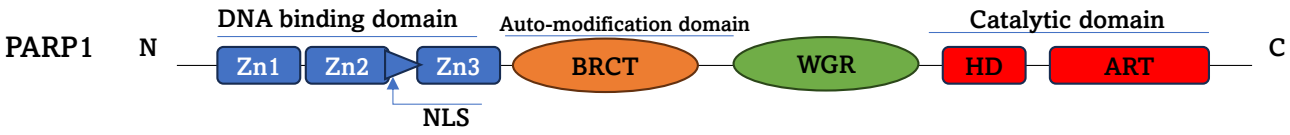

Figure 3. Schematic of PARP1 structure.

1.7 Poly(ADP-ribose) Polymerase 1 function

PARP1 is the most well characterized member in the PARP family. It is ubiquitous in subcellular compartments such as the nucleus. It has been well described for its role in DNA damage repair (Lüscher et al., 2018) (**Figure 4.**). However the list of its functions in other essential cellular processes is growing and now includes signal transduction, acting as a switch between apoptosis-inducing factor (AIF) dependent and independent cell death and regulating epigenetic modifications (David, 2009; Hottiger, 2015; Lüscher et al., 2018). Role of PARP1 has also been implicated in genomic maintenance, circadian rhythm, development and ageing, and cell fate and function (Asher et al., 2010; Harrision et al., 2020; Lüscher et al., 2021; Mangerich & Bürkle, 2012).

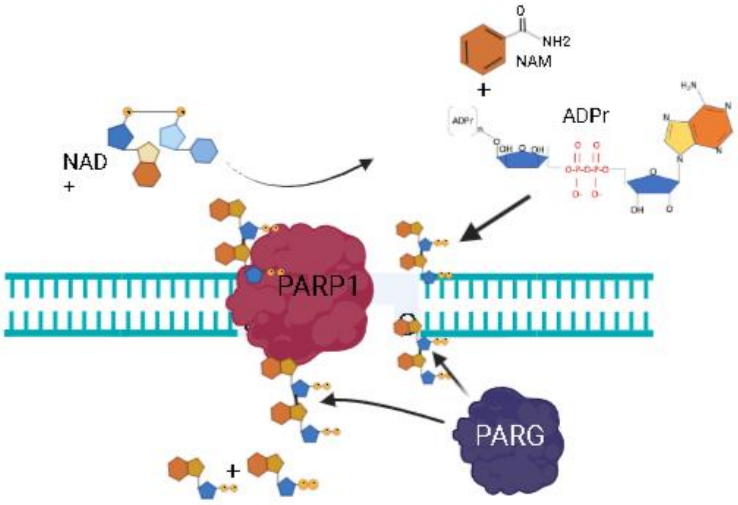

Figure 4. Schematic showing PARP1- and PARG-mediated DNA damage repair. Created with Biorender.

Under mild to moderate genotoxic stress conditions, PARP1 acts as a transcriptional activator and pro-survival protein that maintains cellular homeostasis. PARP1 detects DNA breaks and rapidly PARylates the DNA damage sites by derepressing the histones. PARP1 promotes the recruitment of chromatin remodelling proteins, such as APLF, CHFR, and macroH2A (Hurtado-Bagès et al., 2020; Liu et al., 2017). This provides a more favourable state of chromatin for the DNA repair machinery to acces and repair the damaged DNA site. PARP1 also provides a docking platform for DNA repair proteins, such as XRCC1 to bind and perform its repair function (Pazzaglia & Pioli, 2019) (**Figure 4.**).

In contrast, extensive DNA damage can lead to overactivation of PARP1 and chronic PAR sysnthesis and can deplete the intracellular levels of NAD+, affecting the overall cellular bioenergetics, for example, cellular ATP generation through mitochondrial respiration (Berger, 1985; Ha & Snyder, 1999). Sustained over-activation of PARP1 and continuous NAD+ depletion can lead to an energy crisis and has been shown to cause cell death (i.e. apoptosis, necrosis or parthanatos) (Andrabi et al., 2006; David, 2009; Ha & Snyder,

1999; Koh et al., 2004; Z. Li et al., 2021). Additonally, sustained levels of PAR polymers on chromatin causes a prolonged state of decondensation, leaving the DNA prone to intrinsic and extrinsic stressors (Prokhorova et al., 2021). Previous studies have shown that PARP1 dysregulation during pathophysiologcial conditions affects PAR-directed changes in NAD+ metabolism, promoting inflammation, obesity, diabetes and tumorigensis (Bai, 2015; Devalaraja-Narashimha & Padanilam, 2010; Fehr et al., 2020; Johnson et al., 2022; Mangerich & Bürkle, 2012; Martínez-Morcillo et al., 2021; Pirinen et al., 2014; Szántó & Bai, 2020).

1.8 Role of PARP1 as a transcriptional regulator

PARP1 has been previously implicated as the promoter of inflammatory pathways through the expression of cytokines and transcriptional coactivation of proinflammatory modulators such as Activating Protein 2 (AP2), myogenic transcriptional regulator Ying Yang 1 (YY1), and nuclear factor kappa-light-chain-enhancer of activated B cells (NF-κB) amongst others. The interaction between PARP1 and NF-κB has been studied previously in several cells and tissue types suggesting a higher level of coordination between the two proteins at the basal and stress conditions (Ke et al., 2022; Oliver, 1999; Robaszkiewicz et al., 2016).

A recent study highlighted the role of PARylation by PARP1 in early stage skeletal muscle differentiation. Inhibition of PARP1, using PJ34 impaired differentiation and reduced the levels of Troponin T1 (TNNT1) protein, a subunit of the sarcomere during early stage myogensis, suggesting that PARP1 is important for proper thin filament assembly (Tan et al., 2023). The transcription factor CCAAAT/enhancer binding protein beta (C/EBP), a regulator of myogenic progression, has been previously found to be

PARylated during adipogenesis (Luo et al., 2017). C/EBP has also been separately linked with myogenic progression (Tan et al., 2023) and in the regulation of NF-κB mediated inflammatory responses (Hassa et al., 2005). Interestingly, acetylation of PARP1 occurs via p300/C/EBP, causing the activation of NF-κB. Specifically, PARP1-C/EBP complexes with the p50 subunit to activate NF-κB, thereby initiating a proinflammatory response through the transcription of inflammatory cyto-and chemokines and other related transcription factors (Fehr et al., 2020). In addition, PARP1 has also been shown to activate canonical NF-κB pathway through IKKγ binding (Stilmann et al., 2009). PARP1 has also been shown to repress the myogenic factor Myoblast Determination Protein 1 (MyoD) which regulates the skeletal muscle differentiation through interaction with chromatin-modification complexes (Matteini et al., 2020).

1.9 Role of PARP1 in energy metabolism

NAD+ is a highly compartmentalized co-enzyme central to cellular energy metabolism. It is involved in the reduction-oxidation reactions and acts as a signaling molecule. It is the susbtrate and rate limiting factor for several NAD+ consuming enzymes such as PARPs and Sirtuins. Examples of how PARPs influence energy metabolism are summarized here. Linking genotoxic stress to energy metabolism, PARP1 inhibits glycolysis pathways upon hyperactivation during genotoxic stress. This occurs through a specific PAR binding motif present on hexokinase 1, the rate limiting enzyme in glycolysis (Andrabi et al., 2014; Fouquerel et al., 2014). PARP1 has also been shown to inhibit glyceraldehyde-3-phosphate dehydrogenase (GAPDH), an important enzyme in glycolysis, through PARylation during renal ischemic injury (Devalaraja-Narashimha & Padanilam, 2009). Furthermore, it has been suggested that PAR accumulation plays a role

in shifting the metabolic pathway from glycolysis to oxidative phosphorylation during the onset of early stage myogensis (Tan et al., 2023). PARP1 has also been shown to regulate metabolism simply through altering cellular NAD+ levels. PARP1 depletion or inhibition increases NAD+ levels in *Parp1* KO mice on a C57BL6J background thereby improving metabolism and protecting these mice from high fat diet-induced obesity (Bai, Cantó, et al., 2011; Pirinen et al., 2014). However, as mentioned previously, this finding may be dependent on mouse strain, as *Parp1* null mice on a 129/SVJ background showed exacerbated obesity on a similar diet (de Murcia et al., 1997; Devalaraja-Narashimha & Padanilam, 2010). Increased bioavailability of NAD+ has been shown to increase SIRT1 activity and enhance mitochondrial biogenesis. This in turn provides protection against metabolic dysfunction during diet induced obesity and can improve longevity (Pirinen et al., 2014). For instance, *Parp1* germline knockout mice did not gain body weight on a high fat diet (Lehmann et al., 2015; Pirinen et al., 2014). In addition, these mice demonstrated improved glucose tolerance and enhanced insulin sensitivity, altered feeding entrainment and locomoter activity. PARP1 has also been found to play an important role in both β-islet cell and adipocyte differentiation, both cells that have implications on whole-body metabolism. Specifically, selective inhibition of PARP1 has shown to improve in β-islet cell differentiation and provides protection against diabetes (Dadheech et al., 2022). PARP1 also promotes adipogenic differentiation through the PARylation of C/EBPβ (K. W. Ryu et al., 2018).

1.10 De-Poly-ADP-ribosylation

PAR synthesis and degradation are both required to maintain the often dynamic and transient PAR-directed signalling events. In contrast to PARylation, the removal of PAR chains is referred to as de-poly-ADP-ribosylation (dePARylation), as illustrated in **Figures 1. and 4.**. The degradation of PAR chains is mediated by various catabolizing enzymes. These dePARylating enzymes act by cleaving the glycosidic bond between adjacent ADP-ribose units or between the ADP-ribose unit and an attached amino acid (Lüscher et al., 2018).

The reversal of ADP-ribosylation via deMARylation or dePARylation is done by two distinct families of proteins: macrodomain containing enzymes and DraG-like ADP-ribosyl acceptor hydrolases (Agnew et al., 2018; Catara et al., 2019; O'Sullivan et al., 2019; Rack et al., 2020). The macrodomain containing hydrolases include MacroD1, MacroD2, phosphodiesterase family of NUDIX enzymes (NUDT9 and NUDT16), terminal ADPr glycosylhydrolase 1 (TARG1) and PARG (O'Sullivan et al., 2019). The other class of PAR degrading enzymes includes ADP-ribosyl hydrolase 1 (ARH1) and ADP-ribosyl hydrolase 3 (ARH3) (Mashimo et al., 2014; Niere et al., 2012). While PARG and ARH3 are the only two known dePARylating enzymes capable of incrementally removing PAR polymers, TARG1 can remove either a terminal ADPr monomer or the whole PAR chain attached to the target protein through its terminal. The rest of the enzymes can only hydrolyze a single ADPr monomer bound directly to an amino acid, which is the rate limiting and last step to complete PAR hydrolysis. These enzymes include MacroD1, MacroD2 and the phosphodiesterases family of NUDIX enzymes (NUDT9 and NUDT16) (O'Sullivan et al., 2019; Palazzo et al., 2015). Out of these enzymes, MacroD1, MacroD1 and TARG1 have

been shown to cleave the ester bond of modified glutamate and aspartate residues. ARH1 has specificity for cleaving modified arginine mono-ADPr residues, whereas ARH3 has the exo-glycolytic acitivity to reduce serine residues modified by PAR chains (O'Sullivan et al., 2019; Reber & Mangerich, 2021).

1.11 Poly-ADP Glycohydrolase

PARG is the predominant glycohydrolase enzyme that dePARylates modified target proteins by cleaving the 'O'-glycosidic bond between ADP-ribose units of PAR polymers, liberating ADPr monomers (Hottiger, 2015; Slade et al., 2011). It has several different isoforms formed through alternative splicing, specifically the nuclear 110-kDa protein, the 102, 99 and 60-kDa cytoplasmic proteins, and a 55-kDa mitochondrial protein (Hottiger, 2015). The nuclear PARG (110 kDa) isoform is the most studied hydrolase and is involved in the PAR hydrolyzing activity of the nucleus (**Figure 5.**). PARG hydrolyzes the glycosidic ribose-ribose bonds through its endo-and exo-glycohydrolase activity except for the terminal ADPr unit attached to the substrate which is degraded further by TARG1, MacroD1 or ARH3 (Agnew et al., 2018; Barkauskaite et al., 2015; Hottiger, 2015; Slade et al., 2011). With regards to the biological processes that PARG is involved in, there is an expected overlap with processes that have been described above for PARP1 and PARP2, including DNA damage repair, cell death, transcriptional regulation, epigenetics and cancer (Feng & Koh, 2013). Since PAR degradation acts dynamically in concert with PAR synthesis, the biological implications and pathophysiological effects of dysregulation of PAR degradation is similar to PARylation. While persistent MAR activity on chromatin is deemed non-toxic through previous studies, dysregulated PAR degradation elicits strong

pathophysiological conditions causing sythetic lethality in the absence of ARH3 and PARG in cells (Prokhorova et al., 2021). In addition, germline deletion of *Parg* causes embryonic lethality in mice due to PAR accumulation. (Koh et al., 2004).

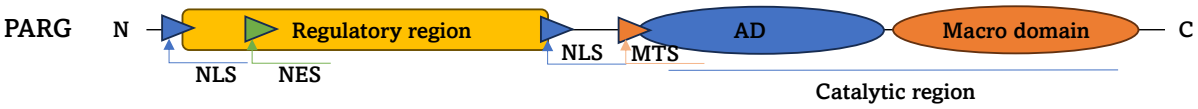

Figure 5. Schematic of nuclear PARG structure.

1.12 Skeletal muscle

The musculoskeletal system accounts for 30-40% of body mass (Relaix et al., 2021). Skeletal muscle is extremely plastic in nature and aids in movement through contraction and force generation (Mukund & Subramaniam, 2020). This organ is highly organized, striated, innervated, and it is attached to bones through tendons. They are composed of actin and myosin filaments which together form the sarcomere, a functional unit of contraction. Myofibrils, the most basic rod-like unit of muscle, are made up of a certain number of sarcomeres. Several bundles of myofibrils together form myofibers and bundles of organized myofibers form fascicles, which then forms the skeletal muscle tissue (**Figure 6.**). Denervation and loss of vascularization of the skeletal muscle leads to atrophy suggesting that it requires a constant energy supply and stimulation, through neuro-muscular junctions, to maintain its muscle contractile function and muscle mass (Mukund & Subramaniam, 2020).

Skeletal muscle is involved in many important biological processes apart from its muscle contractile function, such as maintaining core body temperature and insulating

internal organs (Baskin et al., 2015). Skeletal muscle is a metabolically active tissue and consumes a massive amount of energy, both at rest and in an active state. Moreover, skeletal muscle generates, senses, stores and utilizes nutrients for muscle homeostasis (Goody & Henry, 2018). The energy required for muscle contraction and force generation is achieved through ATP production using glycolytic and oxidative phosphorylation pathways (Mukund & Subramaniam, 2020). Excessive glucose is stored as glycogen in the skeletal muscle and is broken down during future activity (Goody & Henry, 2018b). Excessive nutrient uptake (glucose or fats) can cause stress through increased reactive oxygen species (ROS) generation, mitochondrial dysfunction, and chronic inflammation, leading to obesity and type 2 diabetes. This eventually affects insulin mediated glucose deposition in the body, such as in muscle and liver (Rohm et al., 2022). Evidence suggests that inflammation dysregulates skeletal muscle metabolism, influencing whole-body glucose regulation and insulin sensitivity. This response in the muscle is in part mediated by macrophage infiltration and secretion of proinflammatory molecules affecting muscle metabolism and contributing to insulin resistance (Wu & Ballantyne, 2017). Ultimately, obesity and type 2 diabetes can lead to muscle wasting through loss of proteostasis (Wang et al., 2006).

Loss of muscle mass, function and strength is also common in older individuals with healthy aging. During aging the rate of skeletal muscle deterioration increases, decreasing muscle mass and function and affecting the quality of life in older individuals, and is termed sarcopenia (Deschenes, 2004; Thompson, 2009). With sarcopenia, muscle fibres die and are replaced by connective tissues which lack contractile function and thus fail to generate force, reducing muscle strength. This decrease in muscle mass and strength,

required for proper locomotion and posture maintenance, causes frailty, attenuates overall health and results in a poor quality of life. There are many reasons for the overall decline in muscle health during aging, inlcuding reduced proteastasis, NAD+ depletion, mitochondrial dysfunction, decreased oxidative phosphorylation, increased catabolic activity and induction of anabolic resistance (Covarrubias et al., 2021; Ham et al., 2020; Hiona et al., 2010).

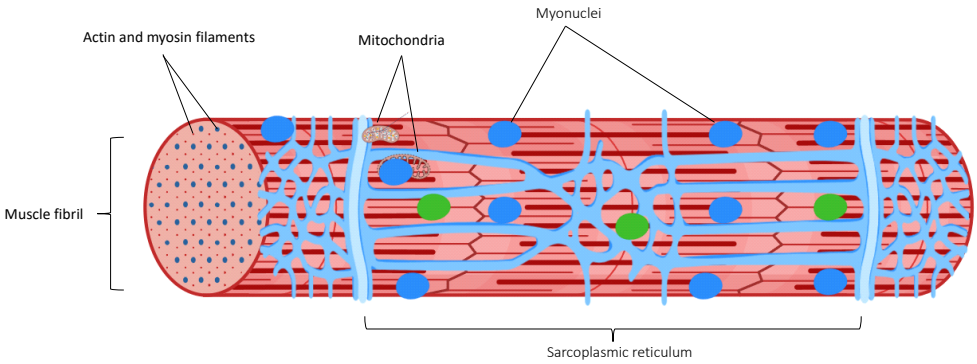

Figure 6. Schematic of a skeletal muscle fiber. Created with Biorender.

1.13 ADP-ribosylation in skeletal muscle

PARP1 overactivation has been associated with increased levels of oxidative stress in skeletal muscle due to the redox imbalance caused by the depletion of NAD+ in myotubes (Bai, Cantó, et al., 2011; Oláh et al., 2015). This in vitro observation gives insight into the process of aging where the activity level of PARP1 was observed to increase in unison with genotoxic stress and the depletion of NAD+ levels in the muscle of older individuals (Cobley et al., 2013). Similarly, in the mdx mouse model of Duchenne Muscular dystrophy (DMD), elevated PARylation has been shown to deplete NAD+, causing impaired mitochondrial function and bioenergetics in the skeletal muscle with

increased inflammation and fibrosis (D. Ryu et al., 2016). To substantiate the link between PARP1 and muscle NAD+ levels, in PARP1-null mice there is an increased abundance of NAD+ in muscle, along with increased mitochondrial biogenesis and enhanced oxidative phosphorylation (Bai, Cantó, et al., 2011). Of note, a recent study demonstrated that knockdown of PARP1 in the skeletal muscle of *Drosophila* increases lifespan, through AMPK activation and restored proteastasis through increased damaged mitochondrial turnover (Guo et al., 2023). This finding and the benefits seen in PARP1-null mice seems in juxtaposition to findings showing that PARP1 mediated PARylation is required for early stage differentiation of myoblasts (Tan et al., 2023). Thus, there is a need to understand the role of PARP1 and PARG in (de)PARylation in skeletal muscle.

1.14 Rationale and research objective:

The role of PARP proteins is well characterized in biological processes such as DNA damage repair, telomere lengthening, chromatin remodelling, immunity and inflammation, stress response, and apoptosis. PARP1 has been targeted in BRCA-1 deficient cancer, due to its known role in single stranded break repair in DNA. It has also been studied in stress related diseases such as metabolic disorders, stroke, cardiovascular diseases, and diabetes (Gibson & Kraus, 2012). However, it is still unclear how PARP1 affects skeletal muscle in normal vs diseased conditions, such as sarcopenia or DMD. Moreover, germline ablation of *Parp1* in mice has generated ambiguous data on the effect of PARP1 in mice fed a high fat diet, with an exacerbated obesity phenotype in mice bred on a 129/SVJ background vs an improved phenotype on a C57BL6J background (Bai, Cantó, et al., 2011; Devalaraja-Narashimha & Padanilam, 2010). Although some muscle phenotypes have been characterized in these studies, not enough data is available to date on muscle-specific ablation of PARP1.

Even though PARG is involved in similar biological functions as PARP proteins, it's role in the regulation of skeletal muscle structure, function, and homeostasis has yet to be characterized. This is especially important given that PARG is the predominant hydrolyzing enzyme which efficiently cleaves long PAR chains (Slade et al., 2011). It therefore remains to be seen how PARG ablation may affect skeletal muscle in normal and pathological conditions such as DMD, aging, obesity, and cancer.

Thus, we have generated mice that lack *Parp1* in mature skeletal muscle following induction (i.e., *Parp1*-iMKO) to elucidate if the activity of PARP1 is required for muscle function and homeostasis. Then, to examine if elevated PARylation levels can affect

muscle, we also generated mice where PARG elimination can be induced in mature skeletal muscle (i.e., *Parg*-iMKO mice). These models will help determine how reduced or elevated levels of general PARylation could yield an altered phenotype in muscle health and function during normal physiological conditions.

1.14.1. Hypothesis:

Parp1 ablation will decrease PARylation and reduce skeletal muscle mass and function, whereas *Parg* deletion will lead to the accumulation of PARylated proteins, thus, improving muscle mass and function.

Aim 1 (Chapter II): To characterize the effect of skeletal muscle-specific *Parp1* deletion in mature mice utilizing biochemical and functional assays.

Aim 2 (Chapter III): To characterize the effect of skeletal muscle-specific *Parg* deletion in mature mice utilizing biochemical and functional assays.

Chapter II: Role of PARP1 in Mature Skeletal Muscle Mass, and Function in Healthy Mice

2.1 Introduction

Skeletal muscle is an organ composed of muscle fibers, connective tissues, nerve tissues and blood vasculature. In general, 30-40% of body mass in humans constitutes skeletal muscle, which is required for locomotion, nutrient storage, and thermoregulation. It is one of the major reservoirs for glycogen and triglyceride storage, which in turn is primarily utilized to produce energy in the form of ATP for muscle contractile function, through glycolysis or oxidative metabolism using carbohydrates or fats as primary substrates (Hargreaves & Spriet, 2020). Healthy muscle mass and function are predictors of longevity, whereas loss of muscle mass and muscle function leads to poor health outcomes such as progressive weakness, and reduced life span (Goody & Henry, 2018b).

Previous work from our lab has identified the overactivation of poly-ADP-ribosylation (PARylation), a post translational modification mediated by poly(ADP-ribosyl) polymerases (PARPs), as a potential mediator of skeletal muscle health in Duchenne muscular dystrophy (DMD) (D. Ryu et al., 2016). PARP enzymes utilize nicotinamide adenine dinucleotide (NAD^+) as a substrate, to covalently attach ADP-ribosyl (ADPr) units to the target proteins on a serine, aspartate, or glutamate residue. Of multiple PARylating enzymes, PARP1 is not only the most active PARylating enzyme but is also a major consumer of NAD^+ and a competitor with other NAD^+ consuming enzymes such as Sirtuins, SARM1, CD38/157 ADP-ribosyl cyclases, and DNA ligase (Hurtado-Bagès et al., 2020b; Rajman et al., 2018). Importantly, PARP1 is a central mediator of cellular stress which is known to be activated by various physiological processes such as differentiation,

development, stress responses, DNA damage, and inflammation (Bai, 2015; Martínez-Morcillo et al., 2021; Reber et al., 2023; Tan et al., 2023). In turn, PARP1 modifies target proteins, induces DNA damage repair, and alters chromatin assembly, transcription regulation, amongst other important cellular functions (Gupte et al., 2017).

PARPs have been shown to be hyperactive in obese human participants (Jukarainen et al., 2016). In addition, pharmacological inhibition of PARP1 in mice fed a high fat diet has been shown to improve mitochondrial function in skeletal muscle while improving the overall phenotype (Pirinen et al., 2014). Increasing evidence suggests that chronically elevated PARylation leads to the depletion of the cellular NAD+ pool that is required by other NAD+ dependent enzymes, such as Sirtuin 1 (SIRT1) (Bai, Cantó, et al., 2011). Whole-body *Parp1* deletion also improves whole-body metabolism on a high fat diet by increasing energy expenditure, glucose oxidation, and mitochondrial biogenesis in metabolically active tissues such as muscle and brown adipose tissues (Bai, Cantó, et al., 2011).

To date no studies have examined the effect of *Parp1* ablation in skeletal muscle function, or its potential systemic effect on whole-body metabolism. Furthermore, the basal metabolic activity of PARP1 in skeletal muscle in healthy adult mice has not been characterized yet, hence we set out to look at the effects of an inducible *Parp1* deletion in the skeletal muscle of mature healthy mice (*Parp1*-iMKO) on a chow diet without any physiological stressors.

2.2 Materials and Methods

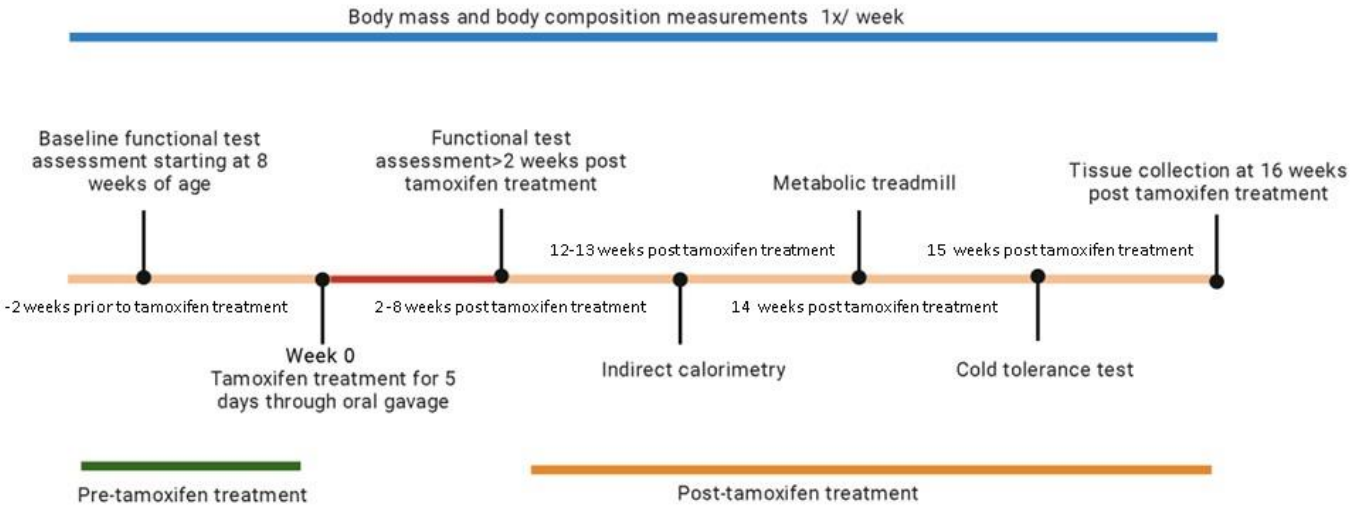

Figure 1. Schematic of the experimental timeline

2.2.1 Animal model

2.2.1.1 Parp1-inducible muscle knockout (iMKO) model

Parp1^{loxP} mice were obtained from Jackson Laboratory (stock no:032650) harboring loxP sites flanking exon 4 of *Parp1* on a C57BL/6N background (C57BL/6N-*Parp1*$^{tm1a(EUCOMM)Hmg)}$). HSA-MCM (Stock No: 025750) mice were obtained from Jackson laboratory for tamoxifen induced gene deletion using human skeletal actin as the promoter for controlled release of Cre-recombinase enzyme, where the Cre-recombinase sequence was flanked by Mutated Estrogen Receptor (MER) ligand binding domain on both C- and N-terminal (Mer-Cre-Mer). In the absence of ligand, MCM fusion protein is bound to Heat Shock Protein-90 (HSP-90) and retained in the cytoplasm. Upon tamoxifen binding, the MCM fusion protein translocates to the nucleus and mediates HSA-driven genomic recombination. HSA-MCM were bred with *Parp1*^{loxP} mice to obtain *Parp1*-iMKO mice in the F2 generation. Tamoxifen was given at 10 µl/gm bodyweight with a dose range not

exceeding 200 mg/kg body weight mixed with corn oil solution and administered through oral gavage to both WT and *Parp1*-iMKO cohorts. Tamoxifen-corn oil solution was administered for 5 days at a dose range described above to induce gene deletion in the mice at 12 weeks of age (**Figure 2.**). Mature muscle-specific *Parp1* deletion (*Parp1*-iMKO) was confirmed two weeks following tamoxifen treatment using qPCR. Data was normalized to *Peptidylprolyl isomerase A* (*Ppia*) gene expression and displayed as fold change over control (*Parp1*-LoxP$^{+/+}$, HSA-MCM$^{-/-}$ mice or *Parp1*-LoxP$^{-/-}$, HSA-MCM$^{+/-}$ mice).

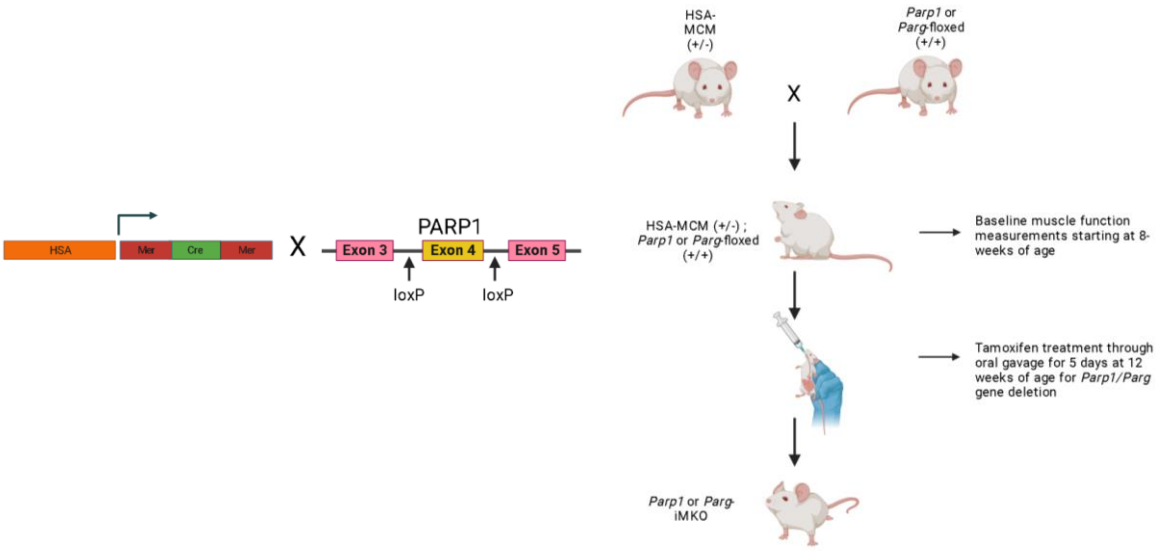

Figure 2. Schematic representation of inducible mature muscle-specific *Parp1* iMKO model. Created with BioRender.com

2.2.1.2 Mouse housing and maintenance

Mice were housed in temperature-controlled rooms kept at sub-thermoneutral temperatures i.e., ~23 ºC with 12:12 light and dark periods and had access to standard diet and water *ad-libitum.* For comprehensive laboratory animal monitoring system (CLAMS) study, the mice were housed at 28ºC-30ºC. All experiments were approved by Animal Care and Veterinary Services Committee at the University of Ottawa (Animal use protocol:

HSe-3236-R2 A1 and Meb3607-R1 A3) and conducted in strict accordance with Canadian Council on Animal Care (CCAC).

2.2.2 RNA isolation and quantitative real-time polymerase chain reaction (qPCR)

For total RNA Isolation, at least 13 milligrams of flash frozen quadriceps were crushed and added in 1ml of TRIzol® reagent (Invitrogen) to isolate high-quality RNA. Samples were homogenized using a 2.8 mm ceramic bead in a Bead Mill homogenizer (Fisherbrand 15340163) for three cycles at 2.09 m/s for 40 seconds with 20 seconds of rest in between the cycles. The aqueous phase, obtained after TRIzol® (Invitrogen) addition and homogenization, was then loaded on to a commercial RNA purification column. Total RNA was extracted according to the manufacturer's protocol as outlined in EZ-10 DNAaway RNA Miniprep Kit – BS88136 (Bio Basic Canada Inc, Markham, Ontario, Canada). RNA yield was quantified by measuring the absorption at 260/280 nm and 260/230 nm using a Nanodrop spectrophotometer-2000 (ThermoFisher Scientific).

cDNA synthesis was transcribed from the isolated total RNA using a ProtoScript II Reverse Transcriptase Kit (NEB #M0368). The diluted cDNA was prepared with SYBR Green (Roche). The quantitative expression of the selected genes was analyzed by LightCycler 480 System (Roche). Data was normalized using the housekeeping gene *Peptidylprolyl isomerase A* (*Ppia*). The primer pairs used for quantitative real-time PCR analysis are as follows:

Table 1. List of primers used for qPCR

Gene	Forward primer	Reverse primer
Adprhl2	AGGCACACGATACCGTCAG	CATGTCCACCTCGTCGAAGG
Atg7	TGACCTTCGCGGACCTAAAGA	CCCGGATTAGAGGGATGCTC

Atrogin1	ACACATCCTTATGCACACTGG	TCTCCATCCGATACACCCACA
MacroD1	CCTCCACCGACTGGAAGGA	CCCCACGGTACAGGGAGATT
MacroD2	ACCTTAGAGGAGAGACGCAAA	GTGGTGCTTCCTGAGTATTTTCT
MuRF1	CCAGGCTGCGAATCCCTAC	ATTTTCTCGTCTTCGTGTTCCTT
Myh1	CGGAGTCAGGTGAATACTCACG	GAGCATGAGCTAAGGCACTCT
Myh2	AAGTGACTGTGAAAACAGAAGCA	GCAGCCATTTGTAAGGGTTGAC
Myh3	AAAAGGCCATCACTGACGC	CAGCTCTCTGATCCGTGTCTC
Myh4	CTTTGCTTACGTCAGTCAAGGT	AGCGCCTGTGAGCTTGTAAA
Myh7	AGACTGTCAACACTAAGAGGGT	TGCCCCAAAATGGATTCGGAT
Myh8	CTGTACGACCAACATCTGGGA	GCACTAGCGTATGTGGAAAAGA
MyoD1	CGGGACATAGACTTGACAGGC	TCGAAACACGGGTCATCATAGA
MyoG	GCAGGCTCAAGAAAGTGAATGA	GTTGGGACCGAACTCCAGT
Parg	GGGGACTCCGCTACCAAAG	ACAGACTGGCGAGATCCACT
Park2	CGTGTGATTTTTGCCGGGAAG	GGTCCACTCGTGTCAAGCTC
Parp1	GGCAGCCTGATGTTGAGGT	GCGTACTCCGCTAAAAAGTCAC
Parp2	CACAGCTTGGTGACTTGTTCT	ACTCAGGCTTCAAAGTTTCCTC
Parp3	CACCCAGAACCTTATCACCAAC	CCTGTGGGGTTTTTCATGGC
Parp4	TCTTGCCAAATACCGTGCTTT	TGCTTAAAAACTCCGTAGCTTCA
Pink1	CACACTGTTCCTCGTTATGAAGA	CTTGAGATCCCGATGGGCAAT
Sqstm1	ATGTGGAACATGGAGGGAAGA	CCCCGATGTCGTAATTCTTGG
Tnks1	GTCTACTCCGTTACACCTGGC	TGAAGAGGTACAAGTCCACCTTT
Tnks2	GATGGCAGAAAGTCAACTCCA	AGCAGGCATTGTGTAGTGGTA
Ulk1	ACATCCGAGTCAAGATTGCTG	GCTGGGACATAATGACCTCAGG

2.2.3 Western blotting

Western immunoblots were completed using standard procedure with muscles collected from WT and *Parp1*-iMKO mice post-dissection in small microcentrifuge tubes and flash frozen in liquid nitrogen and stored at -80ºC.

For tissue homogenization, quadriceps tissues were sandwiched in between 7-8 aluminum sheets on both ends and pulverized over an aluminum block with a hammer. Both the hammer and the aluminum block were pre-cooled with liquid nitrogen. At least 17 milligrams of tissue were collected in a 2 ml reinforced bead mill homogenizer tubes

and stored at -80°C. Subsequently the tissues were thawed and three 2.8 mm ceramic beads (Fisher Scientific 19-340-162) were added along with RIPA lysis buffer (50 mM Tris HCl pH 8, 150 mM NaCl, 1% Triton X-100, 0.5% Sodium Deoxycholate, 0.1% SDS, Protease Inhibitor Cocktail (cOmplete Mini by Roche), Phosphatase Inhibitor (phosStop by Roche), PARP1 inhibitor (1 μM Olaparib final concentration), and PARG inhibitor (100 μM Tannic Acid final concentration). Tissues were homogenized using bead mill homogenizer for three cycles at 2.09 m/s for 40 seconds with 20 seconds of rest in between the cycles. Post homogenization, the tissues were centrifuged twice at 16,000g for 10 minutes at 4 ºC and the supernatant was collected after each spin in a freshly labelled microcentrifuge tube. Protein concentration was determined using a DC protein assay kit from BioRad (Bio-Rad Laboratories, Hercules, California, USA) and the absorbance was measured using the POLARstar Omega plate reader (BMG Labtech).

Lysates were diluted to 1 μg/μL of protein with 4x Laemmli buffer (Bio-Rad Cat# 1610737) supplemented with 10% β-mercaptoethanol (Fisher Bioreagents, BP176-100) and boiled for 5 minutes at 95ºC. Equal volume of lysates was loaded at 10-20 μg in 1.5 mm, 10% SDS-PAGE using TGX Stain-free FastCast Acrylamide Kit (Bio-Rad Cat# 1610173) and Bio-Rad™ Mini Protean Tetra System (Bio-Rad Laboratories, Hercules, California, USA) for protein separation. The SDS-PAGE was run at a constant 90 volts across the gel for 30 minutes and then 120 volts for 50-60 minutes in 1X running buffer at room temperature.

To compare samples loaded on multiple gels for the same experiment, a WT sample lysate was loaded in all the gels as a common loading control. Post separation, the gels were activated once using UV light through StainFree option for protein gels in ChemiDoc

Imaging System (Bio-Rad Laboratories, Hercules, California, USA) for 45 seconds of automatic exposure time. Post activation, the proteins were transferred to a TransBlot Turbo Mini size 0.2 µm nitrocellulose membrane (Bio-Rad) using BioRad™ Mini Trans-Blot apparatus (Hercules, California, USA). After the protein transfer was completed, the membranes were imaged in the ChemiDoc Imaging System (Bio-Rad Laboratories, Hercules, California, USA) with the StainFree blot option and optimal exposure setting. Subsequently, the membranes were then blocked for an hour in 5% BSA (5% w/v bovine serum albumin [Sigma, SKU A7906]) in Tris-buffer saline with Tween (TBST) buffer (50 mM Tris-HCl, pH 7.6; 150 mM NaCl; 0.1% Tween) on a rocking platform at room temperature.

Membranes were probed with primary antibodies (1:1000 anti-Parp-(9532S) Cell Signaling Technologies – Danvers, Massachusetts, USA); (1:1000 anti-PAR –(83732S) Cell Signaling Technologies – Danvers, Massachusetts, USA) and diluted in 5% TBST overnight at 4ºC with gentle rocking. The membranes were then washed with 5% TBST for 5 minutes and then probed with a horseradish peroxidase (HRP)-conjugated secondary antibody (1:10000 anti-Rabbit IgG – (7074S) Cell Signaling Technologies – Danvers, Massachusetts, USA) for 60 minutes, rocking gently at room temperature. Subsequently, the membranes were washed three times in TBST for visualization using ChemiDoc Imaging systems (Bio-Rad Laboratories, Hercules, California, USA).

For protein detection, blotting membranes were incubated with either Clarity™ (1705061) or Clarity Max™ (1705062) Enhanced Chemiluminescence (ECL) substrate (Bio-Rad Laboratories, Hercules, California, USA) and detected with ChemiDoc Imaging System (Bio-Rad Laboratories, Hercules, California, USA). Multiple exposures were taken

for total protein quantification. FIJI (open source; ImageJ) software was used for rolling ball background correction, band size and intensity quantification.

2.2.4 Membrane stripping

Membranes that require a second round of probing with a different antibody were rinsed with TBST and then incubated for 30 minutes with ~10 ml of stripping buffer with gentle shaking at 37ºC (Restore PLUS Western Blot Stripping Buffer, ThermoScientific) to strip the antibodies off the blot. The membranes were washed with TBST and then blocked with a 5% bovine serum albumin (BSA) buffer for blocking for 1 hour before the membrane was reblotted with a secondary antibody and imaged to confirm loss of signal from the previous antibody.

2.2.5 Grip strength assessment

Forelimb grip strength was measured in the WT and *Parp1*-iMKO mice using conventional grip strength test. Assessments were performed blinded to the operator. Both the groups were measured for grip strength 1 week before tamoxifen treatment (at ~ 8 weeks of age), 2 weeks after the treatment and 1 week prior to sacrifice using a standard grip strength meter (Chantillion DFE, Columbus Instruments). The operator allowed the mouse to grasp the bar mounted on a newton meter with its forelimb. Once the mouse grasped the bar comfortably, the meter was set to zero and the mouse tail gently pulled away until the mouse released the bar. The tension was recorded in grams at the time the mouse released its grasp from the bar. The test was performed 5 times consecutively with a 60 second interval between each trial.

2.2.6 Hanging wire test

The hang time test was performed blinded to the operator to assess muscle function and coordination over time in the WT and *Parp1*-iMKO mice strain. Both the groups were assessed for hang time duration 1 week prior to tamoxifen treatment starting at the age of 8 weeks, 2 weeks post-tamoxifen treatment and 1 week prior to the harvest, as stated earlier in the grip strength assessment section. During the test, the animal will be placed on a wire cage lid (Canus Plastics Inc.) with soft bedding underneath to break the fall. Once the mouse grasps onto the wire cage lid, which is inverted upside down and the latency to fall from the wire cage lid is recorded in seconds and the weight of mice is recorded in grams. The maximum latency to fall of the three trials for each mouse was used for data analysis.

2.2.7 Rotarod test

The rotarod test was performed blinded to the operator to assess neuromuscular function in animal groups treated with or without tamoxifen. Tests were performed in male and female mice at least 1 week before tamoxifen treatment and then 2 weeks after tamoxifen treatment and once prior to sacrifice, as stated in the section above. The rotarod apparatus (IITC life Sciences or Ugo Basile) was used to assess motor coordination, function, and fatigue resistance in WT and *Parp1*-iMKO mice. All mice were placed on the horizontal rod (either 3 cm or 7 cm in diameter) facing the back wall of the lane separated by Plexiglas panels. Once all the mice (5 max) were loaded, the rod begins to rotate accelerating from 0 to 45 rpm over 5 minutes and additional 5 minutes at 45 rpm or until the mouse falls off the rod. The amount of time the mouse can stay on the moving rod is recorded as the outcome for further analysis.

2.2.8 Body composition (EchoMRI)

To determine body mass and body composition (lean mass and fat mass) *Parp1*-iMKO and WT animals were placed into a tube and scanned using EchoMRI (EchoMRI-700 Analyzer). The body composition measurement for both the groups began at 8 weeks of age. The body composition assessments were performed blinded to the operator and the measurement were performed 1 week prior to tamoxifen treatment, 2 weeks post-tamoxifen treatment and then once a week for 8 weeks thereafter.

2.2.9 Indirect calorimetry for measurement of total energy expenditure and food intake quantification

Blinded to the operator, at 9 weeks post-tamoxifen treatment, both WT and *Parp1*-iMKO animals were individually housed in an open-circuit Oxymax chamber of the Comprehensive Laboratory Animal Monitoring System (CLAMS; Columbus Instruments, Columbus, OH, US) for 72 hours. The mice were acclimated for 24 hours in the metabolic chambers at 28-30ºC after which the resting energy metabolism data was recorded for another 48 hours before moving them back to their home cages. Resting energy metabolism such as oxygen consumption (V02), Carbon dioxide production (VC02) were recorded electronically at regular intervals during light and dark cycles. Physical activity was measured using the beam break method throughout the time they were housed in the metabolic chambers. Whenever a mouse movement broke the beam on the X-axis (length of the cage), the movement was recorded as an activity which was then analyzed by looking at the differences in physical activity during the light and dark cycle between the group. Food consumption was measured through the entire duration the mice were housed in the metabolic chambers.

2.2.10 Acute metabolic treadmill test

Acute metabolic treadmill tests were performed blinded to the operator to evaluate the difference in submaximal oxygen consumption rate (V02 max) between WT and *Parp1*-iMKO animals 9–12 weeks after tamoxifen treatment using an open flow respirometry chamber enclosed with plexiglass (Oxymax, Columbus Instruments, Columbus, OH, US) at ~23ºC. Mice were acclimated to the treadmill over a 3-day period. Mice were individually placed in the metabolic chambers after their body mass was recorded. The treadmill test lasted for 95 minutes per mouse with three phases of running. A low amperage (acceptable range of 0.2-0.4 mA) electrical stimulus was applied at the rear end of the running belt for running encouragement. Warm-up phase starting at 0.05 m/s for 5 minutes with the increments of 0.05 m/s for every 5 minutes, thereafter for a total of 10 minutes. Phase-1 starting at 0.15 m/s for 5 minutes with an increase in speed by 0.05 m/s for 5 minutes thereafter for up to 10 minutes. During the last phase of treadmill running the mice ran at an increased speed of 0.03 m/s every 3 minutes until the oxygen consumption levels were saturated and the substrate utilization ratio increased over 1. The V02 peak, RER ratio, running speed, distance travelled, and total running duration were recorded for further analysis.

2.2.11 Cold tolerance test

The cold tolerance test was to assess acute shivering thermogenesis and muscle contraction function in the animal groups between 12-15 weeks post-tamoxifen treatment and were blinded to the operator. Initial body temperature was recorded for both the control and *Parp1*-iMKO group animals by inserting a small, lubricated thermometer into the

animal rectum before placing them in individual cages without food but with water *ad-libitum.* Mice were then placed in the cold room at 4ºC, and the rectal temperature was recorded every hour during a 4-hour period. At the end of the test, mice were placed into placed on a heating pad (37ºC) for 15-20 minutes to bring them back to the normal temperature and provided with free access to food and water. Of note, if the body temperature of any animal dropped below 30ºC, the mouse was removed from the cold room and placed on to a heating pad to a 37ºC heating source for 15-30 minutes to warm the animals.

2.2.12 Statistical analysis

All statistical analysis was performed using GraphPad Prism (version 9.5.1). Differences between the groups were analyzed using 2-way ANOVA with Bonferroni's post-hoc test correcting for the multiple comparisons. qPCR data was analyzed using multiple unpaired t-tests. All results were shown as mean ± SEM. A p value < 0.05 was considered statistically significant.

2.3 Results

2.3.1 Validation of mature muscle-specific ablation of *Parp1*

To determine if *Parp1* was ablated in the mature skeletal muscle of adult mice, *Parp1* mRNA expression levels were examined in the quadriceps of male and female *Parp1*-iMKO mice that were collected two weeks post-tamoxifen treatment. *Parp1* mRNA levels were significantly reduced and did not increase even after 14 weeks post-tamoxifen treatment in both sexes (**Figures 3A.** and **S1A.**). The mRNA expression levels of both PARylating (*Parp2*, and *Tnks* 1/2) and dePARylating enzymes (*Parg*, *Arh3* and *MacroD1/D2*) were not differentially regulated between in *Parp1*-iMKO male and female mice following induction (**Figures 3A.** and **S1A.**). Further, MARylating enzymes (*Parp3* and *Parp4*), sometimes also shown to PARylate, were not altered in *Parp1*-iMKO mice. Western immunoblotting confirmed the corresponding reduction in the PARP1 protein expression in the quadriceps tissue of the *Parp1*-iMKO male mice (**Figures 3B.**). Despite the ablation of PARP1 expression, PARylation levels did not change in the *Parp1*-iMKO male mice (**Figure 3C.**), despite showing a trend for reduction, suggesting that other PARP family enzymes are more active during normal physiological states.

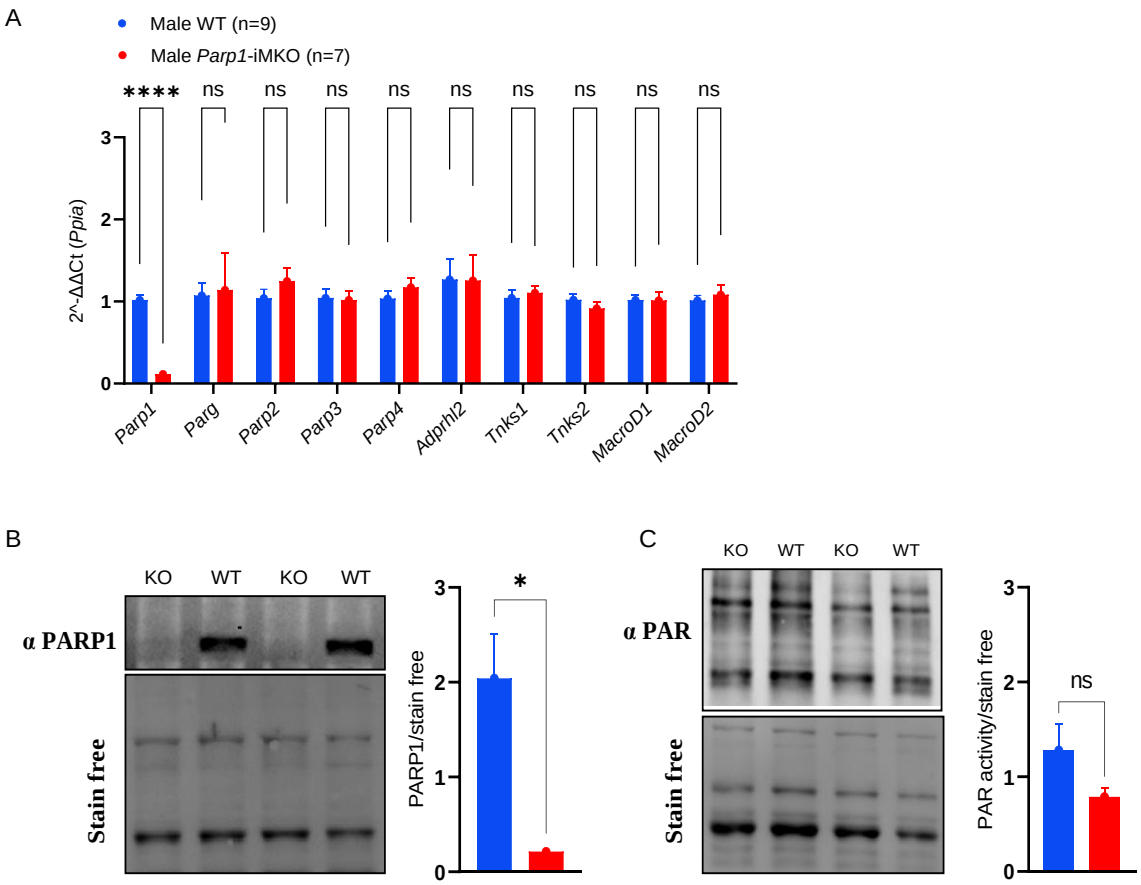

Figure 3 Confirmation of *Parp1* deletion and characterization of mature muscle from male *Parp1*-iMKO mice. (A) mRNA expression levels of *Parp1* and other PAR and MAR synthesizing and degrading enzymes in quadriceps muscle of *Parp1*-iMKO and WT male mice post-tamoxifen treatment (qPCR), (B) PARP1 protein levels and (C) PARylation levels in male WT vs *Parp1*-iMKO. Stats: for qPCR data, unpaired t-tests were performed, graph represent means ± S.E.M for n = 7-9. "*" indicates statistical significance of "p ≤0.05".

2.3.2 *Parp1* deletion does not affect neuromuscular function in male or female mice.

To assess if *Parp1* ablation altered markers of muscle regulation, we examined the expression of myogenic differentiation markers *Myoblast determination protein 1* (*MyoD1*) and *Myogenin factor 4* (*MyoG*), which showed no altered regulation in myogenesis compared to WT controls (**Figures 4A.** and **S1B.**). Furthermore, we looked at

the relative expression levels of Myosin Heavy Chain markers (*Myh*), as indicators of myofiber type. Different muscle fiber types are responsible for distinct contractile functions and are associated with differences in fatigue tolerance and metabolic activity (Emery, 2002). *Myh 3/8* is expressed during early development phase of the muscles, *Myh1/2/4* are expressed in fast-twitch muscle, whereas *Myh7* is expressed in slow-twitch muscle (Dos Santos et al., 2022). The qPCR data demonstrated no consistent change in any of these markers in male or female *Parp1*-iMKO mice, indicating no change in fiber types (**Figure 4A.** and **S1B.**). Furthermore, genes involved in the protein degradation pathway, including autophagic markers such as *Ulk1*, *Atg7*, *Sqstm1*, *Pink1*, *Park2*, and ubiquitin-proteasome degradation markers *Murf1* and *Atrogin1*, were not affected by the deletion of *Parp1* in mature muscle of both male and female mice (**Figures 4B. and S1C.**).

Next, to identify potential physiological differences in skeletal muscle health and neuromuscular function we performed different physical assessments once before the induction of *Parp1* deletion in skeletal muscle through tamoxifen treatment (at 12 weeks of age), 2 weeks after the treatment and once prior to sacrifice. Muscle phenotyping was performed before induction at 8 weeks of age, then again at 2 weeks post-tamoxifen treatment (~14 weeks of age) and once after a month of the second measurement in male and female *Parp1*-iMKO and WT mice. All measures, including mean grip strength with or without correction for body weight (**Figures 4A.**, **S2A.** and **S2D.** and **S2E.**), grip endurance (**Figures 4B.** and **S2B.**) and rotarod performance (**Figures 4C.** and **S2C.**) were similar between *Parp1*-iMKO and WT male or female mice at all time points.

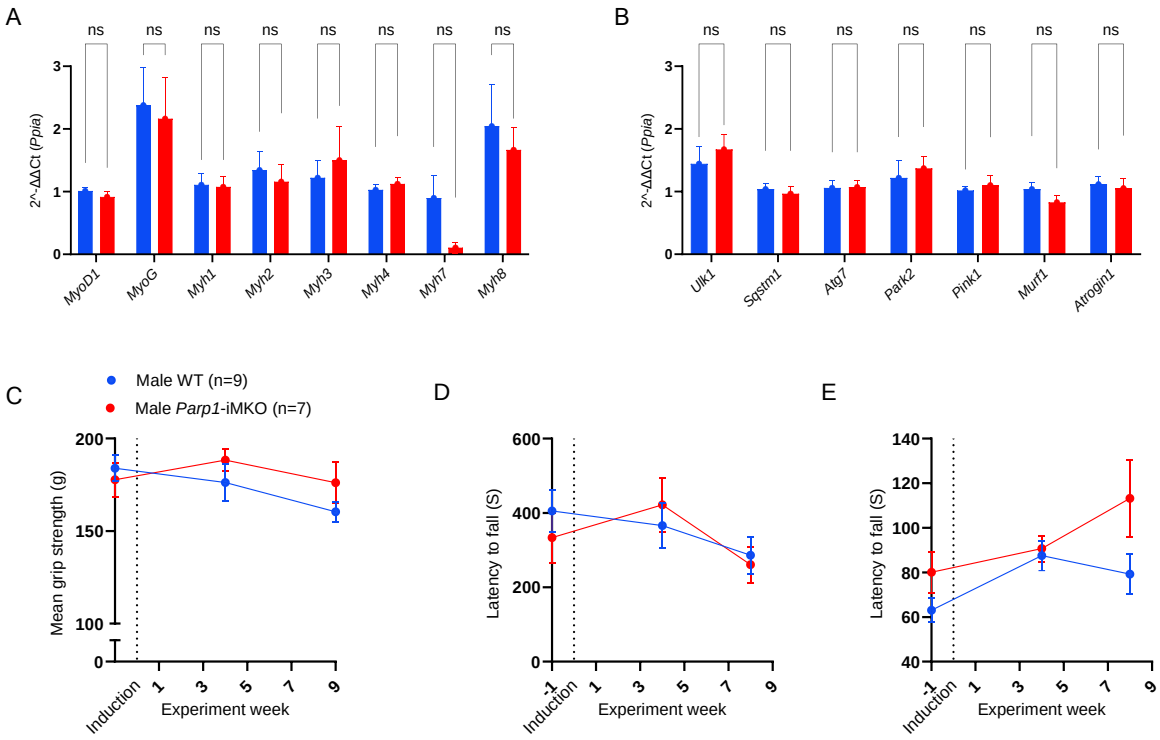

Figure 4. Muscle phenotype was not altered in *Parp1*-iMKO mice. (A) mRNA expression levels for muscle regulation markers (*MyoD1 and MyoG*), myosin heavy chain markers (*Myh1-Myh8*), and (B) autophagy and proteasome-ubiquitination markers in male mice. (C) No changes were observed before or after tamoxifen treatment for grip strength, (D) grip endurance, or (E) neuromuscular function (Rotarod) when comparing *Parp1*-iMKO and WT mice during the entire assessment period. Stats: for qPCR results unpaired t-tests were performed, graph represent means ± S.E.M for n = 7-9. Two-way repeated measures ANOVA with Bonferroni post-hoc analysis for grip strength, grip endurance and rotarod test was performed, graph represent means ± S.E.M for n = 7-9 for males. "*" indicates significance "p≤0.05", "ns" indicates not significant.

2.3.3 *Parp1* ablation does not affect body composition or whole-body metabolism on a regular chow diet in male or female mice

Parp1 ablation has been previously described to alter metabolism in mice on a high fat diet, however, the role of inducible muscle-specific *Parp1* deletion on muscle and whole-body composition and metabolism when on a normal diet has not yet been examined. To investigate the influence of *Parp1* deletion in regulating whole-body

composition we performed EchoMRI and assessed food intake. There was no significant difference in lean or fat mass, bodyweight, or food intake in the *Parp1*-iMKO mice when compared to the control group in either sex (**Figures 5A-F.** and **S3A-E.**). Next, we examined changes in substrate utilization (carbohydrate vs fats) as a fuel source in *Parp1*-iMKO and WT animals. Mean respiratory exchange ratio (RER) between the groups did not differ significantly, suggesting that *Parp1* ablation does not alter metabolism in male or female mice fed a chow diet (**Figures 6A,B.** and **S4A,B.**). Similarly, the mean oxygen consumption rate was not altered (**Figures 6C,D.** and **S4C,D.**). Mean and total ambulatory activity (x-axis) activity of *Parp1*-iMKO mice was not altered compared to WT in either sex (**Figures 6E-G.** and **S4E-G.**). Additionally, we examined the effect of *Parp1* on an acute bout of exercise. The total running distance, speed, and time along with the maximum rate of oxygen consumption (peak VO2) was not altered in the male or female *Parp1*-iMKO mice (**Figures 6H-K.** and **S4H-K.**). Lastly, to assess the influence of *Parp1* expression in skeletal muscle on adaptive thermoregulation, we performed a cold tolerance test which exhibited no changes in male or female *Parp1*-iMKO mice (**Figures 6L.** and **S4L.**).

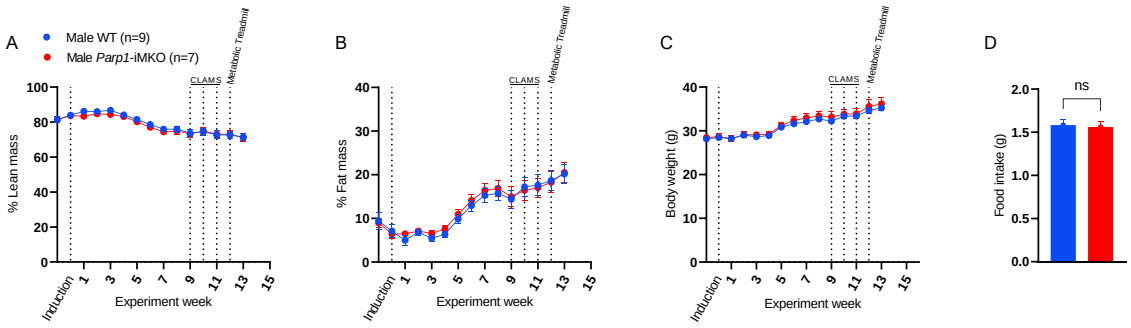

Figure 5. *Parp1*-iMKO male mice exhibited no change in body composition and food intake. *Parp1*-iMKO mice did not significantly differ in their % lean mass (A), % fat mass (B), or body weight (C) when compared to WT. Food consumption remained similar

between groups throughout the 48-hour assessment period. Stats**:** Two-way repeated measures ANOVA with Bonferroni post-hoc analysis, graph represent means ± S.E.M for n = 7-9 for males for body composition analysis. "*" indicates significance "p≤0.05", "ns" indicates not significant. Unpaired t-tests were performed on food intake data, graph represent means ± S.E.M for n = 7-9 for males. "*" indicates statistical significance of "p ≤0.05".

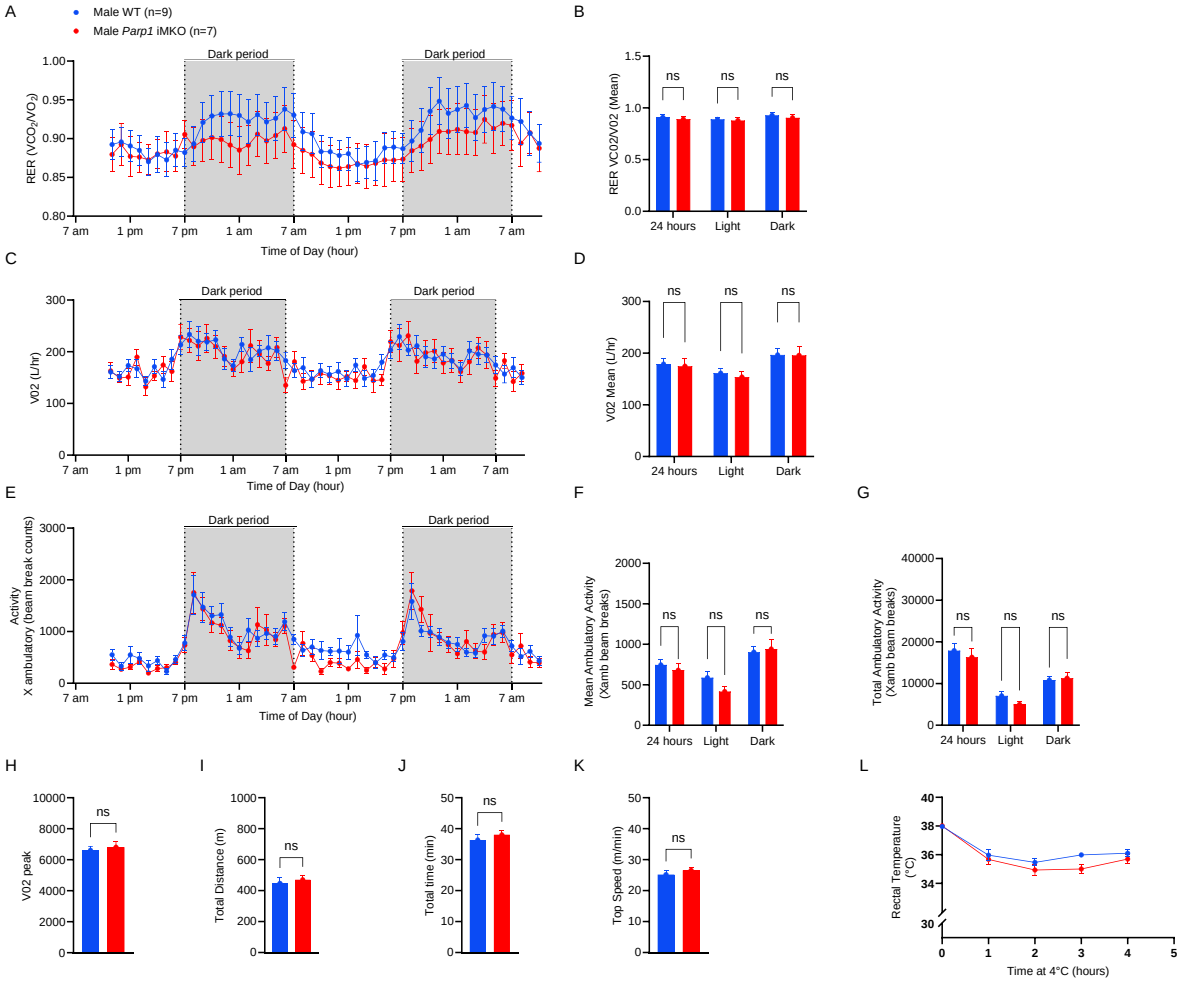

Figure 6. Metabolic activity, locomotion and thermoregulation is not differentially regulated in male *Parp1*-iMKO mice. (A and B) RER ratio did not differ between the groups signifying similar metabolic regulation in the *Parp1*-iMKO compared to the control group. (C and D) oxygen consumption rate was not affected by the deletion of *Parp1* in the *Parp1*-iMKO group in male mice. (E-G) physical activity (x-ambulation) remained the same between the groups throughout the 48-hour assessment period (light and dark phase). No significant difference was observed in the mean and total x-ambulatory motion between the groups. (H-K) acute -test signified no differential regulation in the maximal O2 consumption rate between the groups. Peak V02, total distance, total time and top speed remained comparable between the groups. (L) rectal temperature was measured to assess any difference in thermoregulation between the groups due to cold exposure in male mice

which were insignificant. Stats: Two-way repeated measures ANOVA with Bonferroni post-hoc analysis, graph represent means ± S.E.M for n = 7-9 for males. "*" indicates significance "$p \leq 0.05$", "ns" indicates not significant.

2.4. Discussion

The implications of *Parp1* deletion have been previously examined in the context of metabolism and aging. Piskunova et al. (Piskunova et al., 2008) demonstrated that *Parp1* deletion in 129/SVJ background mice on a standard chow diet had a significant increase in the fatigability at 3 months of age when compared to the control during the hanging wire test. However, this difference diminished over time, and by the age of 17 months, WT and *Parp1* KO had comparable resistance to fatigue. In contrast, the functional assessment tests done in our lab including grip strength, grip endurance and rotarod test identified no significant changes in the muscle strength, fatigue tolerance, and neuromuscular function in the *Parp1*-iMKO mice when compared to the control. However, the difference in the fatigue tolerance shown by (Piskunova et al., 2008) could be attributed to the difference in the mouse strain used. The role of PARP proteins has been previously delineated in several metabolic disorders and linked with chronic inflammation, obesity, and diabetes. However, the results from the *Parp1* whole-body knockout mouse models on high fat diet are ambiguous. Previous studies have demonstrated that *Parp1* inhibition in C57BL6J mice on a high fat diet have leaner mass with higher energy expenditure rate and increased metabolic activity compared to the WT animals mediated through downstream deacetylase activity by SIRT1 and FOXO1 (Bai, Cantó, et al., 2011; Pirinen et al., 2014). In contrast, *Parp1* ablation on a 129/SVJ mouse background led to metabolic dysregulation on high fat diet (Devalaraja-Narashimha & Padanilam, 2010). In contrast to these studies, we first compared body composition between the *Parp1*-iMKO and WT groups on a regular chow

diet. The body composition analysis from EchoMRI did not show any differences in the lean mass, fat mass or body weight of either male or female mice, suggesting that muscle-specific *Parp1* deletion does not affect whole-body metabolism in healthy adult mice. These findings agree with other *Parp1* KO and PARP1 pharmaceutical inhibition studies in mice fed standard chow diets (Lehmann et al., 2015; Pirinen et al., 2014). In line with these findings, the respiratory exchange ratio, maximal oxygen consumption rate and locomotion remained similar between the WT and *Parp1*-iMKO mice. In conclusion, the loss of *Parp1* in mature muscle of healthy mice does not affect whole-body metabolism under normal physiological conditions. In future studies we will examine the effects of a high fat diet on *Parp1*-iMKO mice in skeletal muscle metabolism and on whole-body metabolism, as has been demonstrated in previous studies in *Parp1* null mice or when mice are treated with PARP1 inhibitor (Bai, Cantó, et al., 2011; de Murcia et al., 1997).

2.5 Supplementary data

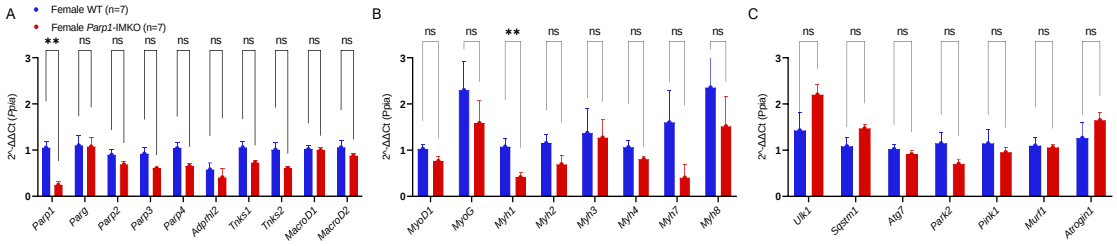

Supplementary Figure 1. Confirmation of *Parp1* deletion and characterization of mature muscle from *Parp1*-iMKO female mice. (A) mRNA expression levels of *Parp1* and other PAR and MAR synthesizing and degrading enzymes in quadriceps muscle of KO and WT female mice post-tamoxifen treatment (qPCR), (B and C) mRNA levels are also shown for muscle regulation markers (*MyoD1* and *MyoG*) and myosin heavy chain markers (*Myh1-Myh8*) as well as markers for protein degradation pathway in female mice. Stats: for qPCR, unpaired t-tests were performed, graph represent means ± S.E.M for n = 7. "*" indicates statistical significance of "p ≤0.05".

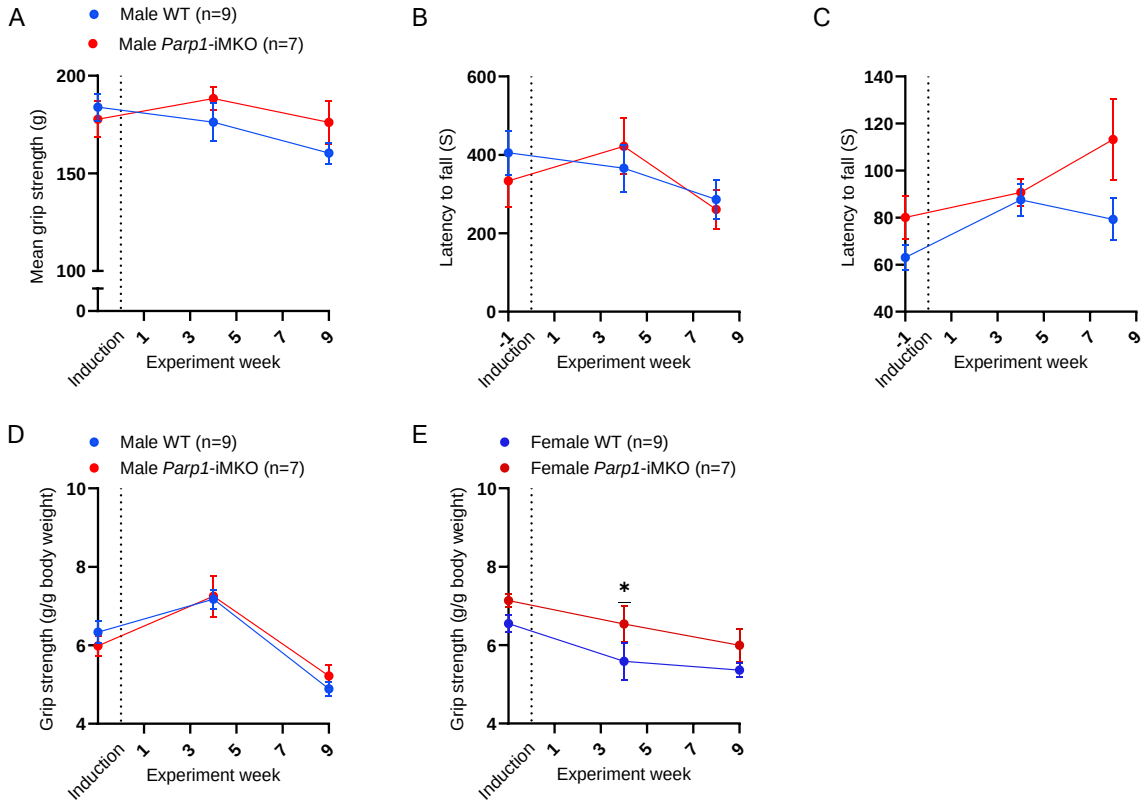

Supplementary Figure 2. Neuromuscular function was not altered in female *Parp1*-iMKO mice. (A) no changes were observed before or after tamoxifen treatment for grip

strength, grip endurance (B), or neuromuscular function (C) when comparing *Parp1*-iMKO and WT female mice during the entire assessment period. (D) no changes were observed before or after tamoxifen treatment for grip strength (corrected to body weight) in male *Parp1*-iMKO mice compared to the WT when corrected for body weight, (E) female *Parp1*-iMKO mice showed significant increase in the grip strength compared to WT two weeks post-tamoxifen treatment, when corrected for body weight, which diminished over time. Stats: Two-way repeated measures ANOVA with Bonferroni post-hoc analysis, graph represent means ± S.E.M for n = 7-9. "*" indicates significance "p≤0.05", "ns" indicates not significant.

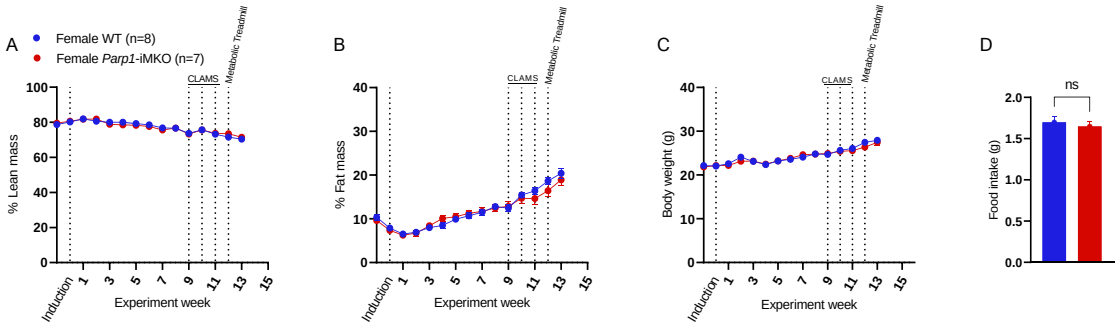

Supplementary Figure 3. *Parp1*-iMKO female mice exhibited similar body composition and food intake as WT mice. Female *Parp1*-iMKO mice did not differ in their % lean mass (A), % fat mass (B), or body weight (C) when compared to WT. Food consumption remained similar between groups throughout the 48-hour assessment period. Stats**:** Two-way repeated measures ANOVA with Bonferroni post-hoc analysis, graph represent means ± S.E.M for n = 7-8 for body composition analysis. "*" indicates significance "p≤0.05", "ns" indicates not significant. Unpaired t-tests were performed on food intake data, graph represent means ± S.E.M for n = 7-9. "*" indicates statistical significance of "p ≤0.05".

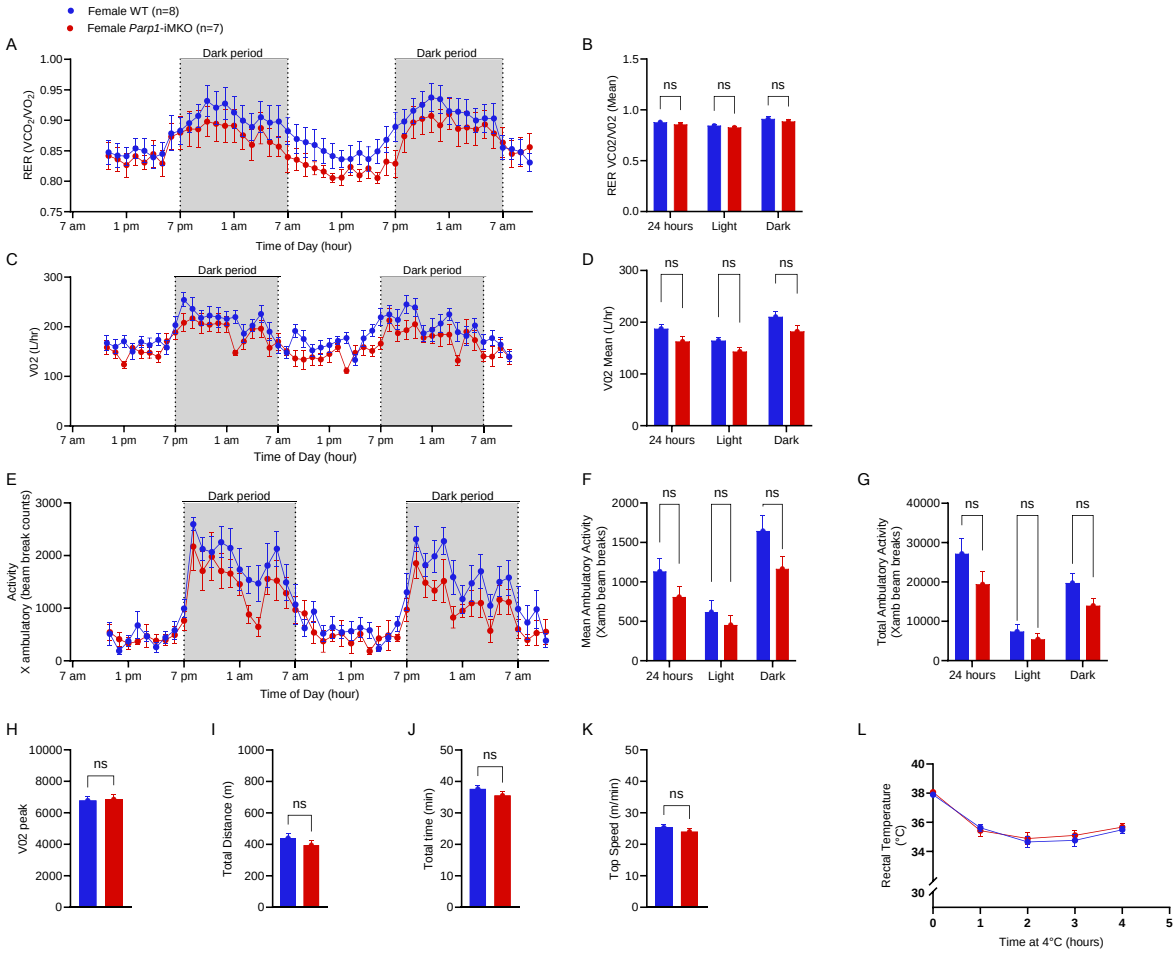

Supplementary Figure 4. Metabolic activity, locomotion and thermoregulation is not differentially regulated in *Parp1*-iMKO female mice. (A and B) RER ratio did not differ between the groups signifying similar metabolic regulation in the *Parp1*-iMKO compared to the control group. (C and D) oxygen consumption rate was not affected by the deletion of *Parp1* in the *Parp1*-iMKO group in female mice. (E-G) physical activity (x-ambulation) remained the same between the groups throughout the 48-hour assessment period (light and dark phase). No significant difference was observed in the mean and total x-ambulatory motion between the groups. (H-K) acute metabolic treadmill test signified no differential regulation in the maximal O2 consumption rate between the groups. Peak V02, total distance, total time and top speed remained comparable between the groups. (L) rectal temperature was measured to assess any difference in thermoregulation between the groups due to cold exposure in female mice which were insignificant. Stats: Two-way repeated measures ANOVA with Bonferroni post-hoc analysis, graph represent means ± S.E.M for n = 7-9 for females. "*" indicates significance "$p \leq 0.05$", "ns" indicates not significant.

Chapter III: Role of PARG in Mature Skeletal Muscle Mass, and Function in Healthy Mice

3.1 Introduction

Poly-ADP-ribosylation (PARylation) is a transient post-translational modification, dynamically regulated by two distinct groups of enzymes working sequentially. This ADP-ribose (ADPr)-mediated modification of target proteins is required for various metabolic and cellular processes such as DNA damage repair, chromosomal integrity, mRNA stability, cell fate and function, transcriptional regulation, to name a few (Lüscher et al., 2018). Poly(ADP-ribose) Polymerases (PARPs) facilitate the addition of ADPr polymers to target proteins which is concomitantly regulated by PAR degrading enzymes such as Poly(ADP-ribose) glycohydrolase (PARG), ADP-ribosyl hydrolases (ARH1/ARH3), or macrodomain containing enzymes i.e., MacroD1 and MacroD2, Terminal ADP-ribose Glycohydrolase 1 (TARG1), and the NUDIX family of hydrolases to maintain PAR metabolism and homeostasis of the target proteins (Krishna kumar & Kraus, 2010; Lüscher et al., 2018). In the past 50 years, the role of PARPs in vivo has been studied extensively, while research on PAR degrading enzymes has been largely overlooked.

The majority of cellular PARylation is catalyzed by PARP1 (Shieh et al., 1998). PARP1 modifies the target site by attaching negatively charged PAR chains at varying lengths up to 200 units and branching at every 20-50 ADPr units, while consuming NAD+ as a required co-substrate (D'Amours et al., 1999; Tanaka et al., 1977). PAR chains are readily hydrolyzed from PARP1 and other nuclear proteins within 1-6 mins by PARG in a process commonly termed dePARylation (Alvarez-Gonzalez & Althaus, 1989). A steady state is achieved when PAR chains are catabolized mostly into free ADPr polymers or

monomers, terminating the signaling associated with PARylation. PARG is responsible for catabolizing the majority of PAR chains from substrate proteins, however, it is not equipped to hydrolyze the ester bond between the most proximal ADPr subunit and the substrate protein. This terminal ADPr unit is hydrolyzed by macro-domain containing enzymes such as TARG1, MacroD1 and MacroD2, in a process termed MARylation.

PARG is constitutively active under normal physiological conditions without physiological stress and hydrolyzes PAR chains through its exo-and endo-glycosidic activity from the substrate protein (BRAUN et al., 1994; O'Sullivan et al., 2019). PARG knockdown in mice, through targeted heterozygous deletion of exons 2 and 3, were viable and fertile, but displayed impaired PAR metabolism and were susceptible to DNA alkylating agents, ionizing radiation, endotoxin shock as well as streptozotocin-induced diabetes, whereas *Parg* null mice are embryonically lethal (Cortes et al., 2004; Koh et al., 2004).

Skeletal muscle is an important organ required for locomotion and storage and regulation of glucose (Hargreaves & Spriet, 2020). It is also involved in modulating whole-body metabolism and overall health. Previously, loss of skeletal muscle (sarcopenia) has been linked with ageing and under pathophysiological conditions (cachexia and DMD) causes mortality (Campelj et al., 2020; Chacon-Cabrera et al., 2017; Pirinen et al., 2014; D. Ryu et al., 2016). The role of PARylation has been previously looked at in the context of muscle function in ageing and shown to be dysregulated at older ages through PARP1 hyperactivation and NAD+ depletion (Cobley et al., 2013). Additionally, elevated PARylation has been implicated in the reduction in NAD+ levels and correlated to pleiotropic effects, such as inflammation, in the mdx mouse model of Duchenne Muscular

Dystrophy (DMD) (D. Ryu et al., 2016). Interestingly, pharmacological inhibition of systemic PARP1-directed PARylation improves fitness and mitochondrial function in skeletal muscle (Pirinen et al., 2014). However, compared to PARP1, the role of PARG in muscle or the action of dePARylation has been mostly overlooked. We therefore set out to delineate the role of PARG in the regulation of skeletal muscle metabolism, and its potential systemic implications, under normal physiological conditions using inducible mature skeletal muscle-specific *Parg* knockout (*Parg*-iMKO) mice.

3.2 Materials and Methods

3.2.1 Animal model

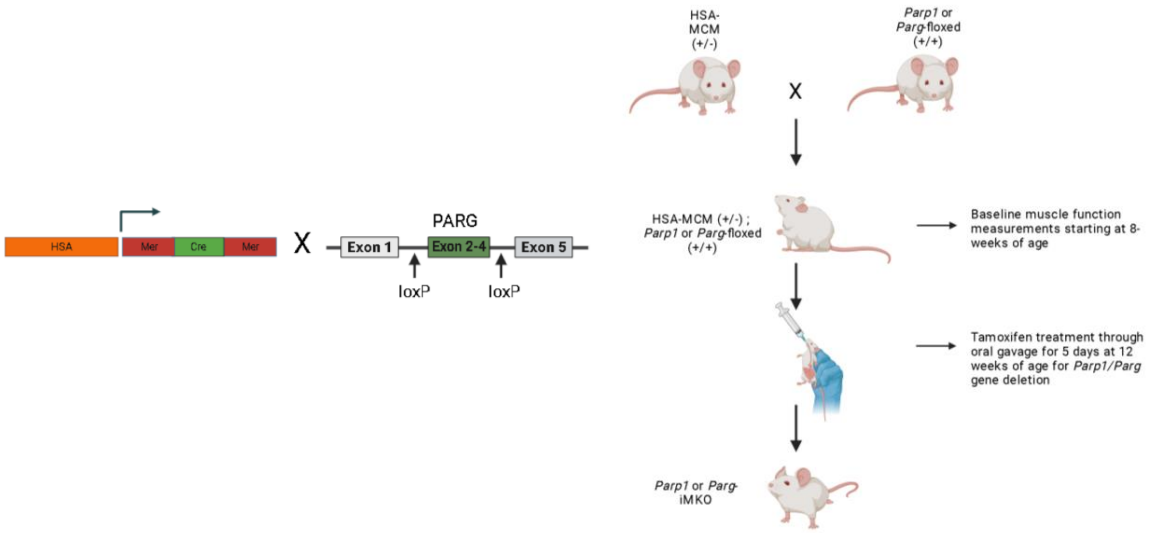

Figure 1. Schematic illustrating the generation of the *Parg*-iMKO mice model. Created with BioRender.com

3.2.1.1 Parg-inducible muscle knockout model

Parg^{loxp} mice were designed and generated with the help of the Canadian Mutant Mouse Repository (CMMR). These mice harbor loxP sites flanking exon 2 to 4 of *Parg* on a C57BL/6N background (C57BL/6N- *Parg*$^{tm2c(KOMP)Mbp/TCP)}$. Human skeletal actin -mer-cre-mer mice (HSA-MCM) (Stock No: 025750) mice were obtained from Jackson Laboratory which express cre-recombinase enzyme following induction with tamoxifen. This is possible given that the HSA promoter driven cre-recombinase sequence was flanked by the Mutated Estrogen Receptor (MER) ligand binding domain on both C- and N-terminal (mer-cre-mer), which is bound to Heat Shock Protein-90 (HSP-90) in the cytoplasm in the absence of tamoxifen. HSA-MCM were bred with *Parg*^{loxP} mice to obtain skeletal muscle-specific *Parg*-iMKO mice in the F2 generation (*Parg*-iMKO); Tamoxifen induction was given at 10 µl/gm bodyweight with a dose range not exceeding 200 mg/kg body weight mixed with corn oil as a solution and administered through oral gavage to both WT and *Parg*-iMKO cohorts. Tamoxifen-corn oil solution was administered for 5 days at a dose range described above to induce gene deletion in the mice at 12 weeks of age. Mature muscle-specific *Parg* deletion in *Parg*-iMKO was confirmed post two weeks of tamoxifen treatment using qPCR. Data was normalized to *Peptidylprolyl isomerase A* (*Ppia*) gene expression and displayed as fold change over control (*Parg*-loxP$^{+/+}$, Cre $^{-/-}$ mice or *Parg*-loxP$^{-/-}$, Cre $^{+/-}$ mice).

3.2.1.2 Mouse phenotyping

Please refer to the Chapter 2.2 (Materials and Methods) above for the description of functional assessment, and experimental timeline, performed on the *Parg*-iMKO mice model, as performed previously while characterizing the *Parp1*-iMKO mouse cohort. All functional assessments were performed blinded.

3.2.2 RNA isolation and quantitative real-time polymerase chain reaction (qPCR)

For total RNA Isolation, at least 13 milligrams of flash frozen quadriceps were crushed and added in 1ml of TRIzol® reagent (Invitrogen) to isolate high-quality RNA. Samples were homogenized in a 2 ml reinforced bead mill tubes (FisherScientific cat#12-340-162) with 3x2.8mm ceramic beads (FisherScientific cat#19-340-162) in a Bead Mill homogenizer (FisherScientific cat#15-340-163) for three cycles at 2.09 m/s for 40 seconds with 20 seconds of rest in between the cycles. The aqueous phase, obtained after TRIzol® (Invitrogen) addition and homogenization, was then loaded on to a commercial RNA purification column. Total RNA was extracted according to the manufacturer's protocol. EZ-10 DNAaway RNA Miniprep Kit - BS88136 (Bio Basic Canada Inc, Markham, Ontario, Canada). RNA yield was quantified by measuring the absorption at 260/280 nm and 260/230 nm using Nanodrop spectrophotometer-2000 (ThermoFisher Scientific).

cDNA synthesis was transcribed from the isolated total RNA using ProtoScript II Reverse Transcriptase Kit (NEB #M0368). The diluted cDNA was used to was prepared with SYBR Green (Roche). The quantitative expression of the selected genes was analyzed by LightCycler 480 System (Roche). Data was normalized using the housekeeping gene

Peptidylprolyl isomerase A (*Ppia*). The primer pairs used for quantitative real-time PCR analysis are as follows:

Table 2. List of primers for qPCR

Gene	Forward primer	Reverse primer
Parg	GGGGACTCCGCTACCAAAG	ACAGACTGGCGAGATCCACT
Adprhl2	AGGCACACGATACCGTCAG	CATGTCCACCTCGTCGAAGG
MacroD1	CCTCCACCGACTGGAAGGA	CCCCACGGTACAGGGAGATT
MacroD2	ACCTTAGAGGAGAGACGCAAA	GTGGTGCTTCCTGAGTATTTTCT
Parp1	GGCAGCCTGATGTTGAGGT	GCGTACTCCGCTAAAAAGTCAC
Parp2	CACAGCTTGGTGACTTGTTCT	ACTCAGGCTTCAAAGTTTCCTC
MyoD1	CGGGACATAGACTTGACAGGC	TCGAAACACGGGTCATCATAGA
MyoG	GCAGGCTCAAGAAAGTGAATGA	GTTGGGACCGAACTCCAGT
Myh1	CGGAGTCAGGTGAATACTCACG	GAGCATGAGCTAAGGCACTCT
Myh7	AGACTGTCAACACTAAGAGGGT	TGCCCCAAAATGGATTCGGAT
Atrogin1	ACACATCCTTATGCACACTGG	TCTCCATCCGATACACCCACA
MuRF1	CCAGGCTGCGAATCCCTAC	ATTTTCTCGTCTTCGTGTTCCTT
Map1lc3B	TTATAGAGCGATACAAGGGGGAG	CTCGTACACTTCGGAGATGGG
Sqstm1	ATGTGGAACATGGAGGGAAGA	CCCCGATGTCGTAATTCTTGG

3.2.3 Muscle explant experiment

3.2.3.1 Materials and reagents

Dimethylsulfoxide (DMSO) (Fisher Scientific; cat# BP231-100), 1mM cisplatin **(**MilliporeSigma**;** cat# P4394-100MG),HEPES Krebs Ringer bicarbonate (HKRB) buffer (MilliporeSigma; cat# K4002-10X1L), RIPA lysis buffer (50 mM Tris HCl pH 8, 150 mM NaCl, 1% Triton X-100, 0.5% Sodium Deoxycholate, 0.1% SDS, Protease Inhibitor Cocktail (cOmplete Mini by Roche), Phosphatase Inhibitor (phosStop by Roche), 2.8 mm ceramic beads (Fisher Scientific 19-340-162), 2 ml reinforced bead mill homogenizing tubes (FisherScientific cat#12-340-162).

3.2.3.2 Muscle explant PARylation activity procedure

All the chemicals and reagents were thawed in a 37°C water bath. Working solutions were prepared in a laminar hood. Quadriceps or TA tissues from both the legs were excised from WT and *Parg*-iMKO mice and were then cut into 12 small pieces. Approximately 10 mg of these tissue explants were incubated in 450 µl of HKRB. 0.1% DMSO in HKRB buffer was used as a vehicle (1ul of DMSO in 999 µl of HKRB). Tissue explants were incubated with shaking at 37°C for 30 mins, both the WT and *Parg*-iMKO tissue explants were treated with vehicle or cisplatin dissolved in HKRB solution for a final concentration of 1 mM and incubated for 30 mins on the shaking incubator at 37°C. After completion of the incubation period, tissues were pipetted out into 2 ml reinforced bead mill tubes (FisherScientific cat#12-340-162) with 3x2.8mm ceramic beads (FisherScientific cat#19-340-162), along with RIPA lysis buffer composed of 50 mM Tris HCl pH 8, 150 mM NaCl, 1% Triton X-100, 0.5% Sodium Deoxycholate, 0.1% SDS, Protease Inhibitor Cocktail (cOmplete Mini by Roche), Phosphatase Inhibitor (phosStop by Roche), PARP1 inhibitor (1 µM Olaparib final concentration), and PARG inhibitor (100 µM tannic acid final concentration) at 10 ul per mg of tissue (~30-40 µl) per sample. Explant tissues were homogenized using bead mill homogenizer for three cycles at 2.09 m/s for 40 seconds with 20 seconds of rest in between the cycles. The explant tissues were then processed for western blotting following the standard western blotting procedure post-homogenization step as mentioned below.

3.2.4 Western blotting

Western immunoblots were completed using standard procedures with muscles collected from WT and *Parg*-iMKO mice post-dissection in small microcentrifuge tubes and flash frozen in liquid nitrogen and stored at -80ºC or from muscle explants as described above.

For tissue homogenization, quadriceps (Quads) or tibialis anterior (TA) tissues were sandwiched in between 7-8 aluminum sheets on both ends and pulverized over an aluminum block with a hammer. Of note, both the hammer and the aluminum block were pre-cooled with liquid nitrogen. At least 17 mgs of tissue were collected in a 2 ml reinforced bead mill homogenizer tubes (FisherScientific cat#12-340-162) and stored at -80°C. Subsequently the tissues were thawed and three 2.8 mm ceramic beads (FisherScientific 19-340-162) were added along with RIPA lysis buffer (described above for Muscle Explant PARylation activity procedure). Tissues were homogenized using bead mill homogenizer for three cycles at 2.09 m/s for 40 seconds with 20 seconds of rest in between the cycles. Post-homogenization, the tissues were centrifuged twice at 16,000g for 10 minutes at 4 ºC and the supernatant was collected after each spin in a freshly labelled microcentrifuge tube. Protein concentration was determined using DC protein assay kit from BioRad (Bio-Rad Laboratories, Hercules, California, USA) and the absorbance was measured using the POLARstar Omega plate reader (BMG Labtech).

Lysates were diluted to 1 μg/μL with 4x Laemmli buffer (Bio-Rad Cat# 1610737) supplemented with 10% β-mercaptoethanol (Fisher Bioreagents, BP176-100) and boiled for 5 minutes at 95ºC. Equal volume of lysates was loaded at 10-20 μg in 1.5 mm 10% SDS-PAGE using TGX Stain-free FastCast Acrylamide Kit (Bio-Rad Cat# 1610173) and

Bio-Rad™ Mini Protean Tetra System (Bio-Rad Laboratories, Hercules, California, USA) for protein separation. The SDS-PAGE was run at a constant 90 volts across the gel for 30 minutes and then 120 volts for 50-60 minutes in 1X running buffer at room temperature.

To compare samples loaded on multiple gels for the same experiment, a WT sample lysate was loaded in all the gels as a common loading control. Post-separation, the gels were activated once using UV light using the StainFree option for protein gels in ChemiDoc Imaging System (Bio-Rad Laboratories, Hercules, California, USA) for 45 seconds of automatic exposure time. Post-activation, the proteins were transferred to a TransBlot Turbo Mini size 0.2µm nitrocellulose membrane (Bio-Rad) using the BioRad™ Mini Trans-Blot apparatus (Hercules, California, USA). After the protein transfer was completed, the membranes were imaged in the ChemiDoc Imaging System (Bio-Rad Laboratories, Hercules, California, USA) with the StainFree blot option and optimal exposure setting. Subsequently, the membranes were then blocked for an hour in 5% BSA (5% w/v bovine serum albumin [Sigma, SKU A7906]) in TBST buffer (50 mM Tris-HCl, pH 7.6; 150 mM NaCl; 0.1% Tween) on a rocking platform at room temperature.

Membranes were probed with primary antibodies (1:1000 anti-Parg-(sc-398563) mouse monoclonal antibody, Santa Cruz Biotechnology, Inc– Dallas, Texas, USA), (1:1000 anti-PAR –(83732S) Cell Signaling Technologies – Danvers, Massachusetts, USA), diluted in 5% TBST overnight at 4ºC with gentle rocking. The membranes were then washed with 5% TBST for 5 minutes and then probed with a HRP (horseradish peroxidase)-conjugated secondary antibody (1:10000 anti-Rabbit IgG – (7074S) Cell Signaling Technologies – Danvers, Massachusetts, USA) for 60 minutes rocking gently at room temperature. Subsequently, the membranes were washed three times in TBST for

visualization using ChemiDoc Imaging systems (Bio-Rad Laboratories, Hercules, California, USA).

For protein detection, membranes were incubated with either Clarity™ (1705061) or Clarity Max™ (1705062) Enhanced Chemiluminescence (ECL) substrate (Bio-Rad Laboratories, Hercules, California, USA) and detected with ChemiDoc Imaging System (Bio-Rad Laboratories, Hercules, California, USA). Multiple exposures were taken for total protein quantification. FIJI (open source; ImageJ) software was used for rolling ball background correction, band size and intensity quantification.

3.2.5 Statistical analysis

All statistical analysis was performed using GraphPad Prism (version 9.5.1). Differences between the groups were analyzed using 2-way ANOVA with Bonferroni's post-hoc test correcting for the multiple comparisons. qPCR data was analyzed using multiple unpaired t-tests. All results were shown as mean ± SEM. A p value < 0.05 was considered statistically significant.

3.3 Results

3.3.1 *Parg* deletion in mature skeletal muscle does not alter expression of (de)PARylating enzymes in male or female mice

At 12 weeks of age, WT and *Parg*-iMKO mice from the first cohort were orally gavaged for 5 days with tamoxifen. Two weeks after tamoxifen treatment, skeletal muscle tissues were harvested for confirmation of *Parg* deletion. *Parg* mRNA levels were significantly reduced in in the quadriceps of *Parg*-iMKO mice compared to the WT animals in both male and female mice. (**Figures 2A.** and **S1A.**). We also assessed expression levels of other known hydrolases and macrodomain containing hydrolases (*Arh3*, *MacroD1* and *MacroD2*) that may compensate for the lack of PARG activity and observed no differences in *Parg*-iMKO male and female mice (**Figures 2A.** and **S1A.**). Similarly, *Parp1* and *Parp2* transcript levels remained comparable between the *Parg*-iMKO and WT animals of both sexes (**Figures 2A.** and **S1A.**). This contrasts with previous studies in HeLa cells that have shown reduced *Parp1* expression after *Parg* depletion (UCHIUMI et al., 2013). Finally, our attempts to validate PARG deletion in *Parg*-iMKO mice failed due to the lack of a suitable antibody (**Supplementary Figure 1B**.), so we performed an *ex-vivo* PARylation activity experiment to confirm the lack of dePARylation activity in *Parg*-iMKO mouse muscle. To this end, we excised the quadriceps from male *Parg*-iMKO and WT mice and treated these explant pieces with cisplatin to induce DNA damage and PAR accumulation. The treatment with cisplatin showed higher levels of PARylation in the *Parg*-iMKO mice compared to the control (**Figures 2B.**), confirming the loss of PARG activity and PAR accumulation.

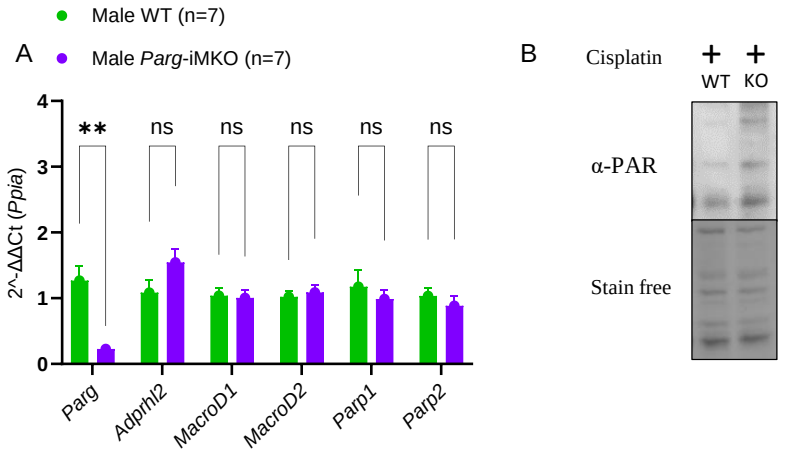

Figure 2 Confirmation of *Parg* ablation in male *Parg*-iMKO mice: (A) *Parg* mRNA expression levels post-tamoxifen induction, and mRNA expression levels of *Parp*s and other hydrolases, (B) western blot for PARylation activity in the WT and *Parg*-iMKO from quadriceps tissues treated with vehicle or cisplatin. Stats: for qPCR, unpaired t-tests were performed, graph represent means ± S.E.M for n = 7-12. "*" indicates statistical significance of "p<0.05."

3.3.2 *Parg* ablation does not affect muscle structure, function, or strength in male or female mice

Previous studies have suggested the importance of PARylation in muscle health, we therefore investigated if the ablation of *Parg* in mature mice would affect markers of muscle regulation, including *myoblast determination protein1* (*MyoD1*) and *Myogenin factor 4* (*MyoG*) (Matteini et al., 2020; Tan et al., 2023a). Here we show no significant differential regulation of *MyoD1* or *MyoG* in *Parg*-iMKO mice of either sex (**Figures 3A.** and **S2A.)**. Additionally, the relative expression levels of fast-twitch and slow-twitch Myosin Heavy Chain markers (*Myh1* and *Myh7*, respectively), as potential indicators of muscle fiber type switching, did not change in the Parg-iMKO male and female animal groups (**Figures 3A.** and **S2A.**). Furthermore, genes involved in the upregulation of the ubiquitin-proteasome degradation pathway during muscle atrophy (*Murf1* and *Atrogin1*)

and autophagic pathway (*Map1lc3b* and *Sqstm1*) were not affected by the deletion of *Parg* in mature muscle of both male and female mice (**Figures 3B.** and **S2B.**).

Next, we performed mouse phenotyping beginning at 8 weeks of age, before tamoxifen treatment, for both male and female animals from the control and *Parg*-iMKO cohorts. Each group was subjected to physical assessments starting at baseline. The first grip strength, grip endurance and rotarod measurements were taken at 8 weeks of age, *Parg* deletion was induced at 12 weeks of age, the second measurement for all the three functional tests were taken 2 weeks after tamoxifen treatment (at ~14 weeks of age), the last measurements were taken approximately one month after the second measurement in both male and female *Parg*-iMKO and WT mice. Mean grip strength showed a trend for reduced grip strength in the second and third measurements post-tamoxifen in male *Parg*-iMKO mice ($p=0.0572$ and $p=0.087$, respectively), but not in female *Parg*-iMKO mice (**Figures 3C.** and **S2C.**). Grip endurance (**Figures 3D.** and **S2D.**) and rotarod performance (**Figures 3E.** and **S2E.**) were similar between *Parg*-iMKO and WT mice for both sexes at all time points without correction for body weight. Furthermore, grip strength did not change significantly when adjusted to body weight between the groups in both male and female *Parg*-iMKO mice compared to the control (**Figures S2F. and S2G.**).

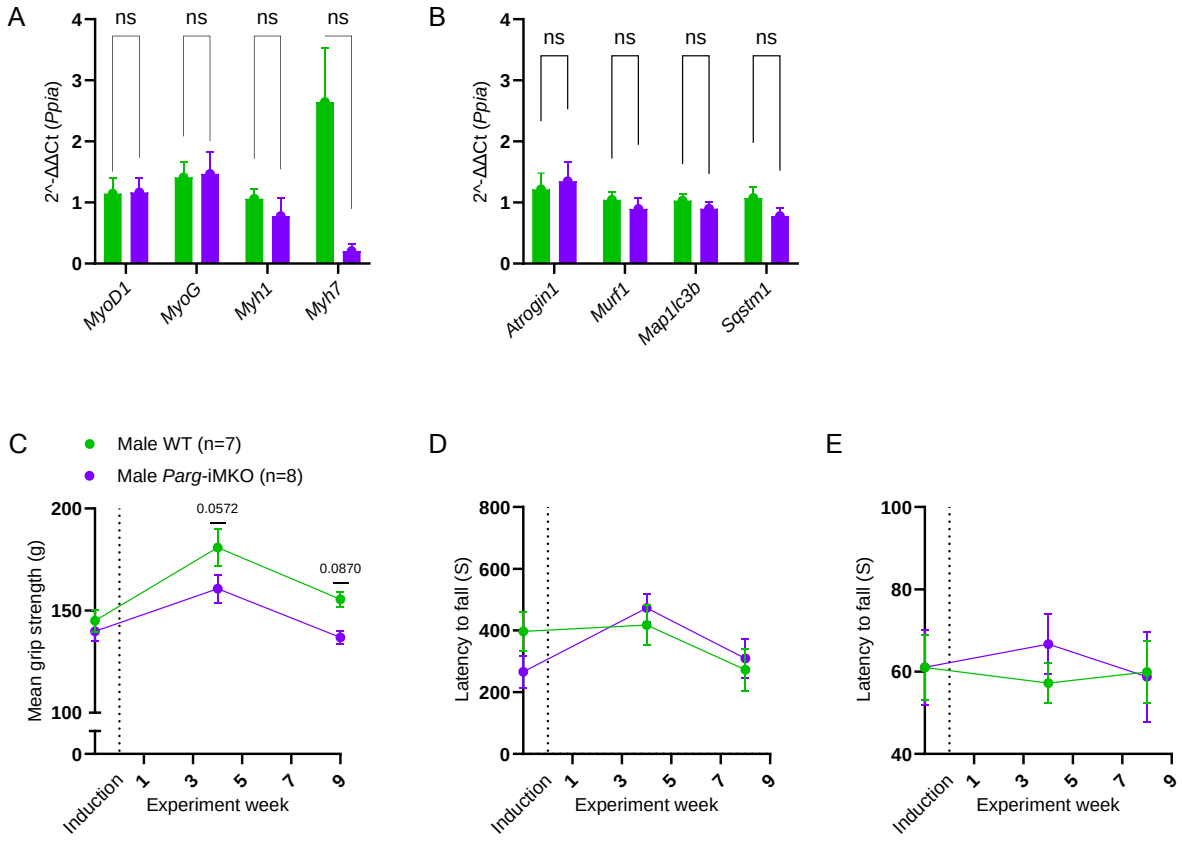

Figure 3. Muscle health and function was not altered in *P*arg-iMKO male mice: (A and B) markers for muscle regulation, and ubiquitination and autophagic markers, respectively. (C) trend in decreased grip strength was observed in the Parg-iMKO male mice, post 2 weeks tamoxifen treatment. (D) grip endurance, (E) or neuromuscular function between the groups did not significantly differ during the entire assessment period in both male. Stats for qPCR, unpaired t-tests were performed, graph represent means ± S.E.M for n = 7-12. Two-way repeated measures ANOVA with Bonferroni post-hoc analysis was used for functional assessment tests, graph represent means ± S.E.M for n = 7-8 for males. "*" indicates significance "p≤0.05".

3.3.3 *Parg* deletion affects energy intake, but not body composition, muscle, or fat mass in male mice

Parp1 germline deletion or pharmaceutical inhibition has been previously shown to improve metabolism in mice on a high fat diet (Bai, Cantó, et al., 2011; Pirinen et al., 2014). Since *Parp1* and *Parg* tightly regulate PAR metabolism in concert, we wanted to

identify whether *Parg* deletion would affect the regulation of skeletal muscle and whole-body metabolism. We measured body composition weekly beginning at 8 weeks of age with no significant differences in *Parg*-iMKO lean or fat mass, or overall bodyweight, compared to the control groups of both sexes before or after tamoxifen induction (**Figures 4A-C.** and **S3A-C.**). Interestingly, despite the lack of change in body composition, the food intake measured for 72 hours between the 9th and 10th week after tamoxifen treatment was found to be higher in the *Parg*-iMKO compared to the WT for both the sexes. (**Figures 4D.** and **S3D.**).

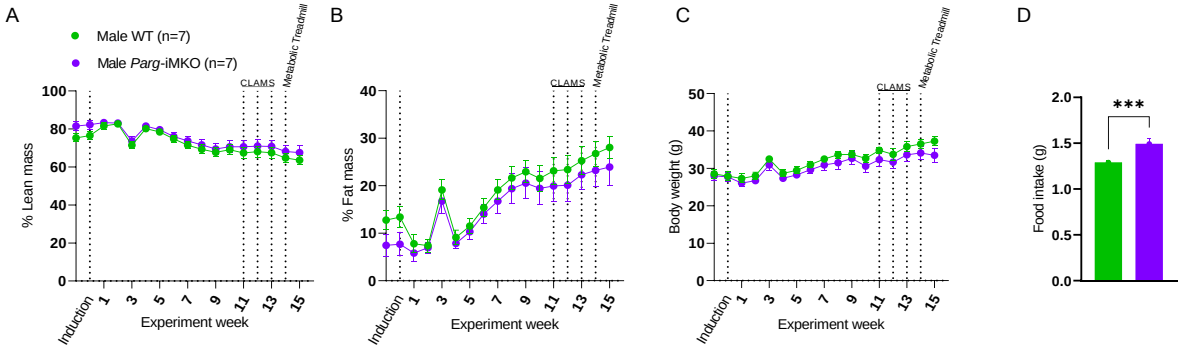

Figure 4. Body composition did not change despite an increase in food intake in male *Parg*-iMKO mice: *Parg*-iMKO mice did not differ in their % lean mass (A), % fat mass (B), or body weight (C) when compared between the groups. *Parg*-iMKO consumed more food compared to the control animals (D). Stats: Two-way repeated measures ANOVA with Bonferroni post-hoc analysis, graph represent means ± S.E.M for n = 7-9 for males. For body composition analysis "*" indicates significance "p≤0.05", "ns" indicates not significant. Unpaired t-tests were performed on food intake data, graph represent means ± S.E.M for n = 7-9 for males. "*" indicates statistical significance of "p ≤0.05".

3.3.4 Substrate utilization, physical activity, acute exercise capacity and thermoregulation are not differentially regulated in *Parg*-iMKO mice

We assessed the fuel utilization and total energy expenditure in *Parg*-iMKO mice by calculating the mean respiratory exchange ratio (RER) for 48 hours after an acclimation

period of 24 hours in CLAMS metabolic cages. The RER and mean oxygen consumption rates did not differ significantly in *Parg*-iMKO mice compared to the controls, suggesting that *Parg* ablation in skeletal muscle does not alter basal metabolism in male or female mice fed a chow diet **(Figures 5A-D.** and **S4A-D.)**. Ambulatory activity in the metabolic cage, measured by x-axis beam breaks, was also similar across each group either sex. (**Figures 5E-G.** and **S4E-G.**). Furthermore, we determined the submaximal V02 consumption rate during an acute bout of treadmill running to discern any effect of *Parg* ablation on muscle function. The total running distance, speed, and time, along with the maximum rate of oxygen consumption (VO2), was not altered in the male or female *Parg*-iMKO mice (**Figures 5H-K.** and **S4H-K.**). When performing a cold test at 4°C *Parg*-iMKO male mice exhibited improved thermoregulation at 1- and 3-hour time points compared to the control animals, whereas the female cohorts showed no differences (**Figures 5L.** and **S4L.**)

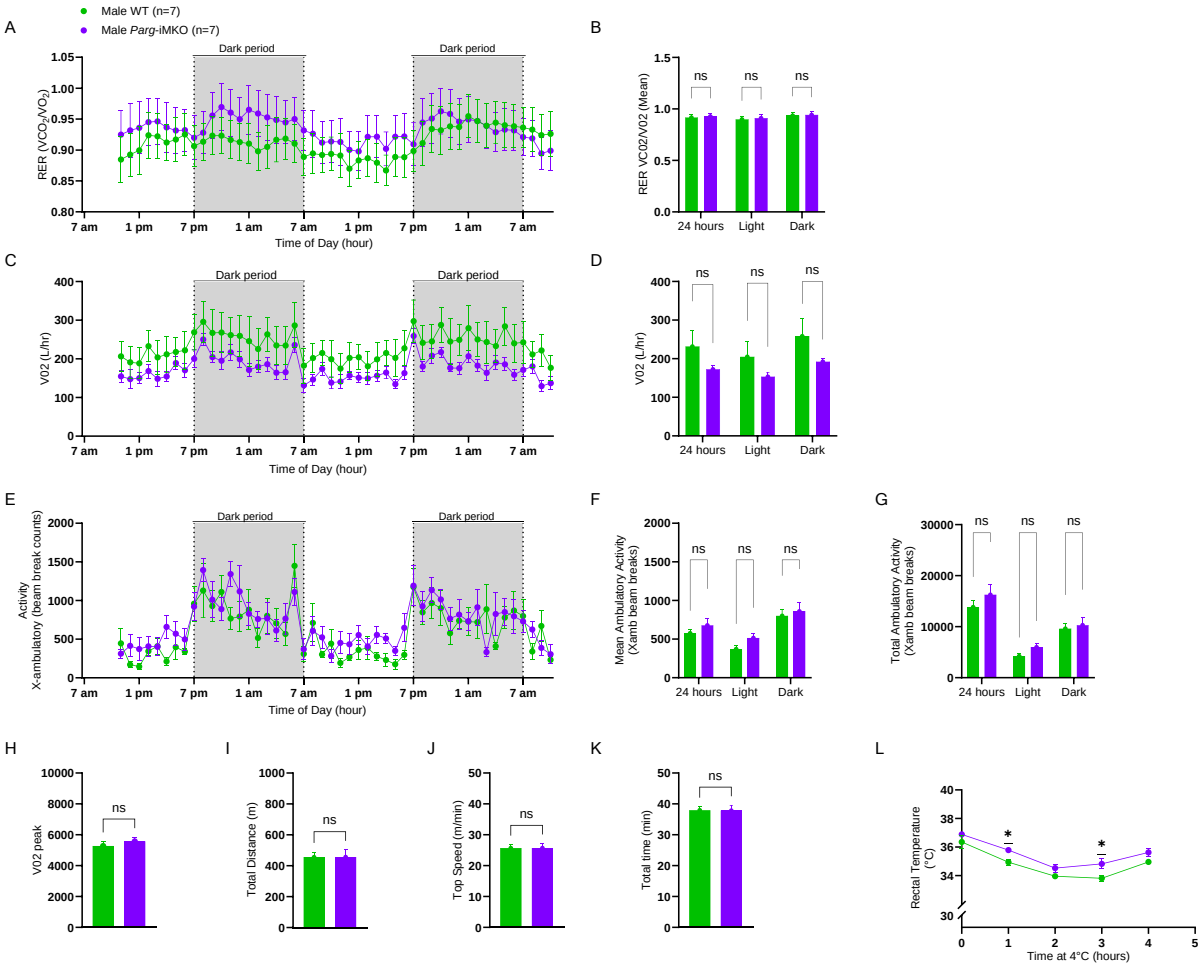

Figure 5. Respiration, physical activity, and thermoregulation is not differentially regulated in the *Parg*-iMKO male mice: (A and B) RER ratio and (C and D) O2 intake did not differ between the groups signifying similar metabolic regulation in the *Parg*-iMKO compared to the control group. (E-G) Ambulatory activity (x-ambulation) remained the same between the groups throughout the entire 48-hour assessment period (light and dark phase). (H-K) The acute metabolic treadmill test exhibited no changes in the submaximal O2 consumption rate between the groups. (H) Peak V02, (I) total distance, (J) top speed and (K) total time remained comparable between the groups. (L) Rectal temperature was measured to assess any difference in thermoregulation between the groups due to cold exposure. *Parg*-iMKO male mice had significantly better thermoregulation at the 1- and 3-hour time points compared to the control. Stats: Two-way repeated measures ANOVA with Bonferroni post-hoc analysis, graph represent means ± S.E.M for n = 7-8 for all the tests performed above. "*" indicates significance "p≤0.05", "ns" indicates not significant.

3.4 Discussion

For decades, research on PARylation has primarily focused on the role of PARPs, particularly PARP1. With regards to muscle, there are only a handful of studies that characterize the role of PARP1 (Bai et al., 2011; Cobley et al., 2013; Devalaraja-Narashimha & Padanilam, 2010; Pirinen et al., 2014; Ryu et al., 2016), whereas the role of PARG in dePARylation has been largely overlooked beyond DNA repair mechanisms in other tissues or cell lines. Even though PARG was discovered 50 years ago (Miwa & Sugimura, 1971; Ueda et al., 1972), and is recognized as the only major dePARylating enzyme inside cells excluding mitochondria (Niere et al., 2012), its importance in PAR degradation has been realized only in the recent past. We therefore set out to examine the role of PARG in modulating skeletal muscle homeostasis under basal physiological conditions. Here we developed a tamoxifen-inducible muscle-specific *Parg* KO model using a Cre-LoxP system in our lab. Skeletal muscle *Parg* deletion was confirmed using qPCR and an explant PARylation assay. Despite the importance of PARG in dePARylation, no change in the body mass, lean mass, or fat mass was observed in *Parg*-iMKO male or female mice fed a chow diet. Grip strength, grip endurance and rotarod assays data did not differ in the *Parg* deficient mice compared to WT under normal physiological conditions. Locomotor assessment, resting energy expenditure, submaximal oxygen consumption upon treadmill running did not suggest any phenotypical changes in *Parg*-iMKO mice compared to the control animals under normal physiological conditions. Interestingly, male, and female *Parg*-iMKO mice had increased energy intake, while only males demonstrated an improved capacity to thermoregulate, compared to sex-matched controls. To summarize, we show that loss of *Parg* in skeletal muscle does not largely affect muscle mass and

function in healthy adult mice fed on chow diet. Further studies are being completed which examine the role of *Parg* on a high fat diet and during cancer-cachexia, potential stressors that may increase PARylation signaling, that will perhaps shed more light on the role of PARG activity in skeletal muscle under physiological stress.

3.5 Supplementary data

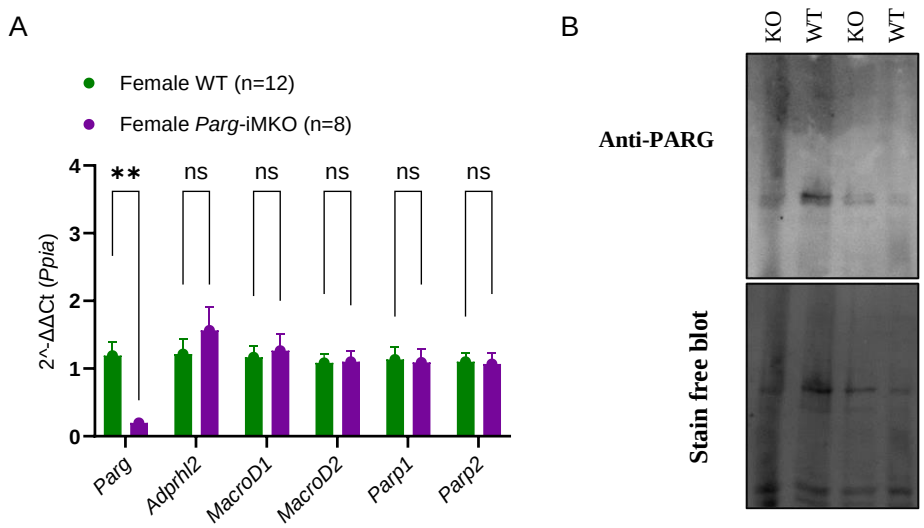

Supplementary Figure 1. Confirmation of *Parg* deletion of *Parg*-iMKO female mice: (A) *Parg* mRNA expression levels post-tamoxifen induction, and mRNA expression levels of *Parp*s and other hydrolases, (B) western blot for PARG loss could not be confirmed due to the unavailability of PARG specific antibody. Stats: for qPCR, unpaired t-tests were performed, graph represent means ± S.E.M for n = 8-12. "*" indicates statistical significance of "$p<0.05$".

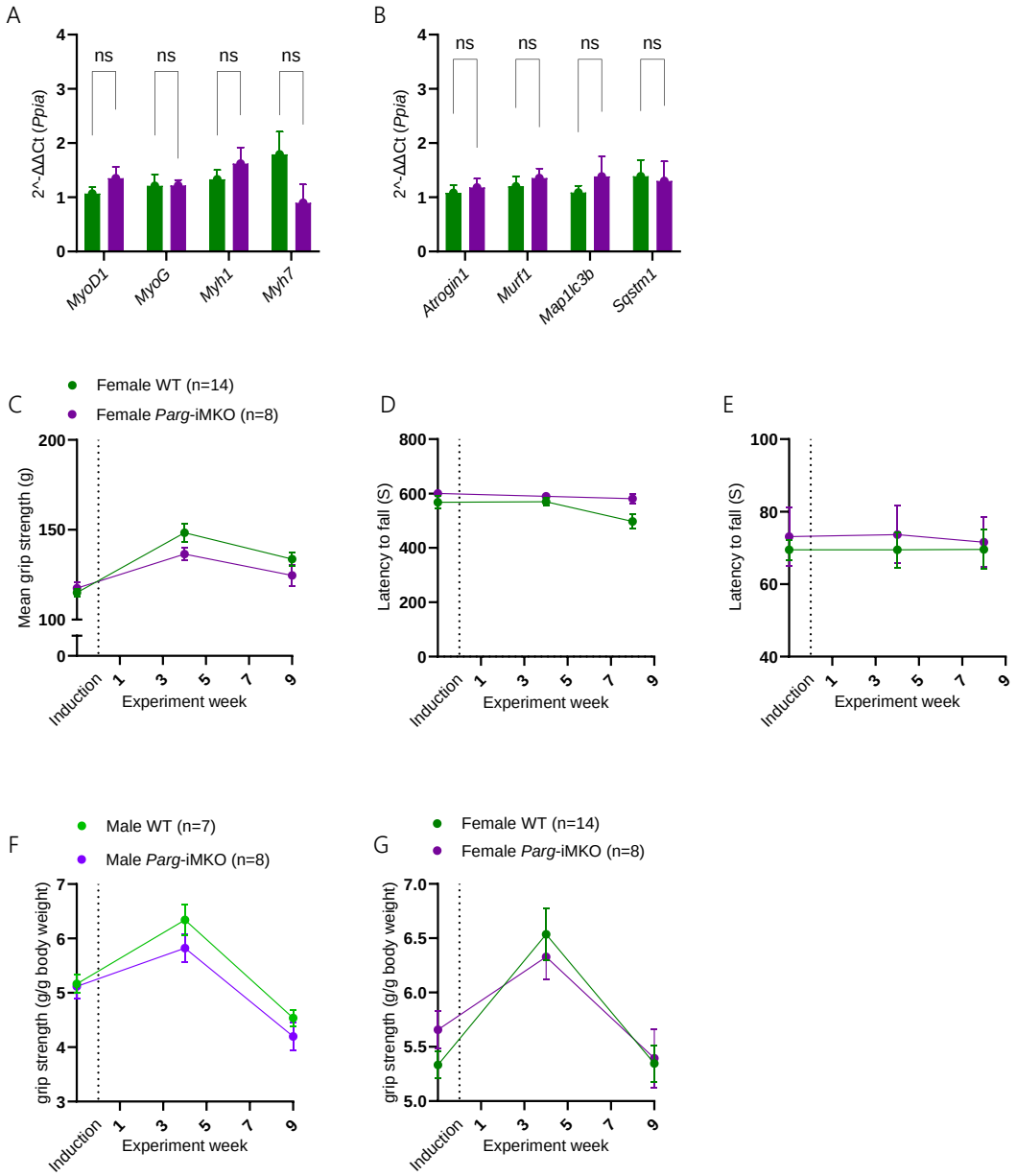

Male and female grip strength adjusted to body weight

Supplementary Figure 2. Muscle health and function was not altered in *Parg*-iMKO female mice: (A and B) markers for muscle regulation, and ubiquitination and autophagic markers, respectively did not differ significantly in *Parg*-iMKO female mice compared to sex-matched WT animals. *Parg* deletion did not have a significant effect on **(**C) mean grip strength, (D) grip endurance and (E) neuromuscular function in female mice compared to the control during the entire assessment period. (F) and (G) grip strength adjusted to body weight in male and female, respectively. Stats for qPCR, unpaired t-tests were performed, graph represent means ± S.E.M for n = 8-12. Two-way repeated measures ANOVA with

Bonferroni post-hoc analysis was used for functional assessment tests, graph represent means ± S.E.M for n = 8-14 for females. "*" indicates significance "p≤0.05".

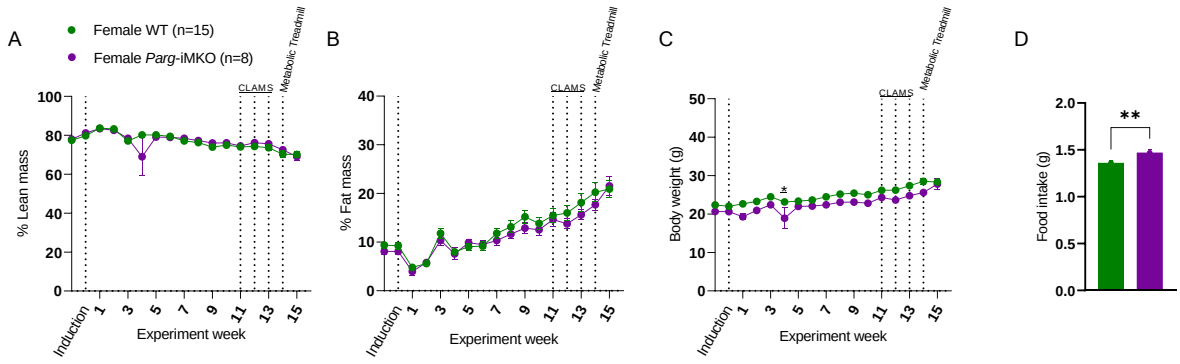

Supplementary Figure 3. Body composition and food intake in *Parg*-iMKO female mice: *Parg*-iMKO female mice did not differ in their % lean mass (A), % fat mass (B), or body weight (C) when compared between the groups. *Parg*-iMKO mice consumed more food compared to the control animals (D). Stats: Two-way repeated measures ANOVA with Bonferroni post-hoc analysis, graph represent means ± S.E.M for n = 8-14 for females. For body composition analysis "*" indicates significance "p≤0.05", "ns" indicates not significant. Unpaired t-tests were performed on food intake data, graph represent means ± S.E.M for n = 8-14 for females. "*" indicates statistical significance of "p ≤0.05

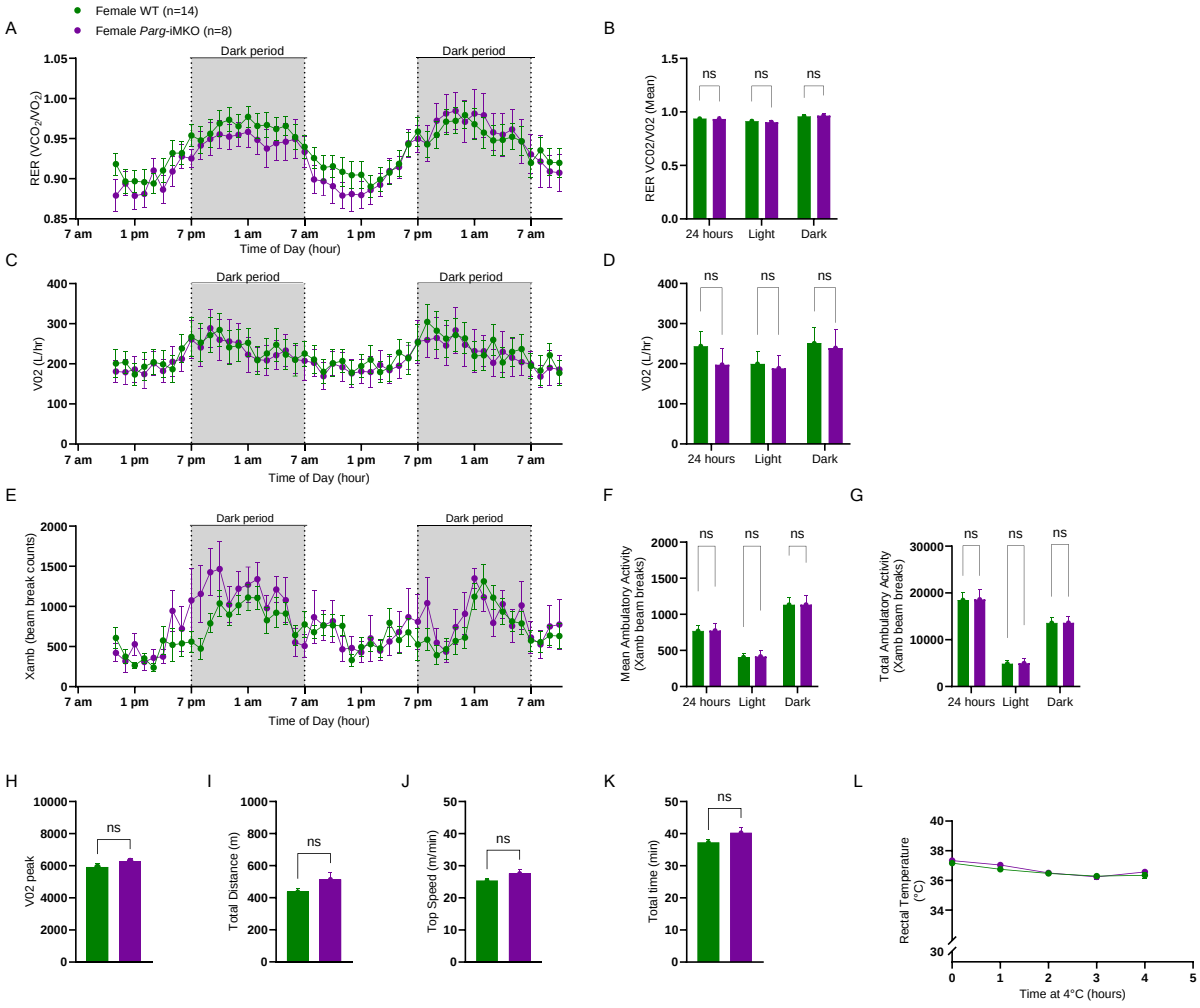

Supplementary Figure 4. Respiration, physical activity, and thermoregulation is not differentially regulated in the *Parg*-iMKO female mice: (A and B) RER ratio and (C and D) O2 intake did not differ between the groups signifying similar metabolic regulation in the female *Parg*-iMKO compared to the control group. (E-G) Physical activity (x-ambulation) remained the same between the groups throughout the entire 48 hours assessment period (light and dark phase). No significant difference was observed in x-ambulatory motion between the group in female mice. (H-K) acute treadmill test signified no differential regulation in the maximal O2 consumption rate between the groups. (H)Peak V02, (I) total distance, (J) top speed and (K) total time remained comparable between the groups. (L) Rectal temperature was measured to assess any difference in thermoregulation between the groups due to cold exposure. *Parg*-iMKO female mice had significantly better thermoregulation at 1- and 3-hour time points compared to the control, which diminished over time. Stats: Two-way repeated measures ANOVA with Bonferroni post-hoc analysis, graph represent means ± S.E.M for n = 8-14 for all the tests performed above. "*" indicates significance "$p \leq 0.05$", "ns" indicates not significant.

Chapter IV

4.1 General Discussion

Despite intensive research on the role PARylation over the last 60 years, mostly delineating its role in response to cellular stress, there is no common consensus describing its role in regulating metabolism under normal physiological conditions in a tissue specific manner. As a PTM, PARylation modulates a wide array of intracellular processes across functionally interconnected tissues, such as liver, pancreas, kidney, skeletal muscle, adipose tissues, and the nervous system, that each govern whole body health (Luo et al., 2017). Given that it is arduous to delineate the effects of PARylation in a tissue specific manner, germline loss-of-function studies and pharmaceutical inhibition of PARP1 in vivo have been employed, yet often producing inconsistent and conflicting data (Bai, Cantó, et al., 2011; Devalaraja-Narashimha & Padanilam, 2010; Erener et al., 2012; Lehmann et al., 2015; Luo & Kraus, 2012). Thus, to investigate (de)PARylation, by addressing the roles of PARP1 and PARG in muscle health, we have generated an inducible conditional-knockout mouse lines to ablate muscle-specific *Parp1* and *Parg* expression in mature healthy mice. Given that skeletal muscle is a predominant regulator of whole-body metabolism and is essential for motility throughout the lifespan, while PARylation has been previously linked to stress responses and metabolism, the role of PARylation in muscle has become an important question to address. Besides the fact that PARylation is usually reported to be less active under normal physiological conditions, and that both PARP1 and PARG are required in early development and cell differentiation processes (Ji & Tulin, 2010), not much is known about their tissue specific roles when not linked to disease progression (Liu et al., 2017).

To determine the role of PARylation in muscle during a normal physiological state, we developed inducible muscle-specific loss-of-function models of *Parp1* and *Parg* using Cre-loxP system on the C57BL6J background that were fed regular chow diet. This thesis then critically examined the role of PARP1 and PARG, the predominant PAR synthesizing and degrading enzymes, on skeletal muscle function, and metabolism in these healthy mature mice under normal physiological conditions.

4.1.1 Effect of the loss of *Parp1* and *Parg* in the regulation of skeletal muscle mass and function.

Our findings from the characterization of *Parp1*-iMKO mice identified no difference in mean grip strength compared to the controls which is in line with (Chacon-Cabrera et al., 2015), where whole-body *Parp1* deletion did not affect the muscle strength or body weight. We did however observe a trend in the reduction in mean grip strength following *Parg* deletion in the *Parg*-iMKO male mice compared to their controls. Furthermore, there were no changes in muscular endurance measured using the hanging wire test in the *Parp1*- and *Parg*-iMKO mice on C57BL6J background, which contrasts with the germline *Parp1* deletion mouse model on 129/SVJ (Piskunova et al., 2008), where the loss of *Parp1* negatively affected the muscle strength and endurance. Although, these differences in results could be attributed to the different mouse strain and the different time points for measurements used in their study.

The body composition analysis of the *Parp1*-iMKO mice suggested comparable mean body weight and percent lean, and fat mass, compared to the controls. The mean body weight and the percent fat mass increased gradually with age in equal manners across animals. Food consumption, resting oxygen consumption rate and resting energy

expenditure, physical activity, submaximal oxygen consumption during exercise, and cold tolerance were comparable between the *Parp1*-iMKO and control mice, which suggests that the loss of *Parp1* does not affect feeding habits, physical activity, or whole-body metabolism. These results appear to contrast with that observed in *Parp1*-null mice, whereas on a C57BL6J background, mice were leaner, accumulated less fat mass, had increased cold tolerance, and improved oxygen consumption rates (Bai, Cantó, et al., 2011). However, the body composition measured by Bai et al. was for a longer duration than our study (46 vs 16 weeks, respectively), and showed significance only at the 16-weeks' time-point, which could explain the differences. In another study that used germline *Parp1* knockouts, but on the 129/SVJ background, Piskunova et al. (Piskunova et al., 2008) showed that loss *Parp1* caused the mice to gain weight on a chow diet, an effect that was not replicated in our skeletal muscle-specific KO. Although their difference emerged in mice at 21 months of age, far beyond the age of our mice.

Despite not observing changes in the food intake of *Parp1*-iMKO mice, we did observe a significant increase in the food intake on average by *Parg*-iMKO male and female mice compared to their controls, which was not corroborated by changes in mean body weight, oxygen consumption or resting energy expenditure. The physical activity and the submaximal oxygen consumption on a metabolic treadmill did not change significantly between the groups. However, *Parg*-iMKO male mice were better at regulating temperature in a cold environment compared to their WT counterparts.

To summarize, our study has shown that the disruption of PARylation signaling through the loss of *Parp1* in muscle does not affect body composition, locomotion, metabolism, or thermoregulation on a normal diet in male or female mice. Whereas *Parg*

deletion leads to increased food consumption and is better at expending energy to regulate their temperature under colder environments in *Parg* null mice. Nonetheless, *Parg* deletion did not affect grip strength, muscle function, physical activity, or metabolism in *Parg*-iMKO mice compared to their controls.

4.1.2 Limitations and future directions:

There are a few caveats related to our study characterizing the inducible muscle-specific-knockout model for both *Parp1* and *Parg*. Firstly, we were unable to use western blotting to confirm the KO of PARG in skeletal muscle due to a lack of functioning PARG specific antibodies. However, we designed an ex vivo PARylation assay, where we observed the accumulation of PAR in the absence of PARG in the quadriceps tissues upon treatment with a DNA damaging agent (cisplatin).

Further, our study focused on the impact of PAR regulation under normal physiological conditions without any insult or stressors, such as muscle injury, disease, aging, or metabolic stress (i.e., a high-fat diet), which may be used in the future to better characterize the role of *Parg* and *Parp1* in muscle. For example, previous studies have shown that PARP1 hyperactivation results in NAD+ depletion, contributing to pathophysiological conditions during ageing(Cobley et al., 2013; Mangerich & Bürkle, 2012). Furthermore, *Parp1* deletion has been shown to improve NAD+ availability for SIRT1-directed activation of mitochondrial biogenesis on a high-fat diet, which is further improved upon exercise (Bai, Cantó, et al., 2011). It would therefore be interesting to compare the effect of disrupted muscle PARylation in trained vs untrained and young vs old mice to better understand the role of PARylation in muscle with different forms of stress. Further studies will also be performed on these two conditional-knockout models

while being fed a high fat diet to tease out the varying role of PARylation in regulating skeletal muscle mass and function during nutritional stress. Cancer cachexia may also be an interesting avenue to examine the role of PARG and PARP1 activity in maintaining muscle mass and strength, given the fact that PARP1 inhibitors are now readily used for cancer treatments while PARG inhibitors are in development for phase I clinical trials to treat cancer (Chacon-Cabrera et al., 2017; Harrision et al., 2020; Houl et al., 2019). Additionally, since *Parp2* has been suggested to catalyze similar functions as *Parp1*,a muscle-specific *Parp1/Parp2* deletion may shed more light on the role of PARylation in skeletal muscle.

Moreover, to further characterize the role of PARylation on muscle, histological assessment of muscle sections has been collected from *Parp1*-iMKO, *Parg*-iMKO and controls that will be examined for differences in muscle fiber types using immunofluorescent staining for type I, type IIA, type IIB and type IIX myosin heavy chain and counterstained with DAPI. Using these images, minimum Ferret diameter will be quantified to determine fiber type specific atrophy. Using immunofluorescence, tissue sections will be stained with anti-PARP1, anti-PARG, and anti-PARylation antibodies to confirm altered PAR accumulation in each of the mouse models. Furthermore, muscle fiber centrally located nuclei will be quantified to capture muscle damage, while TUNEL staining will be performed to detect DNA breaks to assess myonuclear apoptosis or DNA repair defects in *Parp1*/*Parg* deficient mice. Finally, glucose tolerance tests and insulin tolerance tests will be done on *Parp1*/*Parg* deficient mice to quantify the metabolic effects of PARP1 and PARG loss in the skeletal muscle.

Chapter V

5.1 Conclusion

PARylation is an important post-translational modification involved in a wide range of biological functions. PARP1 and PARG, being the predominant enzymes involved in PARylation dynamics, play a key role as PAR synthesizing and degrading enzymes, respectively. PARylation is required for the development and maintenance of important cellular and metabolic functions, whereas hyperactivation of PARylation under severe stress or aging is detrimental to metabolic function and health through excessive NAD+ depletion and mitochondrial dysfunction. However, under normal physiological conditions, altered (de)PARylation in mature skeletal muscle does not modulate muscle homeostasis or metabolism, nor does it alter whole body metabolism. In summary, we have successfully developed and characterized muscle-specific *Parp1* and *Parg* inducible-knockout mouse models, which can be used as a baseline for conducting future studies to better understand the mechanistic role of PARP1 and PARG as modulators of muscle health and metabolism in pathophysiological conditions.

References

Aberle, L., Krüger, A., Reber, J. M., Lippmann, M., Hufnagel, M., Schmalz, M., Trussina, I. R. E. A., Schlesiger, S., Zubel, T., Schütz, K., Marx, A., Hartwig, A., Ferrando-May, E., Bürkle, A., & Mangerich, A. (2020). PARP1 catalytic variants reveal branching and chain length-specific functions of poly(ADP-ribose) in cellular physiology and stress response. *Nucleic Acids Research*, *48*(18), 10015–10033. https://doi.org/10.1093/nar/gkaa590

Agnew, T., Munnur, D., Crawford, K., Palazzo, L., Mikoč, A., & Ahel, I. (2018). MacroD1 Is a Promiscuous ADP-Ribosyl Hydrolase Localized to Mitochondria. *Frontiers in Microbiology*, *9*. https://doi.org/10.3389/fmicb.2018.00020

Alvarez-Gonzalez, R., & Althaus, F. R. (1989). Poly(ADP-ribose) catabolism in mammalian cells exposed to DNA-damaging agents. *Mutation Research/DNA Repair*, *218*(2), 67–74. https://doi.org/10.1016/0921-8777(89)90012-8

Andrabi, S. A., Kim, N. S., Yu, S.-W., Wang, H., Koh, D. W., Sasaki, M., Klaus, J. A., Otsuka, T., Zhang, Z., Koehler, R. C., Hurn, P. D., Poirier, G. G., Dawson, V. L., & Dawson, T. M. (2006). Poly(ADP-ribose) (PAR) polymer is a death signal. *Proceedings of the National Academy of Sciences*, *103*(48), 18308–18313. https://doi.org/10.1073/pnas.0606526103

Andrabi, S. A., Umanah, G. K. E., Chang, C., Stevens, D. A., Karuppagounder, S. S., Gagné, J.-P., Poirier, G. G., Dawson, V. L., & Dawson, T. M. (2014). Poly(ADP-ribose) polymerase-dependent energy depletion occurs through inhibition of glycolysis. *Proceedings of the National Academy of Sciences*, *111*(28), 10209–10214. https://doi.org/10.1073/pnas.1405158111

Asher, G., Reinke, H., Altmeyer, M., Gutierrez-Arcelus, M., Hottiger, M. O., & Schibler, U. (2010). Poly(ADP-Ribose) Polymerase 1 Participates in the Phase Entrainment of Circadian Clocks to Feeding. *Cell*, *142*(6), 943–953. https://doi.org/10.1016/j.cell.2010.08.016

Bai, P. (2015). Biology of Poly(ADP-Ribose) Polymerases: The Factotums of Cell Maintenance. *Molecular Cell*, *58*(6), 947–958. https://doi.org/10.1016/j.molcel.2015.01.034

Bai, P., Canto, C., Brunyánszki, A., Huber, A., Szántó, M., Cen, Y., Yamamoto, H., Houten, S. M., Kiss, B., Oudart, H., Gergely, P., Menissier-De Murcia, J., Schreiber, V., Sauve, A. A., & Auwerx, J. (2011). PARP-2 regulates SIRT1 expression and whole-body energy expenditure. *Cell Metabolism*, *13*(4), 450–460. https://doi.org/10.1016/j.cmet.2011.03.013

Bai, P., Cantó, C., Oudart, H., Brunyánszki, A., Cen, Y., Thomas, C., Yamamoto, H., Huber, A., Kiss, B., Houtkooper, R. H., Schoonjans, K., Schreiber, V., Sauve, A. A., Menissier-de Murcia, J., & Auwerx, J. (2011). PARP-1 Inhibition Increases Mitochondrial Metabolism through SIRT1 Activation. *Cell Metabolism*, *13*(4), 461–468. https://doi.org/10.1016/j.cmet.2011.03.004

Bai, P., Nagy, L., Fodor, T., Liaudet, L., & Pacher, P. (2015). Poly(ADP-ribose) polymerases as modulators of mitochondrial activity. *Trends in Endocrinology & Metabolism*, *26*(2), 75–83. https://doi.org/10.1016/j.tem.2014.11.003

Barkauskaite, E., Jankevicius, G., & Ahel, I. (2015). Structures and Mechanisms of Enzymes Employed in the Synthesis and Degradation of PARP-Dependent Protein ADP-Ribosylation. *Molecular Cell*, *58*(6), 935–946. https://doi.org/10.1016/j.molcel.2015.05.007

Baskin, K. K., Winders, B. R., & Olson, E. N. (2015). Muscle as a "Mediator" of Systemic Metabolism. *Cell Metabolism*, *21*(2), 237–248. https://doi.org/10.1016/j.cmet.2014.12.021

Berger, N. A. (1985). Poly(ADP-Ribose) in the Cellular Response to DNA Damage. *Radiation Research*, *101*(1), 4. https://doi.org/10.2307/3576299

Bernardi, R., Rossi, L., Poirier, G. G., & Scovassi, A. I. (1997). Analysis of poly(ADP-ribose) glycohydrolase activity in nuclear extracts from mammalian cells. *Biochimica et Biophysica Acta (BBA) - Protein Structure and Molecular Enzymology*, *1338*(1), 60–68. https://doi.org/10.1016/S0167-4838(96)00188-4

Bock, F. J., Todorova, T. T., & Chang, P. (2015). RNA Regulation by Poly(ADP-Ribose) Polymerases. *Molecular Cell*, *58*(6), 959–969. https://doi.org/10.1016/j.molcel.2015.01.037

Bradley, D. (2022). The evolution of post-translational modifications. *Current Opinion in Genetics & Development*, *76*, 101956. https://doi.org/10.1016/j.gde.2022.101956

BRAUN, S. A., PANZETER, P. L., COLLINGE, M. A., & ALTHAUS, F. R. (1994). Endoglycosidic cleavage of branched polymers by poly(ADP-ribose) glycohydrolase. *European Journal of Biochemistry*, *220*(2), 369–375. https://doi.org/10.1111/j.1432-1033.1994.tb18633.x

Campelj, D. G., Timpani, C. A., Petersen, A. C., Hayes, A., Goodman, C. A., & Rybalka, E. (2020). The Paradoxical Effect of PARP Inhibitor BGP-15 on Irinotecan-Induced Cachexia and Skeletal Muscle Dysfunction. *Cancers*, *12*(12), 3810. https://doi.org/10.3390/cancers12123810

Catara, G., Corteggio, A., Valente, C., Grimaldi, G., & Palazzo, L. (2019). Targeting ADP-ribosylation as an antimicrobial strategy. *Biochemical Pharmacology*, *167*, 13–26. https://doi.org/10.1016/j.bcp.2019.06.001

Chacon-Cabrera, A., Fermoselle, C., Salmela, I., Yelamos, J., & Barreiro, E. (2015). MicroRNA expression and protein acetylation pattern in respiratory and limb muscles of Parp-1−/− and Parp-2−/− mice with lung cancer cachexia. *Biochimica et Biophysica Acta (BBA) - General Subjects*, *1850*(12), 2530–2543. https://doi.org/10.1016/j.bbagen.2015.09.020

Chacon-Cabrera, A., Mateu-Jimenez, M., Langohr, K., Fermoselle, C., García-Arumí, E., Andreu, A. L., Yelamos, J., & Barreiro, E. (2017). Role of PARP activity in lung cancer-induced cachexia: Effects on muscle oxidative stress, proteolysis, anabolic markers, and phenotype. *Journal of Cellular Physiology*, *232*(12), 3744–3761. https://doi.org/10.1002/jcp.25851

Challa, S., Stokes, M. S., & Kraus, W. L. (2021). MARTs and MARylation in the Cytosol: Biological Functions, Mechanisms of Action, and Therapeutic Potential. *Cells*, *10*(2), 313. https://doi.org/10.3390/cells10020313

Chambon, P., Weill, J. D., & Mandel, P. (1963). Nicotinamide mononucleotide activation of a new DNA-dependent polyadenylic acid synthesizing nuclear enzyme. *Biochemical and Biophysical Research Communications*, *11*(1), 39–43. https://doi.org/10.1016/0006-291X(63)90024-X

Chen, Q., Kassab, M. A., Dantzer, F., & Yu, X. (2018). PARP2 mediates branched poly ADP-ribosylation in response to DNA damage. *Nature Communications*, *9*(1), 3233. https://doi.org/10.1038/s41467-018-05588-5

Chiang, Y. J., Hsiao, S. J., Yver, D., Cushman, S. W., Tessarollo, L., Smith, S., & Hodes, R. J. (2008). Tankyrase 1 and Tankyrase 2 Are Essential but Redundant for Mouse Embryonic Development. *PLoS ONE*, *3*(7), e2639. https://doi.org/10.1371/journal.pone.0002639

Cho, S. H., Ahn, A. K., Bhargava, P., Lee, C.-H., Eischen, C. M., McGuinness, O., & Boothby, M. (2011). Glycolytic rate and lymphomagenesis depend on PARP14, an ADP ribosyltransferase of the B aggressive lymphoma (BAL) family. *Proceedings of the National Academy of Sciences*, *108*(38), 15972–15977. https://doi.org/10.1073/pnas.1017082108

Cobley, J. N., Sakellariou, G. K., Murray, S., Waldron, S., Gregson, W., Burniston, J. G., Morton, J. P., Iwanejko, L. A., & Close, G. L. (2013). Lifelong endurance training attenuates age-related genotoxic stress in human skeletal muscle. *Longevity & Healthspan*, *2*(1), 11. https://doi.org/10.1186/2046-2395-2-11

Cook, B. D., Dynek, J. N., Chang, W., Shostak, G., & Smith, S. (2002). Role for the Related Poly(ADP-Ribose) Polymerases Tankyrase 1 and 2 at Human Telomeres. *Molecular and Cellular Biology*, *22*(1), 332–342. https://doi.org/10.1128/MCB.22.1.332-342.2002

Cortes, U., Tong, W.-M., Coyle, D. L., Meyer-Ficca, M. L., Meyer, R. G., Petrilli, V., Herceg, Z., Jacobson, E. L., Jacobson, M. K., & Wang, Z.-Q. (2004). Depletion of the 110-Kilodalton Isoform of Poly(ADP-Ribose) Glycohydrolase Increases Sensitivity to Genotoxic and Endotoxic Stress in Mice. *Molecular and Cellular Biology*, *24*(16), 7163–7178. https://doi.org/10.1128/MCB.24.16.7163-7178.2004

Covarrubias, A. J., Perrone, R., Grozio, A., & Verdin, E. (2021). NAD+ metabolism and its roles in cellular processes during ageing. *Nature Reviews Molecular Cell Biology*, *22*(2), 119–141. https://doi.org/10.1038/s41580-020-00313-x

Curtin, N. J., & Szabo, C. (2013). Therapeutic applications of PARP inhibitors: anticancer therapy and beyond. *Molecular Aspects of Medicine*, *34*(6), 1217–1256. https://doi.org/10.1016/j.mam.2013.01.006

Dadheech, N., Srivastava, A., Shah, R. G., Shah, G. M., & Gupta, S. (2022). Role of poly(ADP-ribose) polymerase-1 in regulating human islet cell differentiation. *Scientific Reports*, *12*(1), 21496. https://doi.org/10.1038/s41598-022-25405-w

D'Amours, D., Desnoyers, S., D'Silva, I., & Poirier, G. G. (1999a. Poly(ADP-ribosyl)ation reactions in the regulation of nuclear functions. *The Biochemical Journal*, *342 (Pt 2)*(Pt 2), 249–268.

Dantzer, F., & Santoro, R. (2013). The expanding role of PARPs in the establishment and maintenance of heterochromatin. *FEBS Journal*, *280*(15), 3508–3518. https://doi.org/10.1111/febs.12368

Dasovich, M., & Leung, A. K. L. (2023). Molecular tools unveil distinct waves of ADP-ribosylation during DNA repair. *Cell Reports Methods*, *3*(5), 100484. https://doi.org/10.1016/j.crmeth.2023.100484

David, K. K. (2009). Parthanatos, a messenger of death. *Frontiers in Bioscience*, *Volume*(14), 1116. https://doi.org/10.2741/3297

de Murcia, J. M., Niedergang, C., Trucco, C., Ricoul, M., Dutrillaux, B., Mark, M., Oliver, F. J., Masson, M., Dierich, A., LeMeur, M., Walztinger, C., Chambon, P., & de Murcia, G. (1997). Requirement of poly(ADP-ribose) polymerase in recovery from DNA damage in mice and in cells. *Proceedings of the National Academy of Sciences*, *94*(14), 7303–7307. https://doi.org/10.1073/pnas.94.14.7303

De Rycker, M., & Price, C. M. (2004). Tankyrase Polymerization Is Controlled by Its Sterile Alpha Motif and Poly(ADP-Ribose) Polymerase Domains. *Molecular and Cellular Biology*, *24*(22), 9802–9812. https://doi.org/10.1128/MCB.24.22.9802-9812.2004

De Vos, M., Schreiber, V., & Dantzer, F. (2012). The diverse roles and clinical relevance of PARPs in DNA damage repair: Current state of the art. *Biochemical Pharmacology*, *84*(2), 137–146. https://doi.org/10.1016/j.bcp.2012.03.018

Deschenes, M. R. (2004). Effects of Aging on Muscle Fibre Type and Size. *Sports Medicine*, *34*(12), 809–824. https://doi.org/10.2165/00007256-200434120-00002

Devalaraja-Narashimha, K., & Padanilam, B. J. (2009). PARP-1 Inhibits Glycolysis in Ischemic Kidneys. *Journal of the American Society of Nephrology*, *20*(1), 95–103. https://doi.org/10.1681/ASN.2008030325

Devalaraja-Narashimha, K., & Padanilam, B. J. (2010). PARP1 deficiency exacerbates diet-induced obesity in mice. *Journal of Endocrinology*, *205*(3), 243–252. https://doi.org/10.1677/JOE-09-0402

Di Girolamo, M., & Fabrizio, G. (2019). Overview of the mammalian ADP-ribosyl-transferases clostridia toxin-like (ARTCs) family. *Biochemical Pharmacology*, *167*, 86–96. https://doi.org/10.1016/j.bcp.2019.07.004

Dos Santos, M., Backer, S., Auradé, F., Wong, M. M.-K., Wurmser, M., Pierre, R., Langa, F., Do Cruzeiro, M., Schmitt, A., Concordet, J.-P., Sotiropoulos, A., Jeffrey Dilworth, F., Noordermeer, D., Relaix, F., Sakakibara, I., & Maire, P. (2022). A fast Myosin super enhancer dictates muscle fiber phenotype through competitive interactions with Myosin genes. *Nature Communications*, *13*(1), 1039. https://doi.org/10.1038/s41467-022-28666-1

Emery, A. E. H. (2002). Muscular dystrophy into the new millennium. *Neuromuscular Disorders*, *12*(4), 343–349. https://doi.org/10.1016/S0960-8966(01)00303-0

Erener, S., Mirsaidi, A., Hesse, M., Tiaden, A. N., Ellingsgaard, H., Kostadinova, R., Donath, M. Y., Richards, P. J., & Hottiger, M. O. (2012). *ARTD1* deletion causes increased hepatic lipid accumulation in mice fed a high-fat diet and impairs adipocyte function and differentiation. *The FASEB Journal*, *26*(6), 2631–2638. https://doi.org/10.1096/fj.11-200212

Fehr, A. R., Singh, S. A., Kerr, C. M., Mukai, S., Higashi, H., & Aikawa, M. (2020). The impact of PARPs and ADP-ribosylation on inflammation and host–pathogen interactions. *Genes & Development*, *34*(5–6), 341–359. https://doi.org/10.1101/gad.334425.119

Feng, X., & Koh, D. W. (2013). *Roles of Poly(ADP-Ribose) Glycohydrolase in DNA Damage and Apoptosis* (pp. 227–281). https://doi.org/10.1016/B978-0-12-407696-9.00005-1

Fouquerel, E., Goellner, E. M., Yu, Z., Gagné, J.-P., Barbi de Moura, M., Feinstein, T., Wheeler, D., Redpath, P., Li, J., Romero, G., Migaud, M., Van Houten, B., Poirier, G. G., & Sobol, R. W. (2014). ARTD1/PARP1 Negatively Regulates Glycolysis by Inhibiting Hexokinase 1 Independent of NAD + Depletion. *Cell Reports*, *8*(6), 1819–1831. https://doi.org/10.1016/j.celrep.2014.08.036

Gagné, J.-P., Bonicalzi, M.-È., Gagné, P., Ouellet, M.-È., Hendzel, M. J., & Poirier, G. G. (2005). Poly(ADP-ribose) glycohydrolase is a component of the FMRP-associated messenger ribonucleoparticles. *Biochemical Journal*, *392*(3), 499–509. https://doi.org/10.1042/BJ20050792

Gibson, B. A., & Kraus, W. L. (2012). New insights into the molecular and cellular functions of poly(ADP-ribose) and PARPs. *Nature Reviews Molecular Cell Biology*, *13*(7), 411–424. https://doi.org/10.1038/nrm3376

Goody, M. F., & Henry, C. A. (2018). A need for NAD+ in muscle development, homeostasis, and aging. *Skeletal Muscle*, *8*(1), 9. https://doi.org/10.1186/s13395-018-0154-1

Guo, S., Zhang, S., Zhuang, Y., Xie, F., Wang, R., Kong, X., Zhang, Q., Feng, Y., Gao, H., Kong, X., & Liu, T. (2023). Muscle PARP1 inhibition extends lifespan through AMPKα PARylation and activation in *Drosophila*. *Proceedings of the National Academy of Sciences*, *120*(13). https://doi.org/10.1073/pnas.2213857120

Gupte, R., Liu, Z., & Kraus, W. L. (2017). PARPs and ADP-ribosylation: recent advances linking molecular functions to biological outcomes. *Genes & Development*, *31*(2), 101–126. https://doi.org/10.1101/gad.291518.116

Ha, H. C., & Snyder, S. H. (1999). Poly(ADP-ribose) polymerase is a mediator of necrotic cell death by ATP depletion. *Proceedings of the National Academy of Sciences*, *96*(24), 13978–13982. https://doi.org/10.1073/pnas.96.24.13978

Ham, D. J., Börsch, A., Lin, S., Thürkauf, M., Weihrauch, M., Reinhard, J. R., Delezie, J., Battilana, F., Wang, X., Kaiser, M. S., Guridi, M., Sinnreich, M., Rich, M. M., Mittal, N., Tintignac, L. A., Handschin, C., Zavolan, M., & Rüegg, M. A. (2020). The neuromuscular junction is a focal point of mTORC1 signaling in sarcopenia. *Nature Communications*, *11*(1), 4510. https://doi.org/10.1038/s41467-020-18140-1

Hargreaves, M., & Spriet, L. L. (2020). Skeletal muscle energy metabolism during exercise. *Nature Metabolism*, *2*(9), 817–828. https://doi.org/10.1038/s42255-020-0251-4

Harrision, D., Gravells, P., Thompson, R., & Bryant, H. E. (2020). Poly(ADP-Ribose) Glycohydrolase (PARG) vs. Poly(ADP-Ribose) Polymerase (PARP) - Function in Genome Maintenance and Relevance of Inhibitors for Anti-cancer Therapy. *Frontiers in Molecular Biosciences*, *7*, 191. https://doi.org/10.3389/fmolb.2020.00191

Hassa, P. O. (2008). The diverse biological roles of mammalian PARPS, a small but powerful family of poly-ADP-ribose polymerases. *Frontiers in Bioscience*, *13*(13), 3046. https://doi.org/10.2741/2909

Hassa, P. O., Haenni, S. S., Buerki, C., Meier, N. I., Lane, W. S., Owen, H., Gersbach, M., Imhof, R., & Hottiger, M. O. (2005). Acetylation of Poly(ADP-ribose) Polymerase-1 by p300/CREB-binding Protein Regulates Coactivation of NF-κB-dependent Transcription. *Journal of Biological Chemistry*, *280*(49), 40450–40464. https://doi.org/10.1074/jbc.M507553200

Hiona, A., Sanz, A., Kujoth, G. C., Pamplona, R., Seo, A. Y., Hofer, T., Someya, S., Miyakawa, T., Nakayama, C., Samhan-Arias, A. K., Servais, S., Barger, J. L., Portero-Otín, M., Tanokura, M., Prolla, T. A., & Leeuwenburgh, C. (2010). Mitochondrial DNA Mutations Induce Mitochondrial Dysfunction, Apoptosis and Sarcopenia in Skeletal Muscle of Mitochondrial DNA Mutator Mice. *PLoS ONE*, *5*(7), e11468. https://doi.org/10.1371/journal.pone.0011468

Hottiger, M. O. (2015). Nuclear ADP-Ribosylation and Its Role in Chromatin Plasticity, Cell Differentiation, and Epigenetics. *Annual Review of Biochemistry*, *84*(1), 227–263. https://doi.org/10.1146/annurev-biochem-060614-034506

Houl, J. H., Ye, Z., Brosey, C. A., Balapiti-Modarage, L. P. F., Namjoshi, S., Bacolla, A., Laverty, D., Walker, B. L., Pourfarjam, Y., Warden, L. S., Babu Chinnam, N., Moiani, D., Stegeman, R. A., Chen, M.-K., Hung, M.-C., Nagel, Z. D., Ellenberger, T., Kim, I.-K., Jones, D. E., … Tainer, J. A. (2019). Selective small molecule PARG inhibitor causes replication fork stalling and cancer cell death. *Nature Communications*, *10*(1), 5654. https://doi.org/10.1038/s41467-019-13508-4

Hurtado-Bagès, S., Knobloch, G., Ladurner, A. G., & Buschbeck, M. (2020). The taming of PARP1 and its impact on NAD+ metabolism. *Molecular Metabolism*, *38*, 100950. https://doi.org/10.1016/j.molmet.2020.01.014

Iwashita, A., Hattori, K., Yamamoto, H., Ishida, J., Kido, Y., Kamijo, K., Murano, K., Miyake, H., Kinoshita, T., Warizaya, M., Ohkubo, M., Matsuoka, N., & Mutoh, S. (2005). Discovery of quinazolinone and quinoxaline derivatives as potent and selective poly(ADP-ribose) polymerase-1/2 inhibitors. *FEBS Letters*, *579*(6), 1389–1393. https://doi.org/10.1016/j.febslet.2005.01.036

Izumi, T., & Mellon, I. (2021). Base excision repair and nucleotide excision repair. In *Genome Stability* (pp. 293–322). Elsevier. https://doi.org/10.1016/B978-0-323-85679-9.00017-9

Javle, M., & Curtin, N. J. (2011). The role of PARP in DNA repair and its therapeutic exploitation. *British Journal of Cancer*, *105*(8), 1114–1122. https://doi.org/10.1038/bjc.2011.382

Ji, Y., & Tulin, A. V. (2010). The roles of PARP1 in gene control and cell differentiation. *Current Opinion in Genetics & Development*, *20*(5), 512–518. https://doi.org/10.1016/j.gde.2010.06.001

Johnson, S., Karpova, Y., Guo, D., Ghatak, A., Markov, D. A., & Tulin, A. V. (2022). PARG suppresses tumorigenesis and downregulates genes controlling angiogenesis, inflammatory response, and immune cell recruitment. *BMC Cancer*, *22*(1), 557. https://doi.org/10.1186/s12885-022-09651-9

Jwa, M., & Chang, P. (2012). PARP16 is a tail-anchored endoplasmic reticulum protein required for the PERK- and IRE1α-mediated unfolded protein response. *Nature Cell Biology*, *14*(11), 1223–1230. https://doi.org/10.1038/ncb2593

Ke, B., Li, A., Fu, H., Kong, C., Liu, T., Zhu, Q., Zhang, Y., Zhang, Z., Chen, C., & Jin, C. (2022). PARP-1 inhibitors enhance the chemosensitivity of leukemia cells by attenuating NF-κB pathway activity and DNA damage response induced by Idarubicin. *Acta Biochimica et Biophysica Sinica*, *54*(1), 91–98. https://doi.org/10.3724/abbs.2021011

Kiehlbauch, C. C., Aboulela, N., Jacobson, E. L., Ringer, D. P., & Jacobson, M. K. (1993). High Resolution Fractionation and Characterization of ADP-Ribose Polymers. *Analytical Biochemistry*, *208*(1), 26–34. https://doi.org/10.1006/abio.1993.1004

Kim, M. Y., Zhang, T., & Kraus, W. L. (2005). Poly(ADP-ribosyl)ation by PARP-1: `PAR-laying' NAD $^{+}$ into a nuclear signal. *Genes & Development*, *19*(17), 1951–1967. https://doi.org/10.1101/gad.1331805

Koh, D. W., Lawler, A. M., Poitras, M. F., Sasaki, M., Wattler, S., Nehls, M. C., Stöger, T., Poirier, G. G., Dawson, V. L., & Dawson, T. M. (2004). Failure to degrade poly(ADP-ribose) causes increased sensitivity to cytotoxicity and early embryonic lethality. *Proceedings of the National Academy of Sciences*, *101*(51), 17699–17704. https://doi.org/10.1073/pnas.0406182101

Kraus, W. L., & Hottiger, M. O. (2013). PARP-1 and gene regulation: progress and puzzles. *Molecular Aspects of Medicine*, *34*(6), 1109–1123. https://doi.org/10.1016/j.mam.2013.01.005

Krishnakumar, R., & Kraus, W. L. (2010). The PARP Side of the Nucleus: Molecular Actions, Physiological Outcomes, and Clinical Targets. *Molecular Cell*, *39*(1), 8–24. https://doi.org/10.1016/j.molcel.2010.06.017

Kurgina, T. A., Moor, N. A., Kutuzov, M. M., Naumenko, K. N., Ukraintsev, A. A., & Lavrik, O. I. (2021). Dual function of HPF1 in the modulation of PARP1 and PARP2 activities. *Communications Biology*, *4*(1), 1259. https://doi.org/10.1038/s42003-021-02780-0

Langelier, M.-F., Planck, J. L., Roy, S., & Pascal, J. M. (2011). Crystal Structures of Poly(ADP-ribose) Polymerase-1 (PARP-1) Zinc Fingers Bound to DNA. *Journal of Biological Chemistry*, *286*(12), 10690–10701. https://doi.org/10.1074/jbc.M110.202507

Langelier, M.-F., Ruhl, D. D., Planck, J. L., Kraus, W. L., & Pascal, J. M. (2010). The Zn3 Domain of Human Poly(ADP-ribose) Polymerase-1 (PARP-1) Functions in Both DNA-dependent Poly(ADP-ribose) Synthesis Activity and Chromatin Compaction. *Journal of Biological Chemistry*, *285*(24), 18877–18887. https://doi.org/10.1074/jbc.M110.105668

Lehmann, M., Pirinen, E., Mirsaidi, A., Kunze, F. A., Richards, P. J., Auwerx, J., & Hottiger, M. O. (2015). ARTD1-induced poly-ADP-ribose formation enhances PPARγ ligand binding and co-factor exchange. *Nucleic Acids Research*, *43*(1), 129–142. https://doi.org/10.1093/nar/gku1260

Leung, A. K. L., Vyas, S., Rood, J. E., Bhutkar, A., Sharp, P. A., & Chang, P. (2011). Poly(ADP-Ribose) Regulates Stress Responses and MicroRNA Activity in the Cytoplasm. *Molecular Cell*, *42*(4), 489–499. https://doi.org/10.1016/j.molcel.2011.04.015

Li, M., & Yu, X. (2015). The role of poly(ADP-ribosyl)ation in DNA damage response and cancer chemotherapy. *Oncogene*, *34*(26), 3349–3356. https://doi.org/10.1038/onc.2014.295

Li, X., Han, H., Zhou, M.-T., Yang, B., Ta, A. P., Li, N., Chen, J., & Wang, W. (2017). Proteomic Analysis of the Human Tankyrase Protein Interaction Network Reveals Its Role in Pexophagy. *Cell Reports*, *20*(3), 737–749. https://doi.org/10.1016/j.celrep.2017.06.077

Li, Z., Wang-Heaton, H., Cartwright, B. M., Makinwa, Y., Hilton, B. A., Musich, P. R., Shkriabai, N., Kvaratskhelia, M., Guan, S., Chen, Q., Yu, X., & Zou, Y. (2021). ATR prevents Ca^{2+} overload-induced necrotic cell death through phosphorylation-mediated inactivation of PARP1 without DNA damage signaling. *The FASEB Journal*, *35*(5). https://doi.org/10.1096/fj.202001636RRR

Liu, C., Vyas, A., Kassab, M. A., Singh, A. K., & Yu, X. (2017). The role of poly ADP-ribosylation in the first wave of DNA damage response. *Nucleic Acids Research*, *45*(14), 8129–8141. https://doi.org/10.1093/nar/gkx565

Loseva, O., Jemth, A.-S., Bryant, H. E., Schüler, H., Lehtiö, L., Karlberg, T., & Helleday, T. (2010). PARP-3 Is a Mono-ADP-ribosylase That Activates PARP-1 in the Absence of DNA. *Journal of Biological Chemistry*, *285*(11), 8054–8060. https://doi.org/10.1074/jbc.M109.077834

Luo, X., & Kraus, W. L. (2012). On PAR with PARP: cellular stress signaling through poly(ADP-ribose) and PARP-1. *Genes & Development*, *26*(5), 417–432. https://doi.org/10.1101/gad.183509.111

Luo, X., Ryu, K. W., Kim, D.-S., Nandu, T., Medina, C. J., Gupte, R., Gibson, B. A., Soccio, R. E., Yu, Y., Gupta, R. K., & Kraus, W. L. (2017a). PARP-1 Controls the Adipogenic Transcriptional Program by PARylating C/EBPβ and Modulating Its Transcriptional Activity. *Molecular Cell*, *65*(2), 260–271. https://doi.org/10.1016/j.molcel.2016.11.015

Luo, X., Ryu, K. W., Kim, D.-S., Nandu, T., Medina, C. J., Gupte, R., Gibson, B. A., Soccio, R. E., Yu, Y., Gupta, R. K., & Kraus, W. L. (2017b). PARP-1 Controls the Adipogenic Transcriptional Program by PARylating C/EBPβ and Modulating Its Transcriptional Activity. *Molecular Cell*, *65*(2), 260–271. https://doi.org/10.1016/j.molcel.2016.11.015

Lüscher, B., Ahel, I., Altmeyer, M., Ashworth, A., Bai, P., Chang, P., Cohen, M., Corda, D., Dantzer, F., Daugherty, M. D., Dawson, T. M., Dawson, V. L., Deindl, S., Fehr, A. R., Feijs, K. L. H., Filippov, D. V., Gagné, J., Grimaldi, G., Guettler, S., … Ziegler, M. (2021). ADP-ribosyltransferases, an update on function and nomenclature. *The FEBS Journal*. https://doi.org/10.1111/febs.16142

Lüscher, B., Bütepage, M., Eckei, L., Krieg, S., Verheugd, P., & Shilton, B. H. (2018). ADP-Ribosylation, a Multifaceted Posttranslational Modification Involved in the Control of Cell Physiology in Health and Disease. *Chemical Reviews*, *118*(3), 1092–1136. https://doi.org/10.1021/acs.chemrev.7b00122

Mangerich, A., & Bürkle, A. (2012). Pleiotropic Cellular Functions of PARP1 in Longevity and Aging: Genome Maintenance Meets Inflammation. *Oxidative Medicine and Cellular Longevity*, *2012*, 1–19. https://doi.org/10.1155/2012/321653

Mao, Z., Hine, C., Tian, X., Van Meter, M., Au, M., Vaidya, A., Seluanov, A., & Gorbunova, V. (2011). SIRT6 Promotes DNA Repair Under Stress by Activating PARP1. *Science*, *332*(6036), 1443–1446. https://doi.org/10.1126/science.1202723

Martínez-Morcillo, F. J., Cantón-Sandoval, J., Martínez-Navarro, F. J., Cabas, I., Martínez-Vicente, I., Armistead, J., Hatzold, J., López-Muñoz, A., Martínez-Menchón, T., Corbalán-Vélez, R., Lacal, J., Hammerschmidt, M., García-Borrón, J. C., García-Ayala, A., Cayuela, M. L., Pérez-Oliva, A. B., García-Moreno, D., & Mulero, V. (2021). NAMPT-derived NAD+ fuels PARP1 to promote skin inflammation through parthanatos cell death. *PLOS Biology*, *19*(11), e3001455. https://doi.org/10.1371/journal.pbio.3001455

Mashimo, M., Kato, J., & Moss, J. (2014). Structure and function of the ARH family of ADP-ribosyl-acceptor hydrolases. *DNA Repair*, *23*, 88–94. https://doi.org/10.1016/j.dnarep.2014.03.005

Masutani, M., & Fujimori, H. (2013). Poly(ADP-ribosyl)ation in carcinogenesis. *Molecular Aspects of Medicine*, *34*(6), 1202–1216. https://doi.org/10.1016/j.mam.2013.05.003

Matteini, F., Andresini, O., Petrai, S., Battistelli, C., Rossi, M. N., & Maione, R. (2020). Poly(ADP-ribose) Polymerase 1 (PARP1) restrains MyoD-dependent gene expression during muscle differentiation. *Scientific Reports*, *10*(1), 15086. https://doi.org/10.1038/s41598-020-72155-8

Meder, V. S., Boeglin, M., de Murcia, G., & Schreiber, V. (2005). PARP-1 and PARP-2 interact with nucleophosmin/B23 and accumulate in transcriptionally active nucleoli. *Journal of Cell Science*, *118*(1), 211–222. https://doi.org/10.1242/jcs.01606

Menissier de Murcia, J. (2003). Functional interaction between PARP-1 and PARP-2 in chromosome stability and embryonic development in mouse. *The EMBO Journal*, *22*(9), 2255–2263. https://doi.org/10.1093/emboj/cdg206

Miwa, M., & Sugimura, T. (1971). Splitting of the Ribose-Ribose Linkage of Poly(Adenosine Diphosphate-Ribose) by a Calf Thymus Extract. *Journal of Biological Chemistry*, *246*(20), 6362–6364. https://doi.org/10.1016/S0021-9258(18)61798-3

Mukund, K., & Subramaniam, S. (2020). Skeletal muscle: A review of molecular structure and function, in health and disease. *WIREs Systems Biology and Medicine*, *12*(1). https://doi.org/10.1002/wsbm.1462

Niere, M., Mashimo, M., Agledal, L., Dölle, C., Kasamatsu, A., Kato, J., Moss, J., & Ziegler, M. (2012). ADP-ribosylhydrolase 3 (ARH3), Not Poly(ADP-ribose) Glycohydrolase (PARG) Isoforms, Is Responsible for Degradation of Mitochondrial Matrix-associated Poly(ADP-ribose). *Journal of Biological Chemistry*, *287*(20), 16088–16102. https://doi.org/10.1074/jbc.M112.349183

Obaji, E., Haikarainen, T., & Lehtiö, L. (2018). Structural basis for DNA break recognition by ARTD2/PARP2. *Nucleic Acids Research*, *46*(22), 12154–12165. https://doi.org/10.1093/nar/gky927

Oláh, G., Szczesny, B., Brunyánszki, A., López-García, I. A., Gerö, D., Radák, Z., & Szabo, C. (2015). Differentiation-Associated Downregulation of Poly(ADP-Ribose) Polymerase-1 Expression in Myoblasts Serves to Increase Their Resistance to Oxidative Stress. *PLOS ONE*, *10*(7), e0134227. https://doi.org/10.1371/journal.pone.0134227

Oliver, F. J. (1999). Resistance to endotoxic shock as a consequence of defective NF-kappa B activation in poly (ADP-ribose) polymerase-1 deficient mice. *The EMBO Journal*, *18*(16), 4446–4454. https://doi.org/10.1093/emboj/18.16.4446

O'Sullivan, J., Tedim Ferreira, M., Gagné, J.-P., Sharma, A. K., Hendzel, M. J., Masson, J.-Y., & Poirier, G. G. (2019). Emerging roles of eraser enzymes in the dynamic control of protein ADP-ribosylation. *Nature Communications*, *10*(1), 1182. https://doi.org/10.1038/s41467-019-08859-x

Palazzo, L., Mikoč, A., & Ahel, I. (2017). ADP-ribosylation: new facets of an ancient modification. *The FEBS Journal*, *284*(18), 2932–2946. https://doi.org/10.1111/febs.14078

Palazzo, L., Thomas, B., Jemth, A.-S., Colby, T., Leidecker, O., Feijs, K. L. H., Zaja, R., Loseva, O., Puigvert, J. C., Matic, I., Helleday, T., & Ahel, I. (2015). Processing of protein ADP-ribosylation by Nudix hydrolases. *Biochemical Journal*, *468*(2), 293–301. https://doi.org/10.1042/BJ20141554

Pandey, N., & Black, B. E. (2021). Rapid Detection and Signaling of DNA Damage by PARP-1. *Trends in Biochemical Sciences*, *46*(9), 744–757. https://doi.org/10.1016/j.tibs.2021.01.014

Pazzaglia, S., & Pioli, C. (2019). Multifaceted Role of PARP-1 in DNA Repair and Inflammation: Pathological and Therapeutic Implications in Cancer and Non-Cancer Diseases. *Cells*, *9*(1), 41. https://doi.org/10.3390/cells9010041

Perina, D., Mikoč, A., Ahel, J., Ćetković, H., Žaja, R., & Ahel, I. (2014). Distribution of protein poly(ADP-ribosyl)ation systems across all domains of life. *DNA Repair*, *23*, 4–16. https://doi.org/10.1016/j.dnarep.2014.05.003

Pirinen, E., Cantó, C., Jo, Y. S., Morato, L., Zhang, H., Menzies, K. J., Williams, E. G., Mouchiroud, L., Moullan, N., Hagberg, C., Li, W., Timmers, S., Imhof, R., Verbeek, J., Pujol, A., van Loon, B., Viscomi, C., Zeviani, M., Schrauwen, P., … Auwerx, J. (2014). Pharmacological Inhibition of Poly(ADP-Ribose) Polymerases Improves Fitness and Mitochondrial Function in Skeletal Muscle. *Cell Metabolism*, *19*(6), 1034–1041. https://doi.org/10.1016/j.cmet.2014.04.002

Piskunova, T. S., Yurova, M. N., Ovsyannikov, A. I., Semenchenko, A. V., Zabezhinski, M. A., Popovich, I. G., Wang, Z.-Q., & Anisimov, V. N. (2008). Deficiency in Poly(ADP-ribose)

Polymerase-1 (PARP-1) Accelerates Aging and Spontaneous Carcinogenesis in Mice. *Current Gerontology and Geriatrics Research*, *2008*, 1–11. https://doi.org/10.1155/2008/754190

Poltronieri, P., Celetti, A., & Palazzo, L. (2021). Mono(ADP-ribosyl)ation Enzymes and NAD+ Metabolism: A Focus on Diseases and Therapeutic Perspectives. *Cells*, *10*(1), 128. https://doi.org/10.3390/cells10010128

Prokhorova, E., Agnew, T., Wondisford, A. R., Tellier, M., Kaminski, N., Beijer, D., Holder, J., Groslambert, J., Suskiewicz, M. J., Zhu, K., Reber, J. M., Krassnig, S. C., Palazzo, L., Murphy, S., Nielsen, M. L., Mangerich, A., Ahel, D., Baets, J., O'Sullivan, R. J., & Ahel, I. (2021). Unrestrained poly-ADP-ribosylation provides insights into chromatin regulation and human disease. *Molecular Cell*, *81*(12), 2640-2655.e8. https://doi.org/10.1016/j.molcel.2021.04.028

Qi, H., Price, B. D., & Day, T. A. (2019). Multiple Roles for Mono- and Poly(ADP-Ribose) in Regulating Stress Responses. *Trends in Genetics*, *35*(2), 159–172. https://doi.org/10.1016/j.tig.2018.12.002

Rack, J. G. M., Palazzo, L., & Ahel, I. (2020). (ADP-ribosyl)hydrolases: structure, function, and biology. *Genes & Development*, *34*(5–6), 263–284. https://doi.org/10.1101/gad.334631.119

Rajamohan, S. B., Pillai, V. B., Gupta, M., Sundaresan, N. R., Birukov, K. G., Samant, S., Hottiger, M. O., & Gupta, M. P. (2009). SIRT1 Promotes Cell Survival under Stress by Deacetylation-Dependent Deactivation of Poly(ADP-Ribose) Polymerase 1. *Molecular and Cellular Biology*, *29*(15), 4116–4129. https://doi.org/10.1128/MCB.00121-09

Rajman, L., Chwalek, K., & Sinclair, D. A. (2018). Therapeutic Potential of NAD-Boosting Molecules: The In Vivo Evidence. *Cell Metabolism*, *27*(3), 529–547. https://doi.org/10.1016/j.cmet.2018.02.011

Ramazi, S., & Zahiri, J. (2021). Post-translational modifications in proteins: resources, tools and prediction methods. *Database*, *2021*. https://doi.org/10.1093/database/baab012

Rancourt, A., & Satoh, M. S. (2009). Delocalization of nucleolar poly(ADP-ribose) polymerase-1 to the nucleoplasm and its novel link to cellular sensitivity to DNA damage. *DNA Repair*, *8*(3), 286–297. https://doi.org/10.1016/j.dnarep.2008.11.018

Reber, J. M., Božić-Petković, J., Lippmann, M., Mazzardo, M., Dilger, A., Warmers, R., Bürkle, A., & Mangerich, A. (2023). PARP1 and XRCC1 exhibit a reciprocal relationship in genotoxic stress response. *Cell Biology and Toxicology*, *39*(1), 345–364. https://doi.org/10.1007/s10565-022-09739-9

Reber, J. M., & Mangerich, A. (2021). Why structure and chain length matter: on the biological significance underlying the structural heterogeneity of poly(ADP-ribose). *Nucleic Acids Research*, *49*(15), 8432–8448. https://doi.org/10.1093/nar/gkab618

Reeder, R. H., Ueda, K., Honjo, T., Nishizuka, Y., & Hayaishi, O. (1967). Studies on the polymer of adenosine diphosphate ribose. II. Characterization of the polymer. *The Journal of Biological Chemistry*, *242*(13), 3172–3179.

Relaix, F., Bencze, M., Borok, M. J., Der Vartanian, A., Gattazzo, F., Mademtzoglou, D., Perez-Diaz, S., Prola, A., Reyes-Fernandez, P. C., Rotini, A., & Taglietti. (2021). Perspectives on skeletal muscle stem cells. In *Nature Communications* (Vol. 12, Issue 1). Nature Research. https://doi.org/10.1038/s41467-020-20760-6

Riccio, A. A., Cingolani, G., & Pascal, J. M. (2016). PARP-2 domain requirements for DNA damage-dependent activation and localization to sites of DNA damage. *Nucleic Acids Research*, *44*(4), 1691–1702. https://doi.org/10.1093/nar/gkv1376

Rippmann, J. F., Damm, K., & Schnapp, A. (2002). Functional Characterization of the Poly(ADP-ribose) Polymerase Activity of Tankyrase 1, a Potential Regulator of Telomere Length. *Journal of Molecular Biology*, *323*(2), 217–224. https://doi.org/10.1016/S0022-2836(02)00946-4

Robaszkiewicz, A., Qu, C., Wisnik, E., Ploszaj, T., Mirsaidi, A., Kunze, F. A., Richards, P. J., Cinelli, P., Mbalaviele, G., & Hottiger, M. O. (2016). ARTD1 regulates osteoclastogenesis and bone homeostasis by dampening NF-κB-dependent transcription of IL-1β. *Scientific Reports*, *6*(1), 21131. https://doi.org/10.1038/srep21131

Rohm, T. V., Meier, D. T., Olefsky, J. M., & Donath, M. Y. (2022). Inflammation in obesity, diabetes, and related disorders. *Immunity*, *55*(1), 31–55. https://doi.org/10.1016/j.immuni.2021.12.013

Ryu, D., Zhang, H., Ropelle, E. R., Sorrentino, V., Mázala, D. A. G., Mouchiroud, L., Marshall, P. L., Campbell, M. D., Ali, A. S., Knowels, G. M., Bellemin, S., Iyer, S. R., Wang, X., Gariani, K., Sauve, A. A., Cantó, C., Conley, K. E., Walter, L., Lovering, R. M., … Auwerx, J. (2016). NAD $^+$ repletion improves muscle function in muscular dystrophy and counters global PARylation. *Science Translational Medicine*, *8*(361). https://doi.org/10.1126/scitranslmed.aaf5504

Ryu, K. W., Nandu, T., Kim, J., Challa, S., DeBerardinis, R. J., & Kraus, W. L. (2018). Metabolic regulation of transcription through compartmentalized NAD $^+$ biosynthesis. *Science*, *360*(6389). https://doi.org/10.1126/science.aan5780

Satoh, M. S., & Lindahl, T. (1992). Role of poly(ADP-ribose) formation in DNA repair. *Nature*, *356*(6367), 356–358. https://doi.org/10.1038/356356a0

Schreiber, V., Dantzer, F., Ame, J.-C., & de Murcia, G. (2006). Poly(ADP-ribose): novel functions for an old molecule. *Nature Reviews Molecular Cell Biology*, *7*(7), 517–528. https://doi.org/10.1038/nrm1963

Shieh, W. M., Amé, J.-C., Wilson, M. V., Wang, Z.-Q., Koh, D. W., Jacobson, M. K., & Jacobson, E. L. (1998). Poly(ADP-ribose) Polymerase Null Mouse Cells Synthesize ADP-ribose Polymers. *Journal of Biological Chemistry*, *273*(46), 30069–30072. https://doi.org/10.1074/jbc.273.46.30069

Slade, D., Dunstan, M. S., Barkauskaite, E., Weston, R., Lafite, P., Dixon, N., Ahel, M., Leys, D., & Ahel, I. (2011). The structure and catalytic mechanism of a poly(ADP-ribose) glycohydrolase. *Nature*, *477*(7366), 616–620. https://doi.org/10.1038/nature10404

Smith, S., Giriat, I., Schmitt, A., & de Lange, T. (1998a). Tankyrase, a Poly(ADP-Ribose) Polymerase at Human Telomeres. *Science*, *282*(5393), 1484–1487. https://doi.org/10.1126/science.282.5393.1484

Smith, S., Giriat, I., Schmitt, A., & de Lange, T. (1998b). Tankyrase, a Poly(ADP-Ribose) Polymerase at Human Telomeres. *Science*, *282*(5393), 1484–1487. https://doi.org/10.1126/science.282.5393.1484

Stilmann, M., Hinz, M., Arslan, S. Ç., Zimmer, A., Schreiber, V., & Scheidereit, C. (2009). A Nuclear Poly(ADP-Ribose)-Dependent Signalosome Confers DNA Damage-Induced IκB Kinase Activation. *Molecular Cell*, *36*(3), 365–378. https://doi.org/10.1016/j.molcel.2009.09.032

Sugimura, T., Fujimura, S., Hasegawa, S., & Kawamura, Y. (1967). Polymerization of the adenosine 5′-diphosphate ribose moiety of NAD by rat liver nuclear enzyme. *Biochimica et Biophysica Acta (BBA) - Nucleic Acids and Protein Synthesis*, *138*(2), 438–441. https://doi.org/10.1016/0005-2787(67)90507-2

Szántó, M., & Bai, P. (2020). The role of ADP-ribose metabolism in metabolic regulation, adipose tissue differentiation, and metabolism. *Genes & Development*, *34*(5–6), 321–340. https://doi.org/10.1101/gad.334284.119

Talhaoui, I., Lebedeva, N. A., Zarkovic, G., Saint-Pierre, C., Kutuzov, M. M., Sukhanova, M. V., Matkarimov, B. T., Gasparutto, D., Saparbaev, M. K., Lavrik, O. I., & Ishchenko, A. A. (2016). Poly(ADP-ribose) polymerases covalently modify strand break termini in DNA fragments *in vitro*. *Nucleic Acids Research*, gkw675. https://doi.org/10.1093/nar/gkw675

Tan, A., Younis, A. Z., Evans, A., Creighton, J. V., Coveny, C., Boocock, D. J., Sale, C., Lavery, G. G., Coutts, A. S., & Doig, C. L. (2023a). PARP1 mediated PARylation contributes to myogenic progression and glucocorticoid transcriptional response. *Cell Death Discovery*, *9*(1), 133. https://doi.org/10.1038/s41420-023-01420-2

Tan, A., Younis, A. Z., Evans, A., Creighton, J. V., Coveny, C., Boocock, D. J., Sale, C., Lavery, G. G., Coutts, A. S., & Doig, C. L. (2023b). PARP1 mediated PARylation contributes to myogenic progression and glucocorticoid transcriptional response. *Cell Death Discovery*, *9*(1), 133. https://doi.org/10.1038/s41420-023-01420-2

Tanaka, M., Miwa, M., Hayashi, K., Kubota, K., Matsushima, T., & Sugimura, T. (1977). Separation of oligo(adenosine diphosphate ribose) fractions with various chain lengths and terminal structures. *Biochemistry*, *16*(7), 1485–1489. https://doi.org/10.1021/bi00626a037

Teloni, F., & Altmeyer, M. (2016). Readers of poly(ADP-ribose): designed to be fit for purpose. *Nucleic Acids Research*, *44*(3), 993–1006. https://doi.org/10.1093/nar/gkv1383

Thomas, C., & Tulin, A. V. (2013). Poly-ADP-ribose polymerase: Machinery for nuclear processes. *Molecular Aspects of Medicine*, *34*(6), 1124–1137. https://doi.org/10.1016/j.mam.2013.04.001

Thompson, L. V. (2009). Age-related muscle dysfunction. *Experimental Gerontology*, *44*(1–2), 106–111. https://doi.org/10.1016/j.exger.2008.05.003

UCHIUMI, F., WATANABE, T., OHTA, R., ABE, H., & TANUMA, S.-I. (2013). PARP1 gene expression is downregulated by knockdown of PARG gene. *Oncology Reports*, *29*(5), 1683–1688. https://doi.org/10.3892/or.2013.2321

Ueda, K., Oka, J., Narumiya, S., Miyakawa, N., & Hayaishi, O. (1972). Poly ADP-ribose glycohydrolase from rat liver nuclei, a novel enzyme degrading the polymer. *Biochemical and Biophysical Research Communications*, *46*(2), 516–523. https://doi.org/10.1016/S0006-291X(72)80169-4

Vyas, S., Chesarone-Cataldo, M., Todorova, T., Huang, Y.-H., & Chang, P. (2013). A systematic analysis of the PARP protein family identifies new functions critical for cell physiology. *Nature Communications*, *4*(1), 2240. https://doi.org/10.1038/ncomms3240

Vyas, S., Matic, I., Uchima, L., Rood, J., Zaja, R., Hay, R. T., Ahel, I., & Chang, P. (2014). Family-wide analysis of poly(ADP-ribose) polymerase activity. *Nature Communications*, *5*(1), 4426. https://doi.org/10.1038/ncomms5426

Wahlberg, E., Karlberg, T., Kouznetsova, E., Markova, N., Macchiarulo, A., Thorsell, A.-G., Pol, E., Frostell, Å., Ekblad, T., Öncü, D., Kull, B., Robertson, G. M., Pellicciari, R., Schüler, H., & Weigelt, J. (2012). Family-wide chemical profiling and structural analysis of PARP and tankyrase inhibitors. *Nature Biotechnology*, *30*(3), 283–288. https://doi.org/10.1038/nbt.2121

Wang, X., Hu, Z., Hu, J., Du, J., & Mitch, W. E. (2006). Insulin Resistance Accelerates Muscle Protein Degradation: Activation of the Ubiquitin-Proteasome Pathway by Defects in Muscle Cell Signaling. *Endocrinology*, *147*(9), 4160–4168. https://doi.org/10.1210/en.2006-0251

Wang, X., Mi, S., Zhao, M., Lu, C., Jia, C., & Chen, Y. (2022). Quantitative Analysis of the Protein Methylome Reveals PARP1 Methylation is involved in DNA Damage Response. *Frontiers in Molecular Biosciences*, *9*. https://doi.org/10.3389/fmolb.2022.878646

Wu, H., & Ballantyne, C. M. (2017). Skeletal muscle inflammation and insulin resistance in obesity. *Journal of Clinical Investigation*, *127*(1), 43–54. https://doi.org/10.1172/JCI88880

Zhang, Q., Bhattacharya, S., Pi, J., Clewell, R. A., Carmichael, P. L., & Andersen, M. E. (2015). Adaptive Posttranslational Control in Cellular Stress Response Pathways and Its Relationship to Toxicity Testing and Safety Assessment. *Toxicological Sciences : An Official Journal of the Society of Toxicology*, *147*(2), 302–316. https://doi.org/10.1093/toxsci/kfv130